NAVAL POSTGRADUATE SCHOOL

MONTEREY, CALIFORNIA

THESIS

EVALUATION OF NIGHT VISION DEVICES FOR IMAGE FUSION STUDIES

by

Cheng Wee Kiang

December 2004

Co-Advisors: Alfred W Cooper
Gamani Karunasiri

THIS PAGE INTENTIONALLY LEFT BLANK

REPORT DOCUMENTATION PAGE		Form Approved OMB No. 0704-0188

Public reporting burden for this collection of information is estimated to average 1 hour per response, including the time for reviewing instruction, searching existing data sources, gathering and maintaining the data needed, and completing and reviewing the collection of information. Send comments regarding this burden estimate or any other aspect of this collection of information, including suggestions for reducing this burden, to Washington headquarters Services, Directorate for Information Operations and Reports, 1215 Jefferson Davis Highway, Suite 1204, Arlington, VA 22202-4302, and to the Office of Management and Budget, Paperwork Reduction Project (0704-0188) Washington DC 20503.

1. AGENCY USE ONLY *(Leave blank)*	2. REPORT DATE	3. REPORT TYPE AND DATES COVERED
	December 2004	Master's Thesis

4. TITLE AND SUBTITLE:
Evaluation of Night Vision Devices for Image Fusion Studies

5. FUNDING NUMBERS

6. AUTHOR(S)
Mr Cheng Wee Kiang, The Republic of Singapore

7. PERFORMING ORGANIZATION NAME(S) AND ADDRESS(ES)
Naval Postgraduate School
Monterey, CA 93943-5000

8. PERFORMING ORGANIZATION REPORT NUMBER

9. SPONSORING /MONITORING AGENCY NAME(S) AND ADDRESS(ES)
N/A

10. SPONSORING/MONITORING AGENCY REPORT NUMBER

11. SUPPLEMENTARY NOTES
The views expressed in this thesis are those of the author and do not reflect the official policy or position of the Department of Defense or the U.S. Government.

12a. DISTRIBUTION / AVAILABILITY STATEMENT
Approved for public releases; distribution is unlimited.

12b. DISTRIBUTION CODE
A

13. ABSTRACT (maximum 200 words)

Night Vision Devices (NVD) using Image Intensification (II) technology are among the most important sensors used by ground troops and aviators in night operations for modern combat. With the intensified images from these devices, soldiers can see an enemy's movement better and further in darkness. This thesis explores different test methods in evaluating the performances and sensitivities of several NVDs for future image fusion studies. Specification data such as sensitivity, resolution (Modulation Transfer Function) and pixel size are obtained. Comparative analyses of the collected results are made to characterize the performances of the different NVDs. A new method using MATLAB programming to objectively analyze digitized images for characterization of II based NVDs is proposed. This test method can also be extended to the evaluation of Thermal Imaging (TI) systems for comparative analysis with II NVDs. In addition, the feasibility of testing NVDs using both II and TI technologies, with common operating conditions and target boards is discussed. Finally, the potential of using these digitized images for image fusion studies is verified with the test and evaluation results.

14. SUBJECT TERMS
Night Vision Device, NVD, image intensification, II, thermal imaging, TI, contrast transfer function, CTF, modulation transfer function, MTF, image fusion.

15. NUMBER OF PAGES
137

16. PRICE CODE

17. SECURITY CLASSIFICATION OF REPORT	18. SECURITY CLASSIFICATION OF THIS PAGE	19. SECURITY CLASSIFICATION OF ABSTRACT	20. LIMITATION OF ABSTRACT
Unclassified	Unclassified	Unclassified	UL

NSN 7540-01-280-5500

Standard Form 298 (Rev. 2-89)
Prescribed by ANSI Std. 239-18

THIS PAGE INTENTIONALLY LEFT BLANK

Approved for public releases; distribution is unlimited

EVALUATION OF NIGHT VISION DEVICES FOR IMAGE FUSION STUDIES

Mr. Cheng Wee Kiang
Republic of Singapore
B.Eng, National University of Singapore, 1998

Submitted in partial fulfillment of the
requirements for the degree of

MASTER OF SCIENCE IN COMBAT SYSTEMS TECHNOLOGY

from the

NAVAL POSTGRADUATE SCHOOL
December 2004

Author: Cheng Wee Kiang

Approved by: Alfred W Cooper
Thesis Co-Advisor

Gamani Karunasiri
Thesis Co-Advisor

James H. Luscombe
Chairman, Department of Physics

THIS PAGE INTENTIONALLY LEFT BLANK

ABSTRACT

Night Vision Devices (NVD) using Image Intensification (II) technology are among the most important sensors used by ground troops and aviators in night operations for modern combat. With the intensified images from these devices, soldiers can see an enemy's movement better and further in darkness. This thesis explores different test methods in evaluating the performances and sensitivities of several NVDs for future image fusion studies. Specification data such as sensitivity, resolution (Modulation Transfer Function) and pixel size are obtained. Comparative analyses of the collected results are made to characterize the performances of the different NVDs. A new method using MATLAB programming to objectively analyze digitized images for characterization of II based NVDs is proposed. This test method can also be extended to the evaluation of Thermal Imaging (TI) systems for comparative analysis with II NVDs. In addition, the feasibility of testing NVDs using both II and TI technologies, with common operating conditions and target boards is discussed. Finally, the potential of using these digitized images for image fusion studies is verified with the test and evaluation results.

THIS PAGE INTENTIONALLY LEFT BLANK

TABLE OF CONTENTS

LIST OF FIGURES

LIST OF TABLES

THIS PAGE INTENTIONALLY LEFT BLANK

ACKNOWLEDGMENTS

The author would like to express his gratitude towards Professors Alfred W. Cooper and Gamani Karunasiri for their guidance, advices, encouragements and patience in helping him complete this thesis. He would also like thank Mr. Sam Barone for his kind assistance in the laboratory experiments.

The author would also like to acknowledge the support of this research work from the Temasek Defense Technology Institute, National University of Singapore, under Project Reference Number TDSI/02-010/A, "Multi-IR Band Data Fusion for Target Recognition".

Lastly, the author would like to take this opportunity to acknowledge the tremendous support given by his wonderful and lovely wife, Jeanette. Without her love, patience and encouragement, the completion of this thesis would not have been possible.

THIS PAGE INTENTIONALLY LEFT BLANK

I. INTRODUCTION

A. BACKGROUND

In modern combat, the advantage of being able to see further and better under low light conditions is of paramount importance in determining the outcome of a battle. Due to the tactical advantages of night operations, many battles and raids are now conducted in the cover of the night sky. Though there may be huge tactical advantages in operating at night, there exist problems that need to be addressed. These include the ability to have a clear view through augmentation devices for targeting purposes, differentiate between friendly and enemy forces and maneuver through the battle ground without being detected. As these problems are crucial and critical in determining the success of a battle, it is thus important to equip soldiers with equipment that provides the capability of seeing and fighting under the cover of the night sky.

B. REMOTE NIGHT SENSING

Due to the limitations of the human eye, direct view optical systems and TV cameras, remote sensing under night conditions is typically achieved by two common methods, one being Image Intensification and the other Thermal Imaging. When illumination of the environment drops to an illuminance level of 1 to 10 Lux (twilight), the detection and identification capability of human eyes and optical systems degrades severely due to the lack of incident photons.

One of the methods adopted to address this is to intensify the original object image by multiplying the incident photons by several thousands of times in order to produce a perceivable image. This technology is known as Image Intensification. Night Vision Devices or Goggles, that are widely used by the military, use this technology for enabling night operation capabilities. This technology depends on the reflected light from the object to work effectively. As the incident light on the object is largely dependent on the luminance of the environment, Image Intensification will not work in a totally darkened

environment. Therefore, in order for this technology to work, the natural illuminance level must be at least 10^{-4} Lux, which corresponds to an overcast moonless night sky.

The other method is to make use of temperature differences between the background and target objects to perceive their presence. As all objects that are above absolute 0 K will radiate energy and thereby create a temperature contrast between them, the measurement of this contrast can be used to perform night vision operations. This technology is known as Thermal Imaging. As its name implies, thermal imaging uses the thermal property differences between object materials and their environment to detect the presence of objects. The temperature contrasts are typically sensed by an array of detectors that are subsequently scanned to produce an image of the scene. This night vision technology has the advantage of not depending on the illuminance level of the environment to produce good results. However, as it is highly dependent on temperature contrast, a weak contrast between the background and target object (caused by deliberate actions such as thermal shielding) will degrade the effectiveness of this technology.

With these two unique and independent methods of seeing at night, there is an obvious advantage to combining the outputs from these two technologies to bring night vision capabilities to a higher level. This can possibly be achieved by applying strong image fusion techniques to extract the strengths of both output images to produce a resulting high contrast image. With successful fusion, night operations by the military can be greatly enhanced to create a tactical edge over their enemies.

C. OBJECTIVE

The objective of this thesis is to evaluate several night vision systems to characterize their sensitivities and performances. The systems are tested with

both subjective and objective testing methods when possible. In addition, this thesis also studies the potential in using digitized intensified images for future image fusion studies.

This thesis is separated into five chapters with Chapter I covering a brief introduction. This is followed by Chapter II, which discusses the fundamental theories of Image Intensification (II) systems and the different methods of testing and evaluating them. In addition, image fusion techniques will be discussed. Chapter III covers the testing and evaluation of two existing II systems (Night Quest ITT NQ-160 and Zenith Moonlight NV-100) and a new digital night vision viewer (Nitemax NM-1000). Their measured performances and sensitivities are analyzed and compared. Chapter IV covers the test and evaluation of a new II system (Astroscope 9350) and discusses the results obtained. Comparisons between the new II system and the other systems are also made. The last Chapter concludes the major findings of this thesis and recommends future work to be done.

THIS PAGE INTENTIONALLY LEFT BLANK

II. NIGHT VISION IMAGING

A. IMAGE INTENSIFICATION

Image Intensification is a process whereby low intensity input images are boosted to produce higher intensity output images for useful applications. The technique of image intensification is achieved by multiplying incident light photons in low light conditions by gains of 10,000 to 100,000 to produce outputs which are comparable to images taken during the day [Harney, 2004]. The setup of a typical II system is shown in Figure 1 and the process of image intensification is illustrated in Figure 2.

Reflected light photons are incident through the input faceplate of the II system and are passed through a photocathode where they are converted to photo-electrons. These photo-electrons are accelerated through the Micro-Channel Plate (MCP, introduced only in Generation 2 II system) where the number of photo-electrons is multiplied by gains of 10,000 to 100,000 (depending on the Generation of the II system). The resulting huge numbers of photo-electrons are then accelerated to strike the phosphor screen where they are converted back to photons forming intensified images of the original input scene. This process of converting to electrons, accelerating, multiplying and reconverting of photons will significantly increase the intensity of near IR input images to produce visible output images under low light conditions.

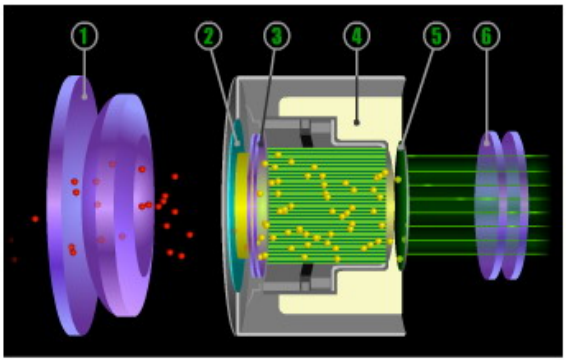

1. Front Lens
2. Photocathode
3. Microchannel Plate
4. High Voltage Power Supply
5. Phosphor Screen
6. Eyepiece

Figure 1. A Typical II System Component Setup [ATN Corp, 2004]

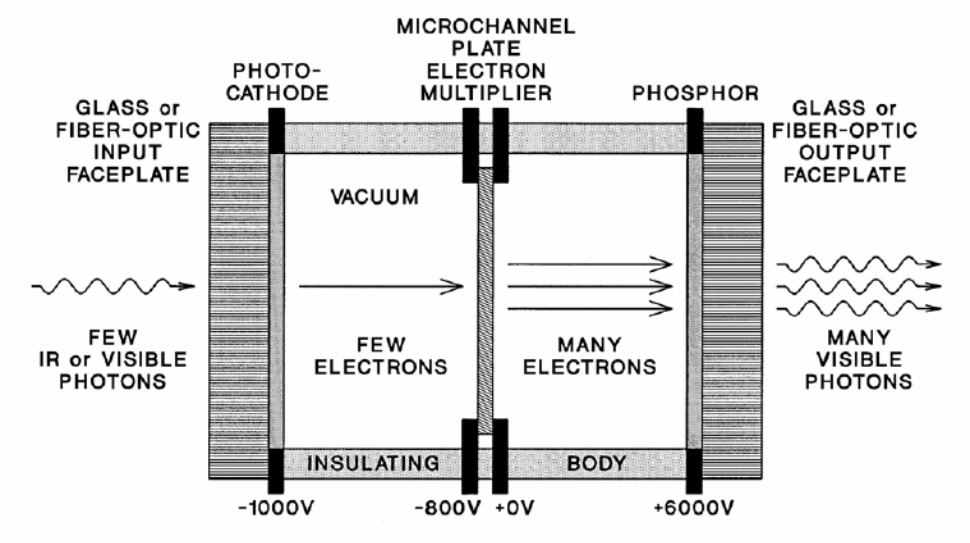

Figure 2. The Image Intensification Process [Harney, 2004]

B. GENERATIONS OF NIGHT VISION IMAGE INTENSIFICATION SYSTEM

II systems, coupled with viewing optics, are used in combat operations since the middle of the 20th century and have developed to the 3rd or even 4th Generation with significant improvements in the quality of the images produced [Harney, 2004]. The improvements are mainly achieved by the development of more efficient and effective internal components using state-of-the-art designs and good material usages.

1. Generation 1 Image Intensification System

The 1st generation of II tubes consists of a simple setup which includes a camera lens, photocathode (S-1 type), a vacuum tube and phosphor screen (P-20). Figure 3 illustrates a Gen 1 II system. In the Gen 1 tubes, the photons striking the photocathode produce electrons that are focused electro-statically and accelerated in the vacuum tube by the 15kV potential, towards the phosphor screen where visible photons are produced. From this simple process, an intensified image is produced. However, one of the major problems in the Gen 1 II system is the relatively low quantum efficiency of the S1 photocathode, which results in a photon-to-output luminous gain of only about 50-100. In order to

overcome this problem, a few Gen 1 tubes were usually coupled together in series to produce an overall system gain of about 10,000 during the early days when II systems are deployed. However, this caused the entire setup to be heavy, bulky and at the same time hazardous due to its high voltage. [Csorba, 1985]

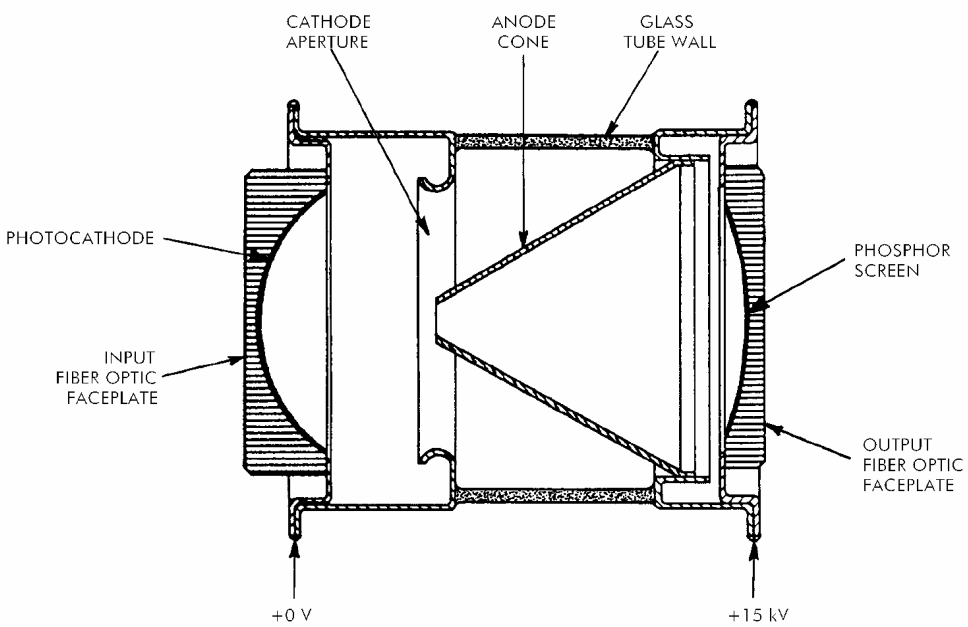

Figure 3. A Gen 1 II System [Csorba, 1985]

2. Generation 2 Image Intensification System

With the limitations of Gen 1 II systems, the next generation (Gen 2) of II system was designed to improve their performances in terms of quantum efficiencies and weight. Gen 2 II system performances are significantly improved with the introduction of the Multi-Channel Plate (MCP) electron multiplier, which is placed between the photocathode and the phosphor screen. The MCP is capable of multiplying the number of incident photo-electrons to amounts of up to thousands of times. The internal MCP is made up of hundreds of thousands or millions of microscopic lead silicate glass tubes bundled in a hexagonal structure. The typical diameter of each micro-channel glass tube is about 8-45 μm. [Harney, 2004]

Figure 4 shows a typical MCP which consists of two face plates (for applying of electrical potential) and a tilted bunch of tubes for electrons to travel

through. Due to the slanted configuration, horizontally moving electrons entering the MCP will strike the tube wall which will in turn result in the reproduction of several other secondary electrons. With this process repeated several other times along the tubes, the number of electrons will be multiplied when they exit the MCP by thousands of times (depending on the quality of the MCP). These large numbers of electrons are then accelerated towards the phosphor screen to produce an image of significantly higher intensity compared to the Gen 1 II system. However, the introduction of the MCP caused a severe loss of resolution at that time due to the relatively large pores of the plate limited by the manufacturing process. [Harney, 2004].

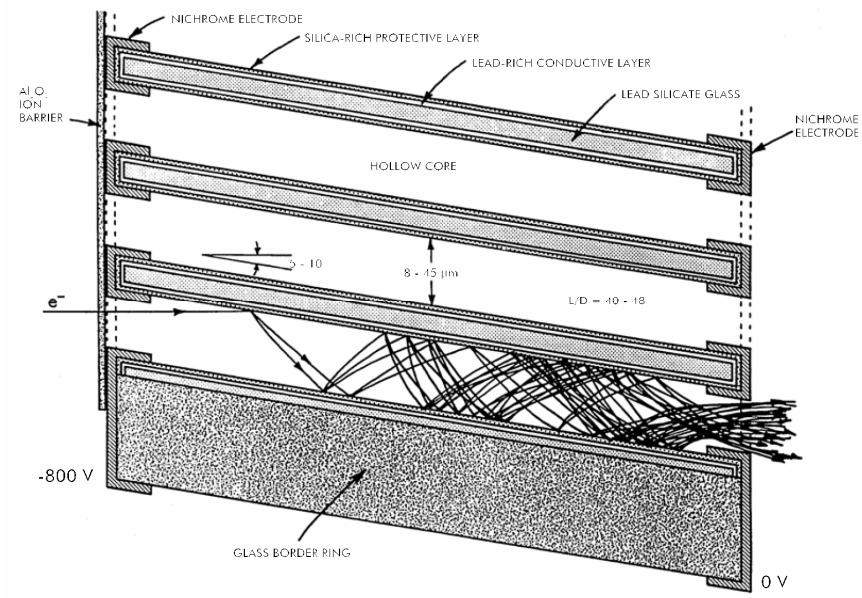

Figure 4. The Internal Structure of a MCP [Harney, 2004]

In addition to the introduction of the MCP, Gen 2 II systems also make extensive use of newer multi-alkali photocathodes such as the red S-20. From Figure 5, it can be observed that the S-20 photocathode has a much higher sensitivity compared to the S-1 photocathode at the visible spectrum range of 400 to 700 nm. It is noted the though Gen 2 II systems perform better than their Gen 1 counterparts, they have no capabilities in performing in the near IR range. Gen 2 II systems come in two different configurations, one being electro-statically

focused (Figure 6) and the other proximity focused (Figure 7). In the electrostatic focused system, electrostatic forces are used to focus the photoelectrons onto the electron multiplier. As the electrostatic forces need distance in order to produce the required focusing function, Gen 2 II systems of this configuration are usually larger in size. For the proximity focused system, the gap between the photocathode and MCP is made very small to prevent photoelectrons from spreading out before they strike the MCP. An obvious advantage of the proximity focused system is that it can be made thinner and consequently lighter than the electrostatic focused systems. Image inversion of the image for these two configurations must be corrected. This can be achieved with the twisted fiber optic plate as shown in Figure 7. [Harney, 2004]

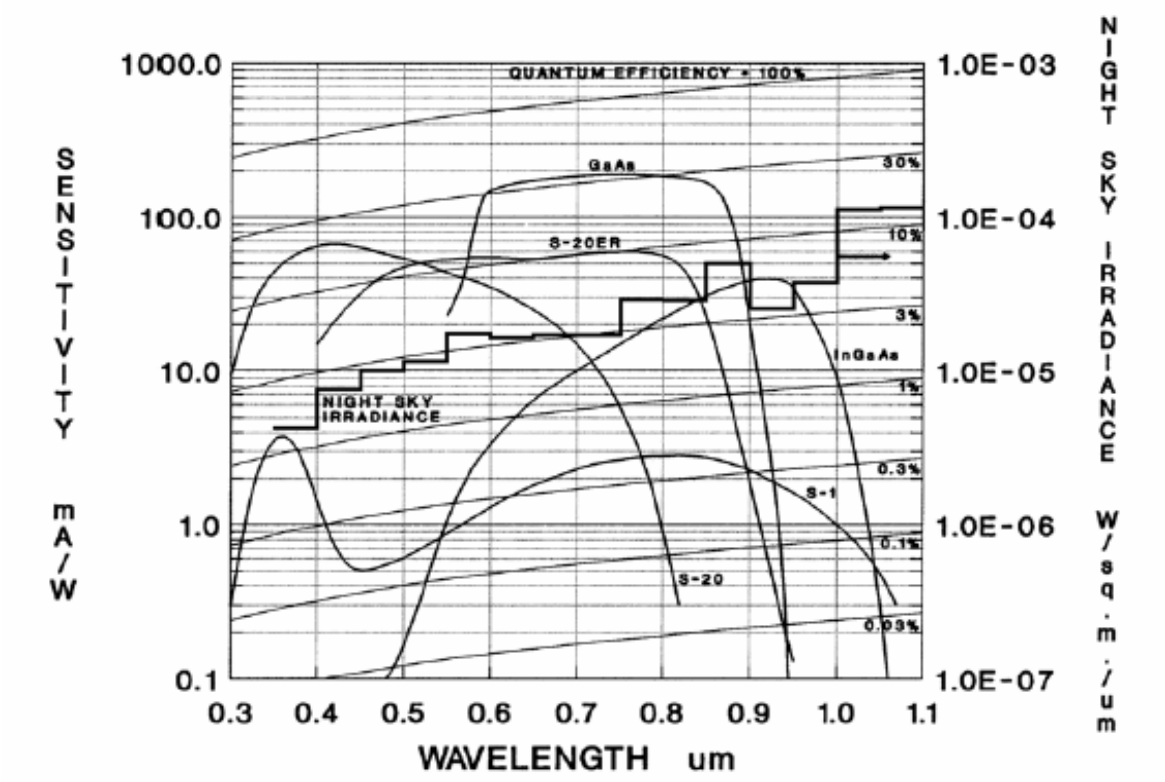

Figure 5. Photocathode Spectral Response and Night Sky Spectrum versus Wavelength [RCA, 1971]

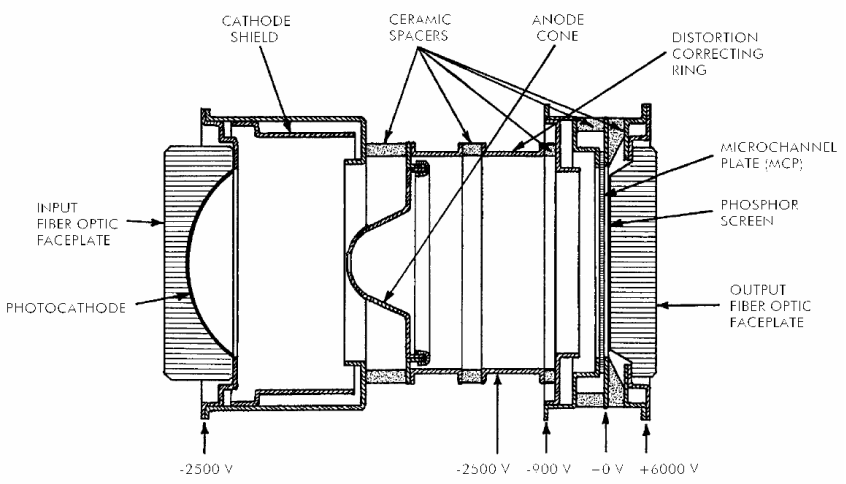

Figure 6. A Gen 2 II System with Electrostatic Focus [Csorba, 1985]

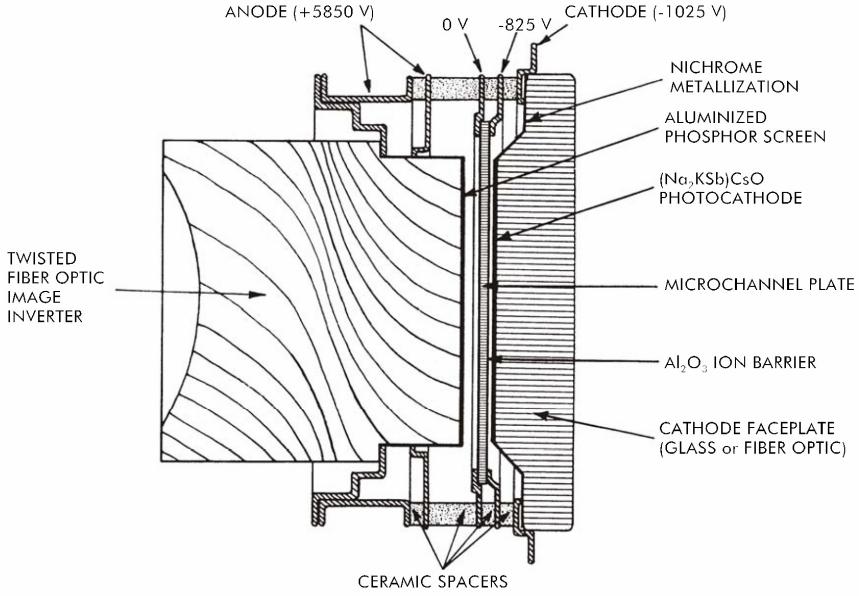

Figure 7. A Gen 2 II System with Proximity Focus [Csorba, 1985]

3. Generation 3 Image Intensification System

The Gen 3 II system is most commonly used in the present Night Vision Devices that are deployed by the military. Gen 3 II systems adopt a Gallium Arsenide (GaAs) photocathode in replacement of the multi-alkali Gen 2 systems. The introduction of the GaAs photocathode offers much higher quantum efficiency, typically by a factor of three [Ji Wei, 2003]. Another advantage of the GaAs photocathode is its extension of sensitivity into the near IR range as shown

in Figure 5. In addition to using the more sensitive GaAs photocathode, Gen 3 II systems also feature improved MCP design whereby the channels are further reduced in diameter to produce better resolution. Further improvements are made to the photocathode with the introduction of the Indium Gallium Arsenide (InGaAs) photocathode which warranted naming a new generation known as Gen 3+. This extends the sensitivity further into the near IR range up to 1 μm as shown in Figure 5. [Csorba, 1985]

Most Gen 3 II systems use the KA (P20) phosphor screen which emits a greenish light of wavelength 555 nm, chosen to match the peak sensitivity of human eyes. This explains the reason behind the greenish background images that are commonly produced by most Night Vision Devices. The advantages of the KA (P20) phosphor screen are in its ability to produce higher conversion efficiency and resolution. In addition, the decay rate of the KA(P20) is also significantly higher as it decays to 0.1 % of its peak output in less than 1msec. Thus, lag is decreased and this results in less “smearing” of the scene when a bright source suddenly appears in front of the II system. Therefore, the KA(P20) phosphor is preferred and more commonly used in aviation tubes where scene movements and changes may be rapid. [Harney, 2004]

In addition to these features, Gen 3 II systems also include an ion barrier film to prevent back accelerating of heavy ions. The protection rendered by this ion barrier can significantly extend the life of Gen 3 II system. Figure 8 illustrates the layout of a typical Gen 3 II system.

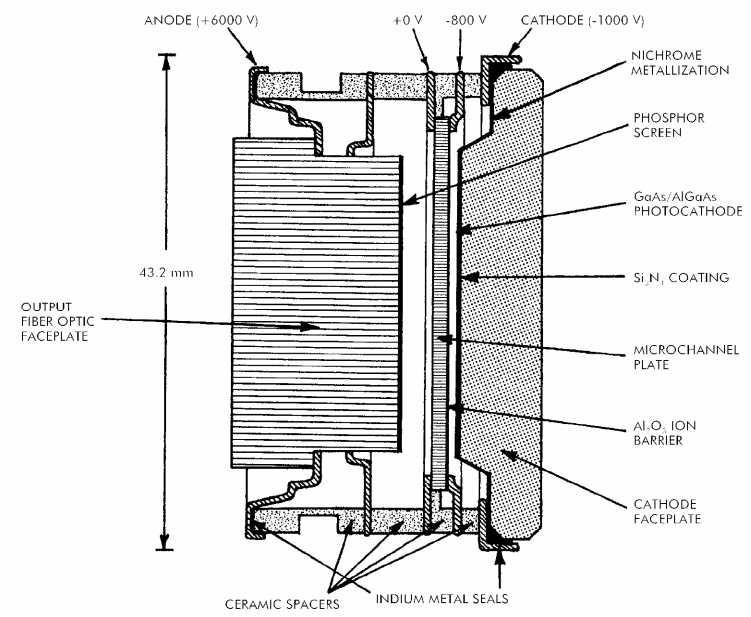

Figure 8. A Gen 3 II System [Csorba, 1985]

C. PHOTOMETRY

One important aspect for the effective operations of Night Vision Devices is the amount of ambient light that is reflected by the target. As the Night Vision Device generates images in the visible spectrum where the human eye can resolve, photometric units are normally used to describe the amount of light reflected from the target. Photometry is the measurement of illumination, which is defined by the electromagnetic radiation perceived by the human eye, and is weighted by the eye luminous efficiency. It is thus restricted to wavelengths ranging from 360 to 830 nm. In short, photometry measures the spectral response of the human eye. [Palmer, 1999] The common units used for photometry measurements are Lux, Footcandles (FC), Footlamberts (FL) with sub-units of lumens and candelas. These units are related to each other in various ways and their corresponding relationships are summarized in the Equations below.

$$1 \text{ Lux} = 1 \text{ Lumen/m}^2 \quad (1)$$

$$1 \text{ FC} = 1 \text{ Lumen/ft}^2 \quad (2)$$

Therefore, $$1 \text{ Lux} = 0.0929 \text{ FC} \quad (3)$$

and, $1\ FL = 1\ Lumen/ft^2/sr = 1\ Candela/ft^2$ (4)

where, $1\ Candela = 1\ Lumen/sr$ (5)

When performing experiments to evaluate the radiant energy at various wavelengths, a human eye is adapted to relatively bright lights to determine its relative effectiveness in producing brightness. This experiment would result in a curve shown in Figure 9 (Photopic). From the curve, it can be observed that the human eye has the greatest responsivity at the wavelength of 555 nm. This explains why this wavelength is chosen for the KA(P20) phosphor screen and also the reason why most NVDs output a greenish image.

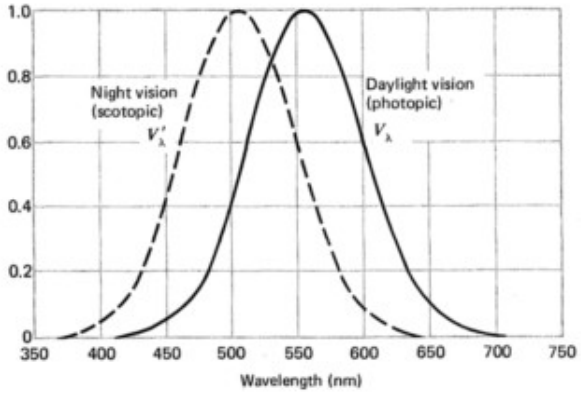

Figure 9. Photopic & Scotopic Luminous Efficiency vs Wavelength [Sitko, 2004]

In the measurement of the night sky scene illumination level, it is a common practice to use the units of photometry to describe it. Table 1 summarizes the different night sky conditions with respect to their corresponding luminous flux density in Lux. [Bond, 1963]

Night Sky	Lux Level
Twilight	10
Deep twilight	1
Full moon	10^{-1}
Quarter moon	10^{-2}
Moonless clear night sky	10^{-3}
Moonless overcast night sky	10^{-4}

Table 1. Night Sky with Corresponding Lux Level

The values in Table 1 will be used as a standard reference when evaluating the Night Vision Devices. In the subsequent chapters, the scene

illumination level of the experiments will be measured using a laboratory photometer. Conversions from FL to Lux, taking into account detector areas and the photo-detector's measurement distances will be made. The conversions will enable the comparison of the measured scene illumination against the night sky conditions.

D. EVALUATION OF NIGHT VISION DEVICES

1. Subjective Test and Evaluation Method

In this test method, the NVDs are evaluated by "experienced" operators trained to observe from a series of bar chart test patterns such as the USAF1951 Test Pattern shown in Figure 10. The operators' tasks are to observe the test pattern from various stand-off distances for different scene illuminations and verify, based on their judgment, the minimum resolvable bar chart for each scenario.

From Figure 10, each bar target on the test pattern will have a corresponding spatial frequency defined by the number of line pairs (one black and one white bar) in a millimeter. The sensitivity of different Night Vision Devices or Goggles can be compared when the scene illumination and their limiting spatial frequencies are plotted against each other. This test method is adopted for most Night Vision Devices or Goggles that are designed as direct view optical systems and do not provide analogue or digital readouts for external analysis. [Task et al, 1993]

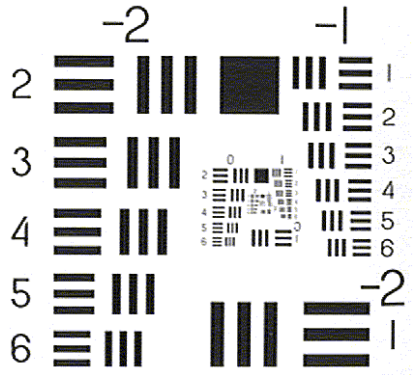

Figure 10. The USAF 1951 Test Pattern [Edmund Optics]

As the outcome of the test and evaluation hinges heavily upon the experience level of the operators, this method is a subjective one and may not be optimal for a good technical evaluation. In order to optimize this evaluation, a large sample of tests with a relatively large number of operators from different combat background experiences may be needed. However, with many operators involved, this may not be a most ideal and cost effective solution, judging from the resources required.

2. Objective Test and Evaluation Method

In objective testing, the dependence on operator skills and experience is eliminated. One of the ways to obtain objective results in evaluating an NVD is by measurement of its Modulation Transfer Function (MTF). In a generic definition, MTF is the measurement of the magnitude of response of a detector when looking at different spatial frequencies. Alternatively, it can also be expressed as the measure of resolution of an imaging system [Boreman, 1998]. The MTF is a sine wave amplitude response which is equal to unity at very low spatial frequencies.

A major reason for MTF being commonly used is that it permits cascading of effects of several major components of an optical system to measure the overall resolution of the entire system. The MTF of an entire system is the product of the individual MTFs of the sub-systems. [RCA, 1974]

When taking measurements with the USAF 1951 Test Pattern, the MTF will determine how much contrast remains between white and black lines on a bar target after they have been projected through the optical assembly. It is a measure of the degradation of an image as it appears at the output screen of the assembly as correlated to the input pattern which is normalized to 100 % contrast at a spatial frequency equal to or less than 0.2 line pairs per millimeter (lp/mm). [Kjellberg, 1998]

Though it is preferred to directly measure MTF when performing analysis, it is often more practical to derive MTF from the Contrast Transfer Function

(CTF). [RCA, 1974] The CTF can be constructed from scans of intensity across an image plane displaying patterns of vertical bars of varying spacing (E.g. shown in Figure 11). Each of these scans will produce a limited square wave for different spatial frequency whose contrast is defined by the maximum and minimum levels in each set. The CTF is defined as the ratio of the image contrast to the object contrast as a function of a square wave spatial frequency. [Holst, 1993]

Figure 11. The Modified USAF 1951 Test Pattern Showing Vertical Bar Patterns Arranged Across a Line [Adapted from Edmund Optics]

From the definition above, CTF can be simply represented by the ratio of the contrast difference between the image and the original object. [Holst, 1993] The contrast for the image and original object is represented by the maximum and minimum intensity levels measured. The measurement of contrast level is described as the separation in intensity between blacks and whites. For a well defined image, the black and white details shown in Figure 11 must appear black and white respectively. The greater the difference in intensity between a black and a white line, the better the contrast. (Refer to Figure 12) [Stack, 2004]

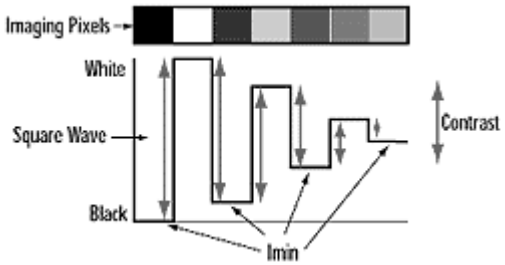

Figure 12. A Pictorial Definition of Contrast [Stack, 2004]

The CTF and Contrast, C, can be represented by the equations below.

$$CTF = \frac{C_{image}}{C_{object}} \tag{6}$$

$$C = \frac{I_{max} - I_{min}}{I_{max} + I_{min}} \tag{7}$$

When looking at the original object, the normalized I_{max}=1 and I_{min}=0 for a perfectly contrasted black and white bar target. From Equation (7), the contrast for the original object, C_{object}=1. Therefore, Equation (6) can be re-organized as below.

$$CTF = \frac{I_{max} - I_{min}}{I_{max} + I_{min}} \tag{8}$$

The CTF is a square wave amplitude response, which, unlike the MTF, cannot be cascaded to evaluate the overall system CTF. However, CTF is often preferred for experimental measurements as it is easier to perform (measurement of contrast differences) when compared to MTF. [RCA, 1974] The conversion between CTF and MTF can be achieved with the Coltman Formulae as depicted below. [Coltman, 1954]

$$MTF = M(N) = \frac{\pi}{4}\left[C(N) + \frac{C(3N)}{3} - \frac{C(5N)}{5} + \frac{C(7N)}{7} - ..... \right] \tag{9}$$

Note that the term C(9N) is omitted as it is zero.

$$CTF = C(N) = \frac{4}{\pi}\left[M(N) - \frac{M(3N)}{3} + \frac{M(5N)}{5} - \frac{M(7N)}{7} + \frac{M(9N)}{9} - ..... \right] \tag{10}$$

From these equations, the MTF response of a NVD can be derived from the experimental CTF measurements. CTF can be measured by a few methods. One of the ‘traditional’ methods is to use an oscilloscope to scan across a line of the image to obtain the square wave that represents the intensity differences across the image. From the scan across a typical target in Figure 11, the

maximum and minimum intensities of each bar target are manually recorded. Subsequently, the CTF and MTF for the optical system are calculated.

An alternative method for measurement of CTF is proposed in this thesis to replace the 'traditional' method. In this method, a digital image of the test pattern is captured and processed. A MATLAB program is written using the image analysis functions to analyze the entire image by assigning intensity levels based on a 256 grayscale (A grayscale model is used as the II system outputs a non-colored image that can be converted to grayscale). A line is then defined in the program to extract the intensity of a line scan across the image. The intensity curve across this line is then analyzed to determine the maximum and minimum intensities for each individual bar target.

In plotting the data obtained from the procedures described above, the CTF and consequently MTF curves must be fitted using an appropriate approximation. One of the curve fitting approximations commonly used is to fit the MTF to a Gaussian form. According to Lloyd, "The well known central limit theorem of probability and statistics has an analog in linear filter theory, which is that the product of N components of band-limited continuous MTF's tends to a Gaussian form as N becomes large." [Lloyd, 1975] As the NVD system consists of at least four components that each has its own MTF performance, the entire system performance can be adequately represented by a Gaussian approximation. Therefore, the system line spread function can be represented by the generic form as shown below. [Lloyd, 1975]

$$r(x) = e^{\left(-x^2 / 2\sigma^2\right)} \tag{11}$$

In the equation above, r(x) is the representation for MTF while x is the spatial frequency. σ is the standard deviation of the line spread function. With this approximation, the CTF and MTF can be fitted and a typical Gaussian fitted MTF curve is shown in Figure 13.

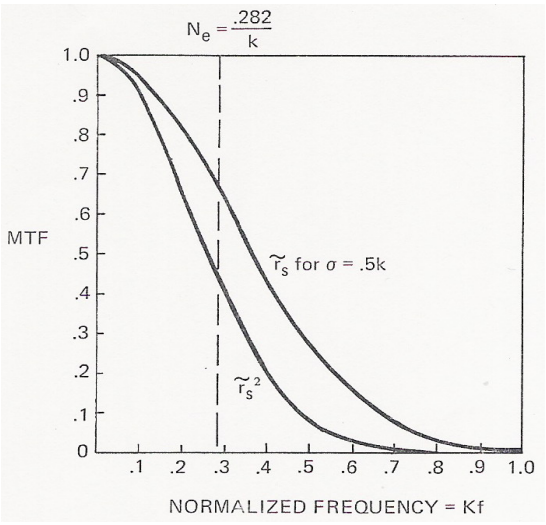

Figure 13. Example of a Gaussian Fitted MTF [Lloyd, 1975]

It is apparent that the objective test method is the preferred test method for NVDs as the uncertainty factors caused by operators (such as moods and fatigue) are taken out of the equation. This will ensure that the evaluations of the NVDs are performed in a fair and unbiased manner. For this thesis, the evaluation of the new NVD is performed based on both tests methods (subjective and objective) for comparison purposes.

E. IMAGE FUSION

With the advances in digital image processing techniques, it is now possible to fuse Intensified and Thermal images of the same scene together in a common format. The performance of fusion not only enables the production of chromatic images from two different sensor outputs, it also combines images obtained from different disparate bands from the electromagnetic spectrum efficiently. [McDaniel, 1998]

Advanced Automatic Target Recognition (ATR) and Image Enhancement algorithms are used to combine multi-spectral sensory output images into a single image that has minimum loss in content. This would relieve the operator of the burden of looking at multiple sensor scenes to achieve situational awareness. In achieving good image fusion, the output must provide the operator with a single clear scene of the pertinent information he requires. In addition, it must not

possess any artifacts that would interfere in the interpretation of the present scene. [Burt, 1993]

Several Multi-resolution fusion techniques that are capable of feature extraction have been proposed for performing image fusion of multi-spectral images. One such technique is the 'Pyramid-based Fusion' whereby a composite image is formed by extracting the salient features (such as edges of an object) from the same scene images obtained by different sensors. This extraction process is known as pyramid transform. A selection process is then performed to choose the most salient features obtained to be used to form the composite image. The composite image, which contains the best salient features of the original images, is subsequently obtained by an inverse pyramid transform. [Burt, 1993]

Another technique, known as 'Discrete Wavelet Transform' is also commonly used for image fusion works. "Discrete Wavelet Transform is based on the decomposition of a signal using an orthonormal family of basis functions." [Wolfram Research, 2004]. This iterative process involves the decomposition of the original image into one low resolution image and three other images that emphasize the vertical, horizontal and diagonal fluctuations of the scene respectively. After the maximum decomposition level is achieved, the information of the salient features of the image in each direction is then obtained. By fusing salient features of several wavelet transformed images of the same scene, a composite image can be constructed.

Apart from the Multi-resolution technique discussed, other image fusion techniques using Statistical and Numerical approaches are also available to achieve pixel level fusion of multi-spectral sensor images. The military community is also actively looking into cooperative use of multi-spectral sensor images for image fusion works. It is noted that although the focus of this thesis does not include detailed analysis of image fusion, the work is expected to lead to foreseen applications in future.

III. EVALUATION OF EXISTING NIGHT VISION DEVICES AND DIGITAL NIGHT VISION VIEWER

A. FOCUS OF TEST AND EVALUATION

In this chapter, tests performed on two existing NVDs (Night Quest ITT NQ-160 and Zenith Moonlight NV-100) in the school's inventory and a newly acquired Digital Night Vision Viewer (Nitemax NM-1000) are described. The procedures for each set of tests are discussed. The results obtained are summarized and the evaluation of the sensitivities and performances of the systems are discussed.

B. EVALUATION OF EXISTING NVD

1. Method

a. Experiment Setup

In this quantitative test, the equipment is setup in a completely darkened room to ensure accuracy of the photometric readout of the reflected light from the test pattern. The equipment for this experiment includes two night vision devices; one is the ITT NQ-160 Gen 3 monocular scope (Figure 14) with a specified resolution of 57-64 line pairs per millimeter (lp/mm) and the other is the Zenith Moonlight NV-100 Gen 2 (equivalent) monocular scope (Figure 15) with a specified resolution of 25 lp/mm. The specifications of the two scopes are summarized in Table 2. The intensity of light projected on the test pattern is controlled by a variac-driven incandescent source and the illumination conditions are measured using the Model 2020 photometer (Figure 16). The setup of the photometer in measuring the scene illumination on the Test Pattern is shown in Figure 17.

Figure 14. The ITT NQ-160

Figure 15. The Zenith Moonlight NV-100

Description	ITT NQ-160	NV-100
II System Type	Gen 3	Gen 2 (Equivalent)
System Resolution (lp/mm)	57-64	25
Gain	50,000	10,000
Magnification	1x	4.3x
Field of View (°)	40	10
Objective Lens	F/1.4	F/1.5
Voltage (V)	3	3
Battery Life (Hrs)	30	20
Weight (g)	454	1270
Length (mm)	185	216
Height (mm)	92	89
Width (mm)	54	63.5

Table 2. Specifications of the Two NVD Scopes

Figure 16. The 2020 Photometer and Variac Driver (Right)

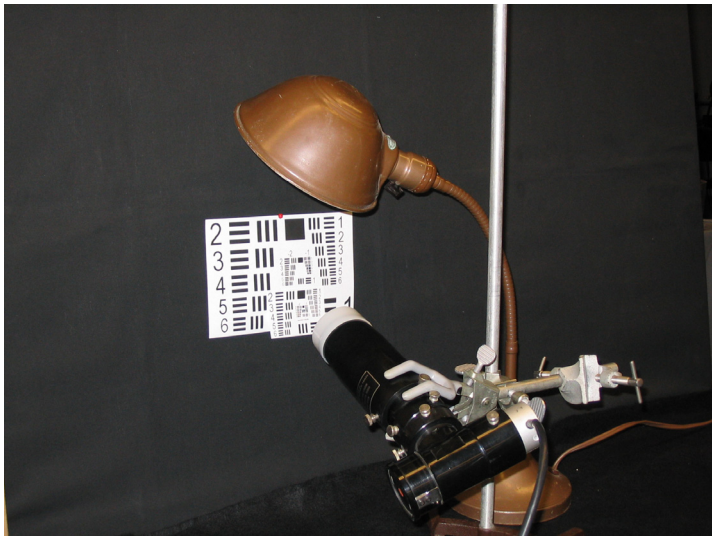

Figure 17. Experimental Setup for Measurement of Scene Illumination

b. USAF 1951 Test Pattern

The USAF 1951 Test Pattern is a widely used target for testing visible imaging systems. It consists of a series of horizontal and vertical pairs of three bar targets with varying spatial frequencies in lp/mm. A sample of the test pattern used in this experiment is shown in Figure 18. On this Test Pattern, there is a total of eight groups of six horizontal and vertical pairs of three bar targets, to provide a wide range of spatial frequencies for effective testing. The spatial frequencies for the bar targets are shown in Table 3. In this test, the Test Pattern

is mounted on a black opaque background for minimal undesired background reflections to reduce errors from the photometer measurements.

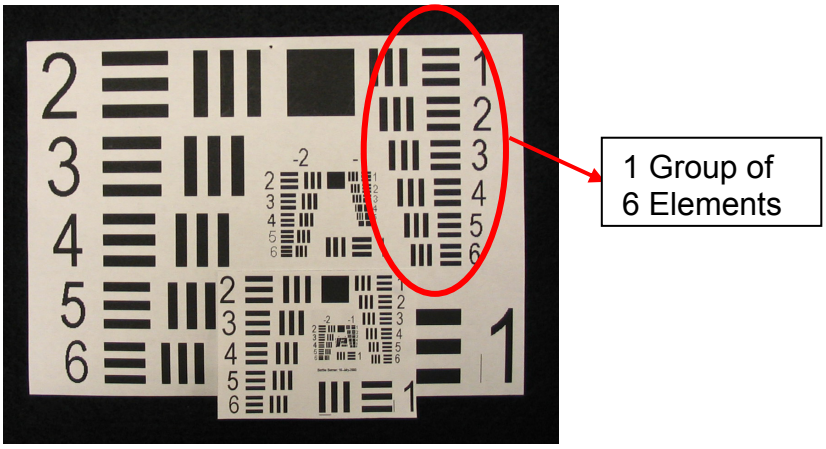

Figure 18. The USAF 1951 Test Chart [Adapted from Edmund Optics]

	Groups							
Elements	-4[1]	-3[1]	-2	-1	0	1	2	3
1	0.100	0.200	0.250	0.500	1.000	2.000	4.000	8.000
2	0.112	0.224	0.281	0.561	1.120	2.240	4.490	8.980
3	0.126	0.252	0.315	0.629	1.260	2.520	5.040	10.100
4	0.142	0.283	0.354	0.707	1.410	2.830	5.660	11.300
5	0.159	0.318	0.397	0.794	1.590	3.170	6.350	12.700
6	0.178	0.356	0.445	0.891	1.780	3.560	7.130	14.300

Table 3. The USAF 1951 Bar Chart Spatial Resolution

c. Photometric Readings

The 2020 photometer measures the scene illumination in terms of Footlamberts (FL) in Lumens per Steradian per Square foot ($lm/sr/ft^2$) [Gamma Scientific Inc]. This measured value has to be converted to Footcandles (FC in lm/ft^2 and subsequently to Lux in lm/m^2 for comparison to the night sky conditions. Based on the Electro-Optics Handbook [RCA 1978], the conversion from FL to FC and then to Lux can be achieved with the following expression:

$$1\ \mathrm{FC} = 1\ \mathrm{FL} \times \frac{1}{\pi} \times \Omega \quad (\mathrm{lm}/\mathrm{ft}^2) \tag{12}$$

$$1\ \mathrm{Lux} = 1\ \mathrm{FC} \times 10.764 = 1\ \mathrm{FL} \times \Omega \times \frac{10.764}{\pi} \tag{13}$$

[1] Note that groups -4 and -3 are 2.5x enlargement of the -2 and -1 groups respectively.

The solid angle, Ω (in sr) subtended by the target to the photo-detector is given by the expression:

$$\Omega = \frac{A_d}{R^2} = \frac{\pi(r_d)^2}{R^2} \tag{14}$$

where A_d is the area of the detector, r_d is the radius of the detector and R is the range from the center of the target to the detector. In this setup, R is 10 cm and r_d is 1.65 cm. From equation (14), the solid angle is found to be 0.0855 sr. Therefore, Equation (13) can be simplified to a direct conversion from FL to Lux as shown below.

$$1\ \text{Lux} = 1\ \text{FL} \times 0.2930 \tag{15}$$

d. Test Procedures

Before the test is performed, the photometer is calibrated according to the steps described in its operational instructions [Gamma Scientific, 1969] in a room of total darkness. This calibration process is required to minimize the readout error from the photometer. Once calibrated, the variac driver is adjusted to allow the incandescent source to produce the minimum amount of light projected on the target which is detectable by the NVDs. In this case, the value is 0.01 FL.

The ITT NQ-160 is the main scope that is analyzed in this test. The scope is first placed at a distance of S = 3 m away from the Test Pattern. The smallest bar target on the Test Pattern that can be resolved at this distance is recorded. The scope is then moved away from the target by 0.1 m and a second observation on the same bar target is made. If the same target can be resolved, the scope is again moved back another 0.1 m. This procedure is repeated until the same bar target cannot be resolved and the distance S from the test pattern is then recorded. This will be maximum distance to the smallest resolvable bar target at the starting distance of 3 m.

By taking into account the distance from the Test Pattern, the spatial frequency, *v* can then be converted from lp/mm to lp/mrad using the expression below.

$$f = S \times v \tag{16}$$

where *f* is the spatial frequency in lp/mrad.

After the 1st set of readings, the variac driver is adjusted to the next higher scene illumination level. The procedure as described in the previous paragraph is then repeated for this new scene illumination. Subsequently, the illumination is increased for more sets of readings until the scene illumination reaches a stage where the scopes are saturated and no reasonable images can be resolved.

The same procedures and conditions are repeated on the NV-100 scope to obtain its sensitivity for comparison purposes. The results from the experiment are summarized in the next section.

2. Results

Table 4 summarizes the readings taken from the ITT NQ-160 scope. From the experimental data, the scene illumination in Lux and limiting spatial frequency in lp/mrad is plotted for the ITT NQ-160.

Photometer Reading		Set 1			Set 2		
FL	Lux	*v* (lp/mm)	S (m)	*f* (lp/mrad)	*v* (lp/mm)	S (m)	*f* (lp/mrad)
0.02	0.0059	0.252	3.0	0.7560	0.252	3.0	0.7560
0.04	0.0117	0.252	3.1	0.7812	0.252	3.1	0.7812
0.06	0.0176	0.252	3.2	0.8064	0.252	3.2	0.8064
0.08	0.0234	0.252	3.3	0.8316	0.252	3.3	0.8316
0.10	0.0293	0.283	3.0	0.8490	0.283	3.0	0.8490
0.20	0.0586	0.283	3.1	0.8773	0.283	3.1	0.8773
0.40	0.1172	0.283	3.2	0.9056	0.283	3.2	0.9056
Photometer Reading		Set 3			Set 4		
FL	Lux	*V* (lp/mm)	(m)	*f* (lp/mrad)	*v* (lp/mm)	S (m)	*f* (lp/mrad)
0.02	0.0059	0.252	3.0	0.7560	0.252	3.0	0.7560
0.04	0.0117	0.252	3.1	0.7812	0.252	3.1	0.7812
0.06	0.0176	0.252	3.2	0.8064	0.252	3.2	0.8064
0.08	0.0234	0.252	3.3	0.8316	0.252	3.3	0.8316
0.10	0.0293	0.283	3.0	0.8490	0.283	3.0	0.8490
0.20	0.0586	0.283	3.1	0.8773	0.283	3.1	0.8773
0.40	0.1172	0.283	3.2	0.9056	0.283	3.2	0.9056
Photometer Reading		Set 5			Set 6		
FL	Lux	*v* (lp/mm)	S (m)	*f* (lp/mrad)	*v* (lp/mm)	S (m)	*f* (lp/mrad)
0.02	0.0059	0.252	3.0	0.7560	0.252	3.0	0.7560
0.03	0.0088	-	-	-	0.252	3.1	0.7812
0.04	0.0117	0.252	3.1	0.7812	0.252	3.2	0.8064
0.06	0.0176	0.252	3.2	0.8064	0.252	3.3	0.8316
0.08	0.0234	0.252	3.3	0.8316	0.252	3.3	0.8316
0.10	0.0293	0.283	3.0	0.8490	0.283	3.0	0.8490
0.20	0.0586	0.283	3.1	0.8773	0.283	3.1	0.8773
0.40	0.1172	0.283	3.2	0.9056	0.283	3.2	0.9056

Table 4. Tabulated Results of ITT NQ-160

The next table (Table 5) summarizes the results taken from the NV-100 which is tested under the same conditions as the ITT NQ-160. As the NV-100 scope has a 4.3X magnification factor in its optical lens, the limiting spatial frequency is normalized by the magnification factor so that a like-to-like comparison with the ITT NQ-160 is possible. The same conversion of the scene illumination and limiting spatial frequency is also performed on these data.

Photometer Reading		Set 1			Set 2		
FL	Lux	*v* (lp/mm)	S (m)	*f* (lp/mrad)	*v* (lp/mm)	S (m)	*f* (lp/mrad)
0.02	0.0059	0.318	3.0	0.2219	0.318	3.0	0.2219
0.03	0.0088	0.318	3.1	0.2293	0.318	3.1	0.2293
0.04	0.0117	0.318	3.2	0.2367	0.318	3.2	0.2367
0.05	0.0147	0.318	3.3	0.2440	0.318	3.3	0.2440
0.06	0.0176	0.318	3.4	0.2514	0.318	3.4	0.2514
0.07	0.0205	0.356	3.1	0.2567	0.356	3.1	0.2567
0.08	0.0234	0.356	3.2	0.2649	0.356	3.2	0.2649
0.09	0.0264	0.356	3.3	0.2732	0.356	3.3	0.2732
0.10	0.0293	0.356	3.4	0.2815	0.356	3.4	0.2815
0.20	0.0586	0.356	3.5	0.2898	0.356	3.5	0.2898
0.30	0.0879	0.356	3.6	0.2980	0.356	3.6	0.2980
0.40	0.1172	0.356	3.7	0.3063	0.356	3.7	0.3063
0.50	0.1465	0.356	3.8	0.3146	0.356	3.8	0.3146
0.60	0.1758	0.356	3.9	0.3229	0.356	3.9	0.3229
0.70	0.2051	0.356	4.0	0.3312	0.356	4.0	0.3312
0.80	0.2344	0.356	4.1	0.3394	0.356	4.1	0.3394
0.90	0.2637	0.356	4.2	0.3477	0.356	4.2	0.3477

Table 5. Tabulated Results of NV-100

From the results in Table 4 & 5, the graph of limiting spatial frequency against scene illumination is plotted for both scopes. Figure 19 illustrates the sensitivity plots for the two scopes.

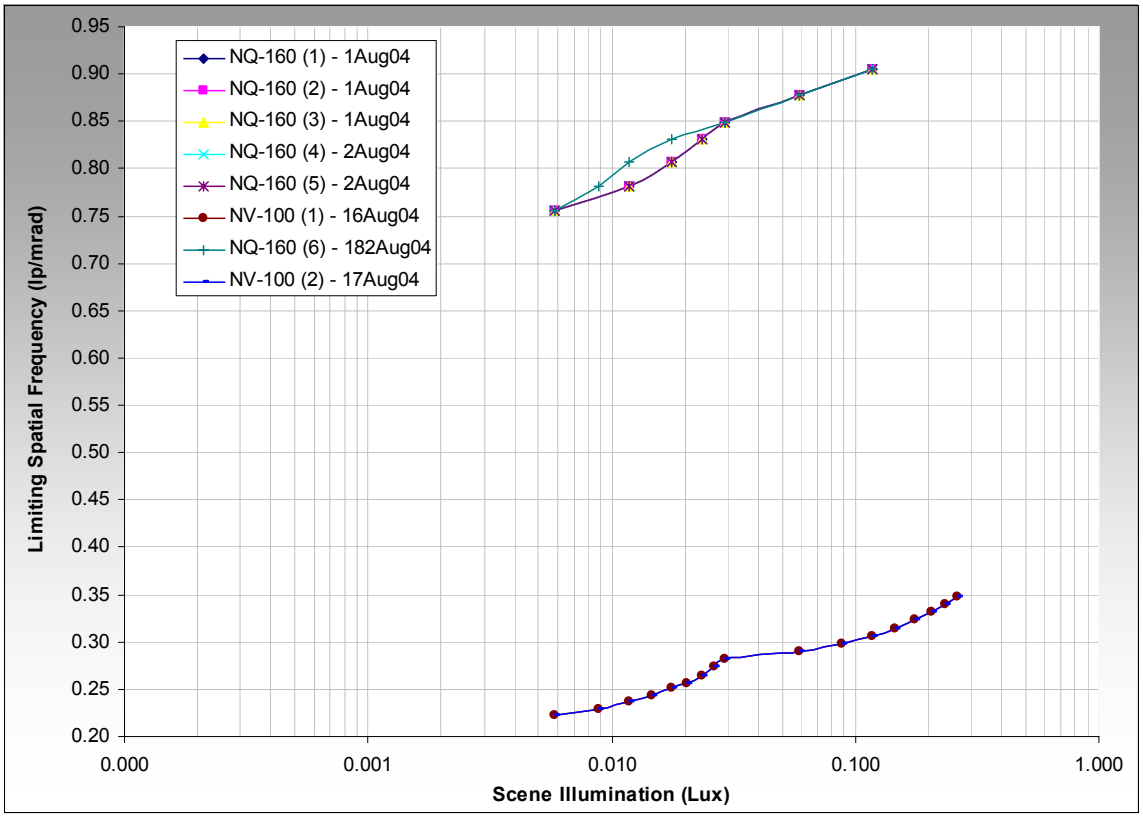

Figure 19. Sensitivity Plots of ITT NQ-160 & NV-100

3. Discussion

From the plots in Figure 19, it is also observed that the limiting spatial frequency increases as the scene becomes brighter. This is consistent with II technology where a brighter scene would mean more photons being absorbed by the image intensification process and eventually translate to a brighter output image. The operator is able to resolve smaller targets at the same distance when scene illumination increases. However, there is a limit to which the scene illumination can be increased. At a point when the scene becomes too bright, saturation of the scope will occur. For the ITT NQ-160, saturation occurs at 0.1172 Lux (Full moon) while the NV-100 saturates at 0.2637 Lux. These results indicate that the dynamic ranges of the two scopes are not wide and therefore their operations may be restricted up to Full Moonlight conditions only.

The plots in Figure 19 indicate that the ITT NQ-160 is more sensitive as compared to the NV-100. This is consistent with the fact that the ITT NQ-160

utilizes a Gen 3 II system which is of a significantly higher gain, while the NV-100 uses a Gen 2 equivalent II system with a lower gain of only about 10,000. Therefore, the ITT NQ-160 will be able to produce images of higher resolution. The technology differences in the Gen 2 and 3 II systems are evident in the plots, as the ITT NQ-160 is observed to perform about three times better than the NV-100. These results demonstrate the significant improvements between the Gen 2 and 3 II systems in which the GaAs photocathode is introduced.

Though not as sensitive, the NV-100 has an added advantage in its 4.3X magnification. When used at the same observation distance, the magnification enables the NV-100 to see further and resolve smaller bar targets as compared to the ITT NQ-160. This feature would be very useful for field operations as most observations in the field are done at stand-off distances to avoid detection by enemies. Therefore, there is significant operational advantage in having optical zoom capabilities in NVDs.

Another observation is that the ITT NQ-160 is significantly lighter than the NV-100, and this is a major advantage to soldiers carrying them in the battlefield. With a lighter scope mounted on his helmet or handheld, the soldier's endurance can be improved in the demanding battle conditions.

In summary, the improvements from a Gen 2 to a Gen 3 II system are shown in this evaluation and the importance of optical zoom is also noted. In addition, operating a light-weight NVD has a tactical advantage as a heavier load would affect the performance of a soldier in the long term.

C. EVALUATION OF NITEMAX NM-1000

The Nitemax NM-1000 is an extended-range viewing system manufactured by Infrared Imaging Inc. It is capable of operating in both day and night conditions producing digital images that can be transferred to any viewing devices via its RCA video output. In the day, the NM-1000 performs like a regular CCD camera system. For night operations, the NM-1000 utilizes infrared (IR) diodes for scene illumination to allow maximum viewing distance and clarity for

low light conditions. Figure 20 shows the compact and lightweight Nitemax NM-1000 system.

Figure 20. The Nitemax NM-1000

1. Method

a. Digital Image Capturing

The NM-1000 is a camera system that does not have an internal device for digital image storage purposes. As such, a screen capture hardware is required to capture and store the digital images that are produced by the NM-1000. In this evaluation, the Imperx Video Capture Card with PCMCIA adaptor is used (Figure 21). This card is capable of capturing up to 640x480 pixels with 24 bit RGB display. Options are also available for up to 24 bit grayscale display capture for grayscale or black and white outputs from the NM-1000.

Figure 21. The Imperx Video Capture Card

b. Scene Illumination

The scene illumination is achieved by adjusting the output level of the IR diodes that operate in the near IR region. A totally darkened scene can be significantly illuminated by these IR diodes. Figures 22 & 23 compare the same scene with minimum and maximum illumination by the NM-1000 IR diodes.

One of the proposed ways of measuring the scene illumination created by these IR diodes is by making use of the 2020 photometer. However, it should be noted that the photometer is a photometric device which is capable of measuring only the visible spectrum of light. As IR is out of the visible range, the readings obtained from the photometer are only relative read-outs and these cannot be used to compare against the scene illumination measured in the evaluation of the existing NVDs.

The readout from the 2020 photometer provides readings in Footlamberts (FL), which was discussed in the earlier section. In order to correct for the solid angle subtended by the infrared diodes to the photo-detector, a conversion will be made to the scene illuminations to convert them FL to FC using Equations (12) and (14).

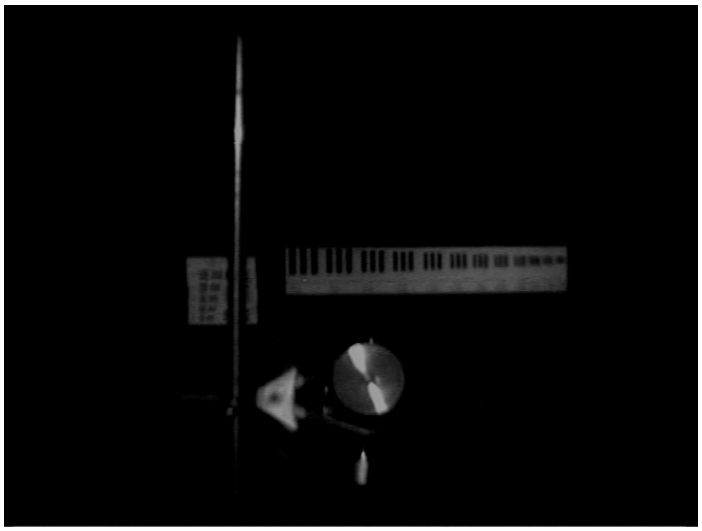

Figure 22. Nitemax Scene Image at minimum illumination

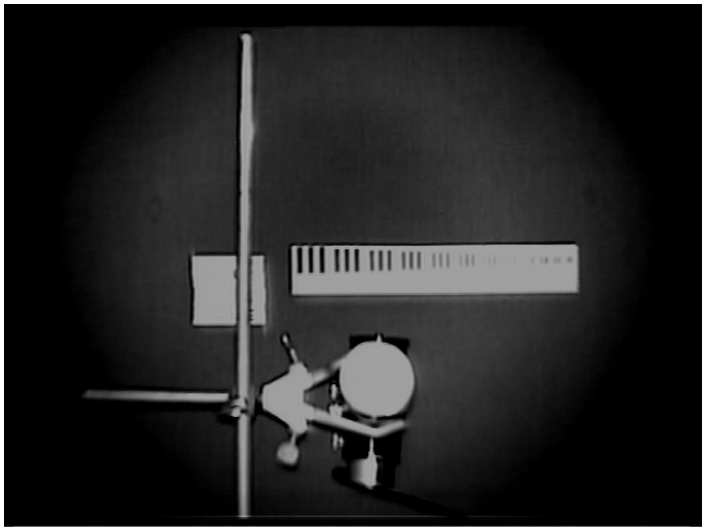

Figure 23. Nitemax Scene Image at maximum illumination

c. Test Pattern

In this test, the Test Pattern is a modified version of the USAF-1951 Test Pattern. The vertical bar targets from the USAF-1951 Pattern are extracted and lined up across a horizontal line as shown in Figure 24. In this modified test pattern, the 2.5X enlarged elements from groups -2 and -1 (i.e. groups -4 and -3 from Table 3) are used and this Test Pattern includes a total of twelve vertical bar targets. The reason for lining up the bar targets in a horizontal manner is to facilitate the MATLAB analysis program in which a horizontal line is scanned across the digital image. The spatial frequencies of the bar targets used for this test are summarized in Table 6.

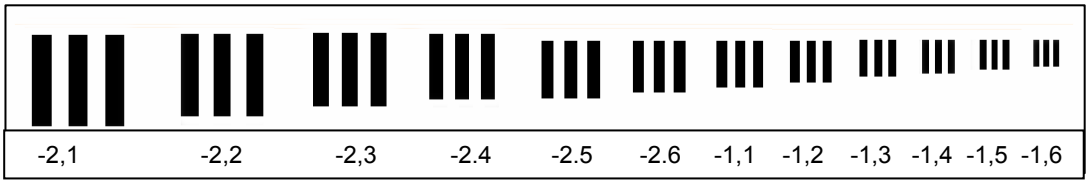

Figure 24. The Modified USAF-1951 Test Pattern [Adapted from Edmund Optics]

	Groups	
Elements	-2	-1
1	0.100	0.200
2	0.112	0.224
3	0.126	0.252
4	0.142	0.283
5	0.159	0.318
6	0.178	0.356

Table 6. The Spatial Frequencies of Modified Test Pattern (2.5x Enlargement)

d. Test Procedures

In this test, the modified Test Pattern is mounted on the same black opaque background with the photometer situated just below the pattern (facing the Nitemax NM-1000) to measure the intensity levels of the IR diodes. The setup of the target board area for this evaluation is shown in Figure 25. The Nitemax NM-1000 is then placed at a distance of 1.5 m from the target board and the IR diodes intensity level is adjusted to the minimum level where the test pattern is observable from the LCD screen. The digital readout from the NM-1000 is captured through the screen capture card and a 640x480 pixel image of the target is obtained. The IR diode intensity is then increased in sequence until the scene is saturated, with digital images captured for each intensity increment. The photometer readout is also noted for each intensity level that is increased. The test is repeated for distances of 2 and 2.5 m, and a series of digital images with their corresponding photometer readings obtained.

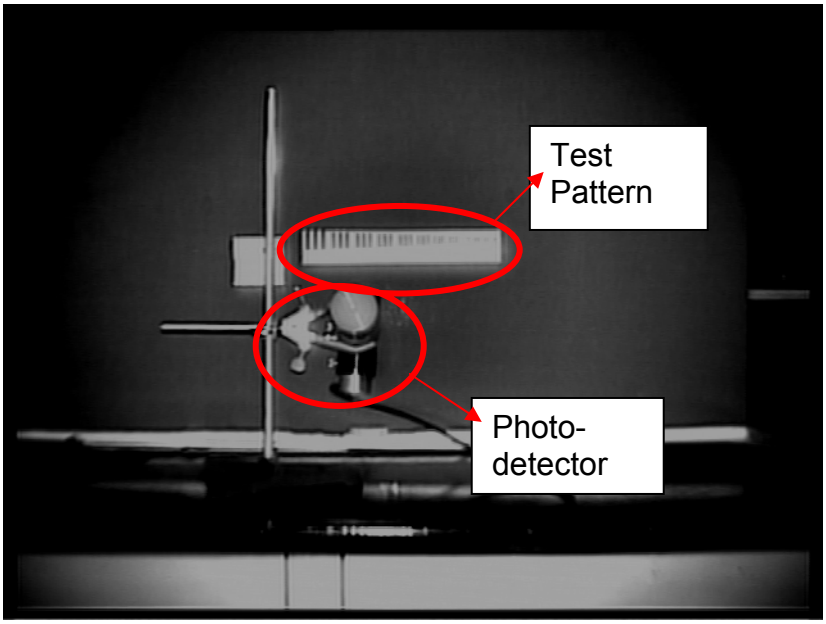

Figure 25. Test Setup for the Nitemax NM-1000

2. Results

a. Experimental Results Tabulation

The scene illuminations measured in FL and their corresponding conversion to FC using Equations (12) & (14) are summarized in Table 7. From the results, the images from the common scene illumination of about 5E-7 FC and 1.5E-6 FC are extracted to perform analysis.

Distance = 1.5m		Distance = 2m		Distance =2.5m	
FL	FC	FL	FC	FL	FC
0.003	**5.5E-07**	0.002	1.8E-07	0.001	5.5E-08
0.005	9.1E-07	0.005	**4.6E-07**	0.002	1.1E-07
0.008	**1.5E-06**	0.007	6.4E-07	0.003	1.7E-07
0.011	2.0E-06	0.011	1.0E-06	0.006	3.3E-07
0.019	3.5E-06	0.017	**1.6E-06**	0.009	**5.0E-07**
0.023	4.2E-06	0.027	2.5E-06	0.015	8.3E-07
0.029	5.3E-06	0.032	2.9E-06	0.023	**1.3E-06**
0.046	8.4E-06	0.035	3.2E-06	-	-
0.057	1.0E-05	0.044	4.0E-06	-	-
-	-	0.052	4.8E-06	-	-

Table 7. Conversion of Footlamberts (FL) to Footcandles (FC) for Different Distances

A sample set of the digital images obtained from the Nitemax NM-1000 at scene illumination of about 5E-7 FC and 1.5E-6 FC is shown in Figures 26 through 28 for distances of 1.5, 2 and 2.5 m respectively.

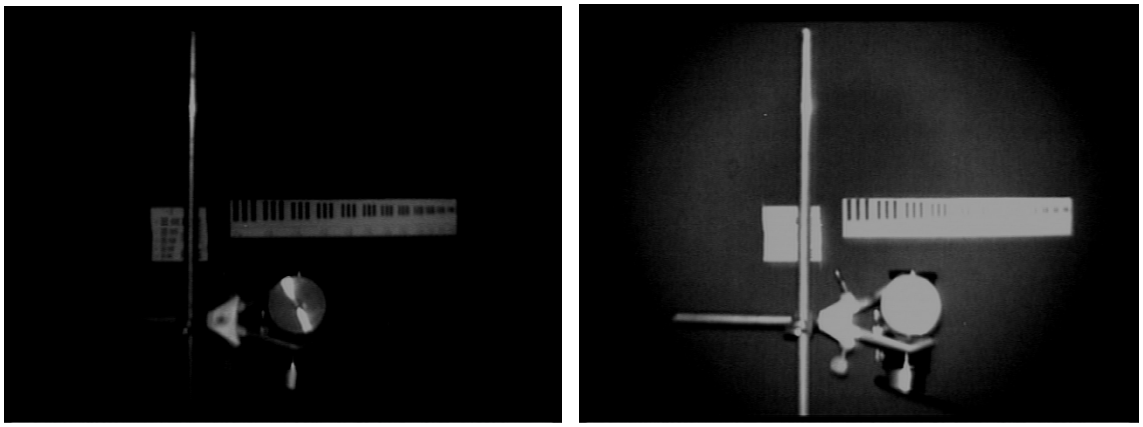

Figure 26. Scene Illumination of 5E-7 FC (Left) and 1.5E-6 FC (Right) for 1.5m

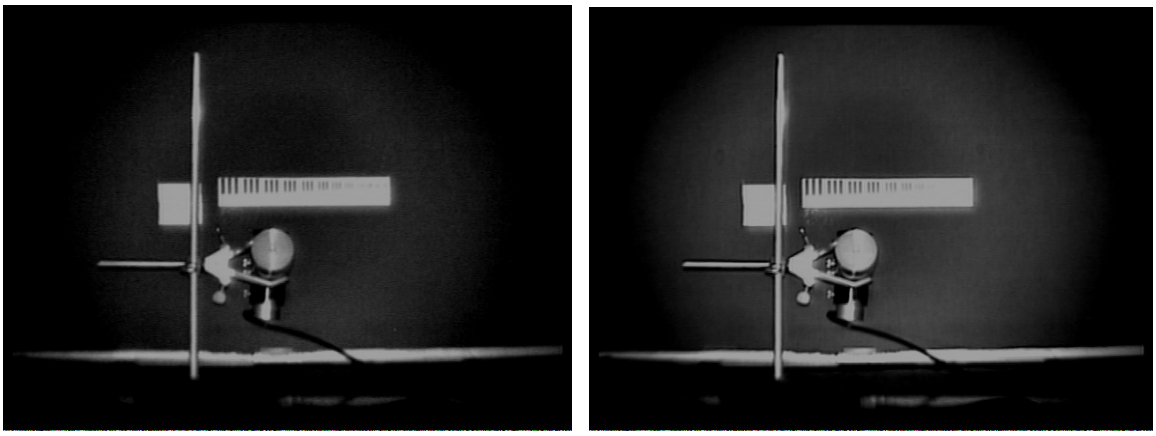

Figure 27. Scene Illumination of 5E-7 FC (Left) and 1.5E-6 FC (Right) for 2m

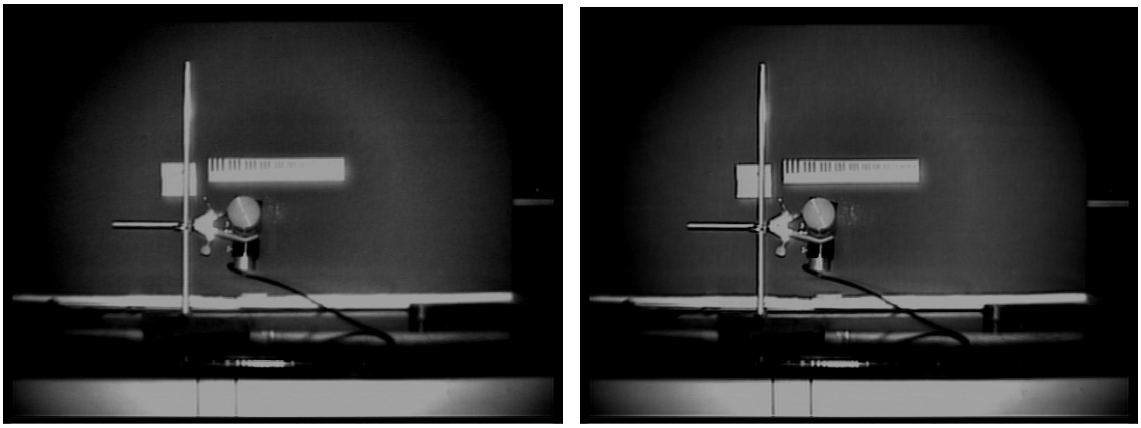

Figure 28. Scene Illumination of of 5E-7 FC (Left) and 1.5E-6 FC (Right) for 2.5m

The digital images of the scene are cropped to show just the Test Pattern for analysis of their respective contrast intensities. For this analysis, a MATLAB program was written to analyze the images obtained from the Nitemax NM-1000. Using the image processing functions in MATLAB, the image of the Test Pattern is analyzed pixel by pixel with a grayscale contrast intensity of 0-255, with black represented by 0 and white represented by 255. The plots in Figures 29 through 34 show the contrast levels of the Test Pattern scanned horizontally across one pixel row at 1.5, 2 and 2.5 m respectively. The detail of the MATLAB codes is appended in Appendix B.

As observed in the Figures below, the bar targets on the Test Pattern can be segregated and each target is represented by a near sinusoid curve with two peaks (for the two white bars that are between the three black bars). From the contrast plot of each bar target, the Contrast Transfer Function (CTF) of the individual bar target can be calculated using Equation (8) that was discussed earlier.

$$CTF = \frac{I_{max} - I_{min}}{I_{max} + I_{min}} \tag{8}$$

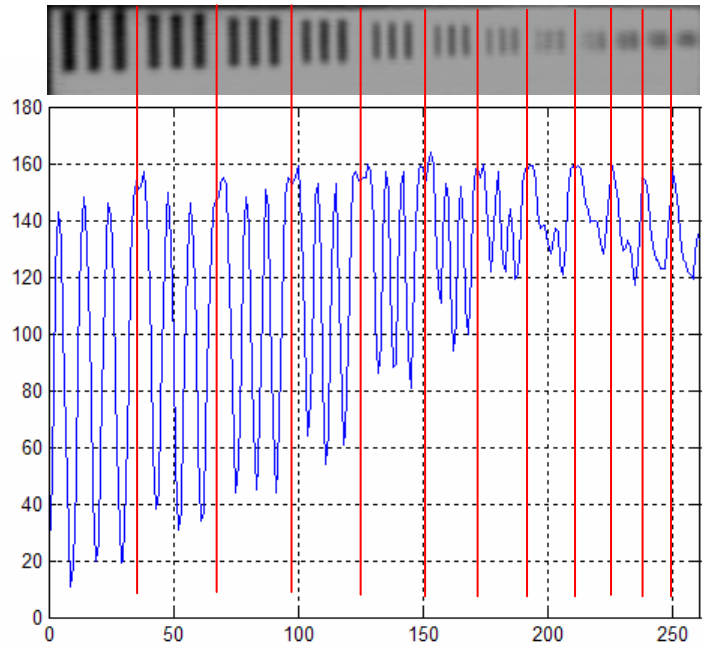

Figure 29. Contrast Intensity Plot for Scene Illumination of 5E-7 FC at 1.5 m

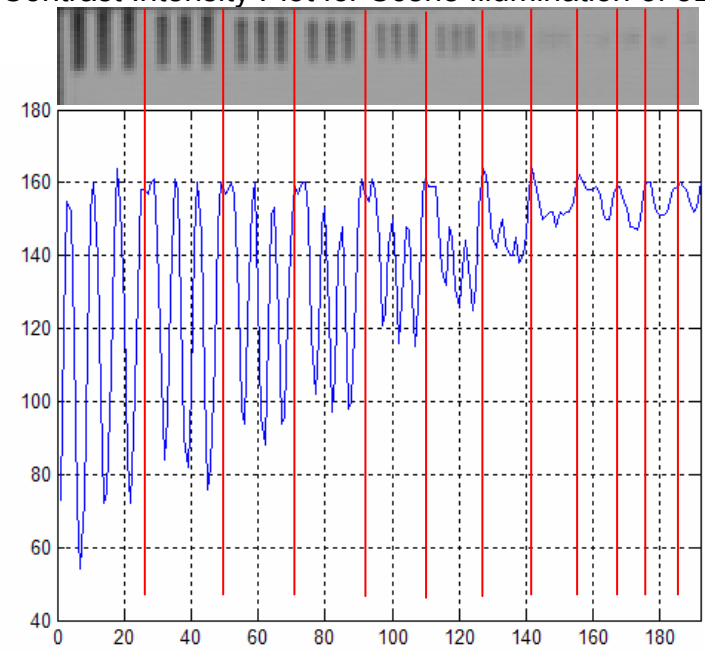

Figure 30. Contrast Intensity Plot for Scene Illumination of 5E-7 FC at 2.0 m

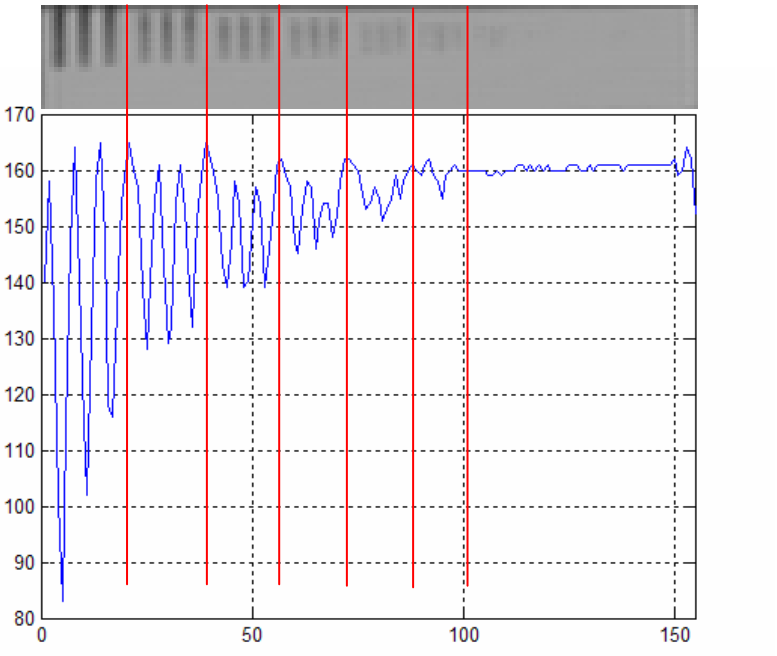

Figure 31. Contrast Intensity Plot of Scene Illumination of 5E-7 FC at 2.5 m

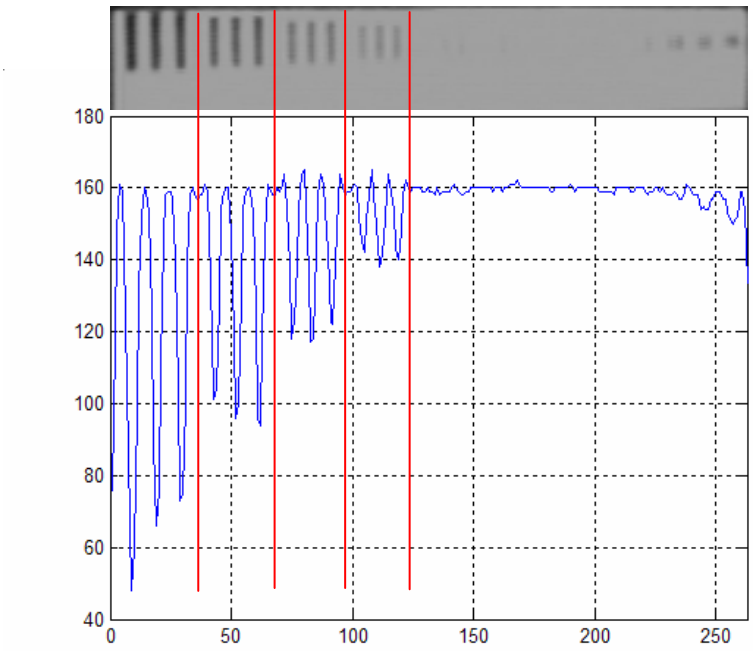

Figure 32. Contrast Intensity Plot of Scene Illumination of 1.5E-6 FC at 1.5 m

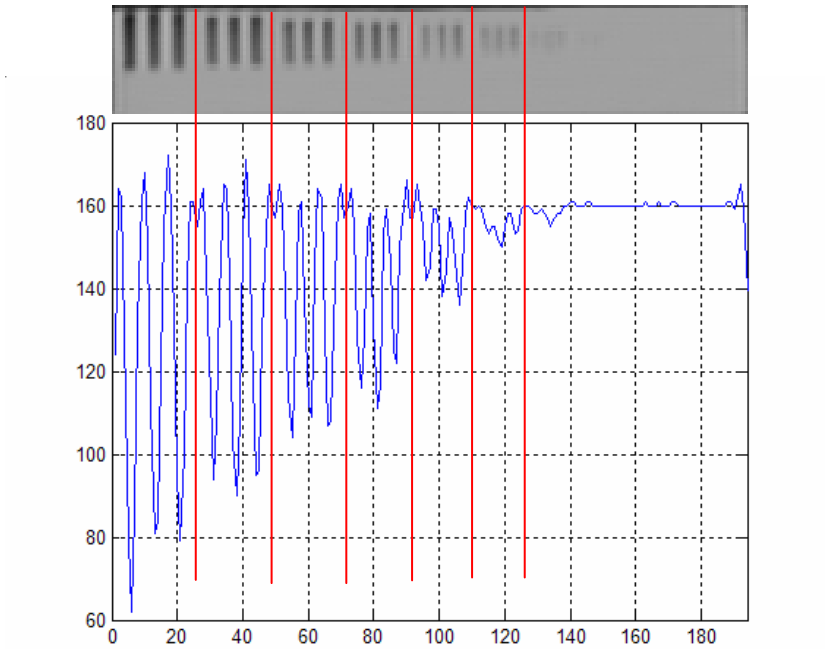

Figure 33. Contrast Intensity Plot of Scene Illumination of 1. 5E-6 FC at 2.0 m

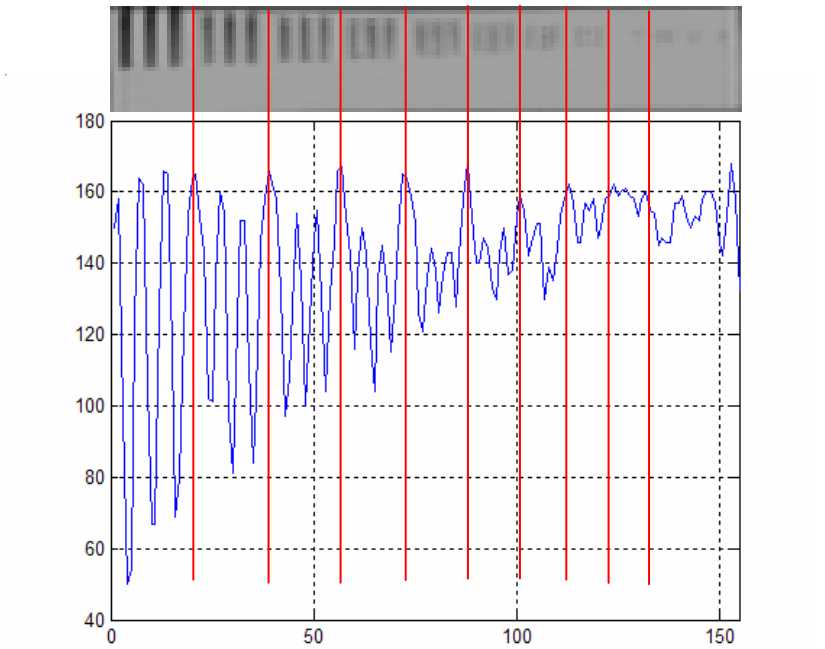

Figure 34. Contrast Intensity Plot of Scene Illumination of 1.5E-6 FC at 2.5 m

b. CTF and MTF Curve Fit

From the plots in Figures 29 through 34, the CTF can be tabulated using Equation (8). Tables 8 and 9 summarize the CTF and Spatial frequencies

for all the plots at the two scene illumination levels. From these results, the experimental CTF points can be plotted against Spatial Frequency and this is shown in Figures 36 & 37 for the both scene illuminations.

I_{max}	I_{min}	CTF	Spatial Frequency, *v* (lp/mm)	Distance (m)	Spatial Frequency, *f* (lp/mrad)
145	20	0.758	0.100	1.5	0.150
150	35	0.622	0.112	1.5	0.168
145	43	0.543	0.126	1.5	0.189
150	55	0.463	0.142	1.5	0.213
158	80	0.328	0.159	1.5	0.239
150	95	0.224	0.178	1.5	0.267
157	120	0.134	0.200	1.5	0.300
162	55	0.493	0.100	2.0	0.200
160	77	0.350	0.112	2.0	0.224
160	90	0.280	0.126	2.0	0.252
152	99	0.211	0.142	2.0	0.284
148	115	0.125	0.159	2.0	0.318
147	125	0.081	0.178	2.0	0.356
150	138	0.042	0.200	2.0	0.400
164	83	0.328	0.100	2.5	0.250
161	129	0.110	0.112	2.5	0.280
158	140	0.060	0.126	2.5	0.315
158	146	0.039	0.142	2.5	0.355
158	151	0.023	0.159	2.5	0.398

Table 8. CTF vs Spatial Frequency for Scene Illumination of 5E-7 FC

I_{max}	I_{min}	CTF	Spatial Frequency, *v* (lp/mm)	Distance (m)	Spatial Frequency, *f* (lp/mrad)
160	49	0.531	0.100	1.5	0.150
160	95	0.255	0.112	1.5	0.168
163	118	0.160	0.126	1.5	0.189
163	139	0.079	0.142	1.5	0.213
172	62	0.470	0.100	2.0	0.200
172	90	0.313	0.112	2.0	0.224
165	105	0.222	0.126	2.0	0.252
163	113	0.181	0.142	2.0	0.284
160	137	0.077	0.159	2.0	0.318
158	150	0.026	0.178	2.0	0.356
163	50	0.531	0.100	2.5	0.250
160	80	0.333	0.112	2.5	0.280
152	98	0.216	0.126	2.5	0.315
148	103	0.179	0.142	2.5	0.355
142	120	0.084	0.159	2.5	0.398
149	130	0.068	0.178	2.5	0.445

Table 9. CTF vs Spatial Frequency for Scene Illumination of 1.5E-6 FC

From the discussions in Chapter II, the CTF curve can be fitted by a Gaussian approximation. The CTF curve approximation can be represented by a more elaborate equation that is extracted from the Origin 6.1 curve fitting software. [OriginLab, 2000]

$$CTF = CTF_0 + \frac{A}{w\sqrt{\pi/2}} e^{\frac{-2(f-f_c)^2}{w^2}} \tag{17}$$

The constants CTF_0, A, w and f_c can be derived from the Origin software which performs the automatic curve fitting of the CTF data points using a Gaussian fit. A sample of the Gaussian curve fit is shown in Figure 35 (Note that for this analysis, y=CTF and x=f). The fitted CTF curves from the experiments for the two different scene illuminations are shown in Figures 36 & 37 respectively. The parameters of the Gaussian approximation for both scene illuminations of the Nitemax NM-1000 are summarized in Table 10. From the fitted CTF curves, the MTF can be tabulated from the Coltman Formulae shown below. These are also plotted in Figures 36 & 37 for both scene illuminations.

$$MTF = M(N) = \frac{\pi}{4}\left[C(N) + \frac{C(3N)}{3} - \frac{C(5N)}{5} + \frac{C(7N)}{7} - ..... \right] \tag{9}$$

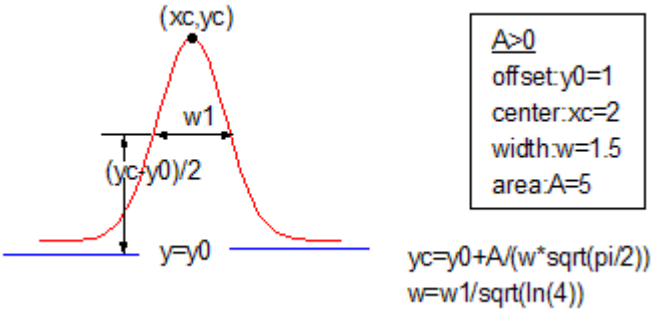

Figure 35. A Typical Gaussian Curve Fit [OriginLab, 2000]

Parameters	5E-7 FC	1.5E-6 FC
CTF_0	-0.0850	0.0792
f_c	0.0000	-0.2827
w	0.3433	0.4828
A	0.4692	1.0861

Table 10. Gaussian Approximation Parameters for Nitemax NM-1000

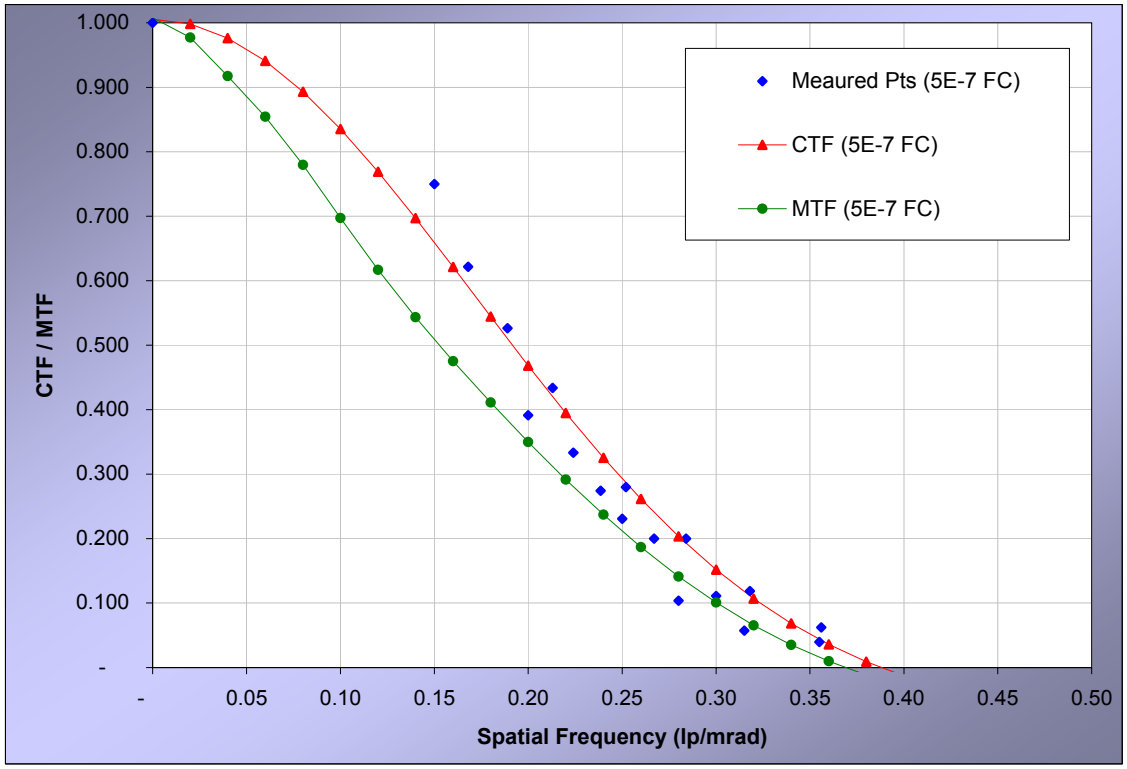

Figure 36. CTF & MTF Plots for the Nitemax at Scene Illumination 5E-7 FC

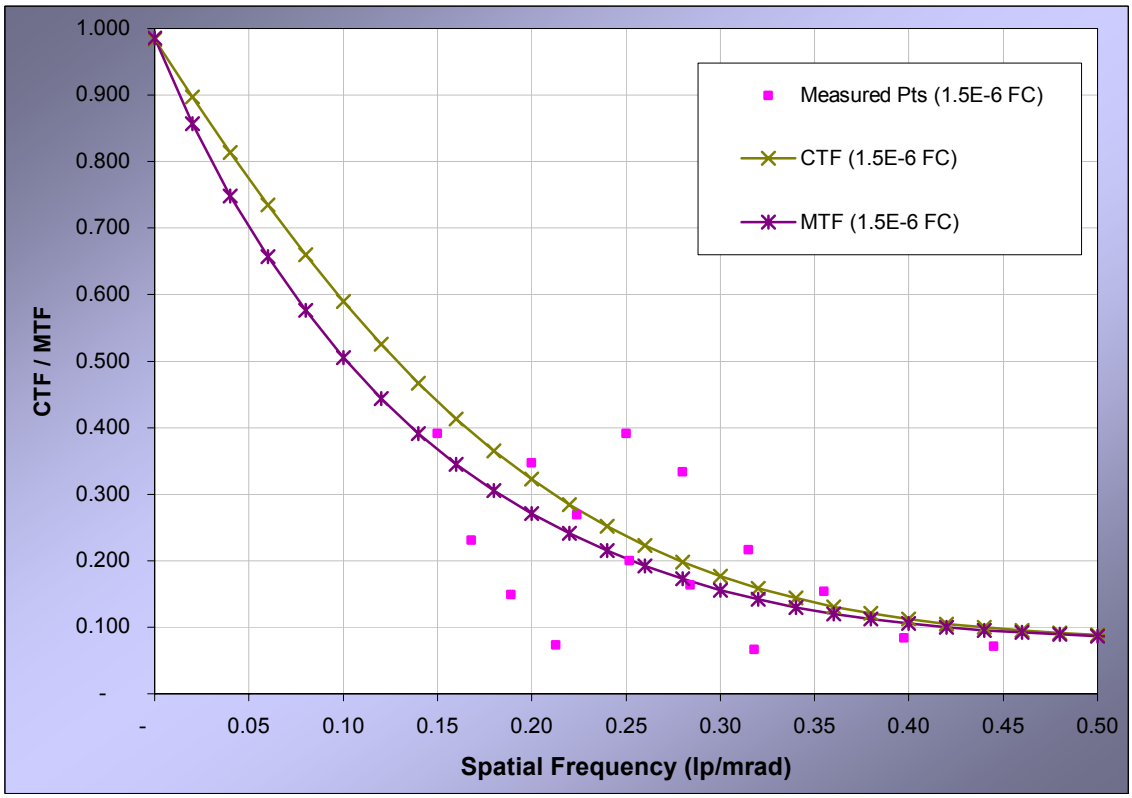

Figure 37. CTF & MTF Plots for the Nitemax at Scene Illumination 1.5E-6 FC

3. Discussion

a. Comparison with NVD

The main advantage of the NM-1000 over a conventional II system is its capability to work in both day and night conditions. It also has another advantage over II systems of being able to operate in extreme low light conditions with its built-in IR diodes. However, without the augmentation of the IR diodes, the NM-1000 will lose its night vision capability. In addition, the operational range of the NM-1000 has yet to be tested and therefore cannot be verified. In summary, the Nitemax NM-1000 can only be considered as an extended range CCD camera with no image intensification capability and thus cannot be classified as a NVD.

b. CTF and MTF

From the fitted CTF and tabulated MTF plots observed, it is noted that the CTF is better fitted for Figure 36 as compared to Figure 37. The experimental data points are relatively consistent without too much deviation from the fitted CTF. Figure 36 indicates a cut-off frequency for the CTF at about 0.39 lp/mrad while the cutoff spatial frequency for MTF is observed about 0.37 lp/mrad. Figure 36 has shown relative consistency to typical CTF/MTF curves and therefore can be used to represent the MTF of the Nitemax NM-1000 reasonably. As Figure 36 represents a better CTF curve fit for the experiment data, it is used for representation of the average CTF and MTF of the Nitemax NM-1000 for subsequent comparative analysis. The scatter of data in Figure 37 is too large for confident use of the curve fit.

c. Operations

The NM-1000 is classified as a civilian surveillance tool by its manufacturer and therefore has not been ruggerdised during manufacturing. As such, it is highly likely to be unsuitable for military operations. One other disadvantage is that the system's LCD screen projects a large amount of light to the environment and thus will not be suitable for tactical surveillance operations.

However, there is significant potential for the NM-1000 to be deployed as a surveillance camera for protection of key installations. By virtue of

its capability to feed live images, a network of such systems can be deployed around important buildings to provide 24/7 surveillance. This would eliminate the need for projection of flood lights for normal CCD cameras to work at night. In addition, the low cost NM-1000 also makes it very attractive and can potentially replace some of the NVDs used in non-critical military operations, such as base observation posts and field sentries.

THIS PAGE INTENTIONALLY LEFT BLANK

IV. EVALUATION OF ASTROSCOPE 9350 NIGHT VISION DEVICE

A. FOCUS OF TEST AND EVALUATION

In this chapter, the test and evaluation of a newly acquired NVD, the Astroscope 9350, is carried out subjectively and objectively, based on the methods discussed in Chapter II. The measured sensitivities from the subjective test are discussed and compared against those obtained from the ITT NQ-160 and NV-1000. For the objective test, the MTF of the Astroscope 9350 is compared against the Nitemax NM-1000.

B. THE ASTROSCOPE 9350

The Astroscope 9350 is marketed by Electrophysics Corp with a modular concept of operations. It can be adapted to several different types of camera systems such as C-Mount CCD cameras, digital SLR cameras and camcorders. The modularity of this system also offers convenience in changing the lens system when required. The basic components of the Astroscope 9350 are shown in Figure 38. The heart of the Astroscope 9350 is the Central Intensifier Unit (CIU) which is essentially a Gen 3 II system. The CIU (9350CIU3-A) acquired for this thesis is the top of the line Gen 3 Aviation class II system which offers the highest resolution, sensitivity and contrast as compared to the other CIUs from the 9350 series. This CIU is also designed and built to significantly reduce halo and blooming effects for stringent aviation operational requirements. The specifications of the Astroscope 9350 are summarized in Table 11.

In this test and evaluation, the Astroscope 9350 is adapted to a C-Mount Panasonic TV Camera WV-CD11. This solid state, single chip image sensor, camera is capable of producing images of up to 404x256 pixels in resolution. The complete setup of the Astroscope 9350 with the Panasonic TV Camera is shown in Figure 39.

Figure 38. Basic Components of Astroscope 9350
(Clockwise from top left, Power unit and C-mount adapter, Objective lens, C-mount device for objective lens, Central Intensifier Unit)

Description	Astroscope 9350
II System Type	Gen 3
System Resolution (lp/mm)	64
Gain	50,000
Magnification	1x
Field of View (°)	24
Objective Lens	F/1.3
Voltage (VDC)	3-15
Weight (g)	1360
Length (mm)	145
Height (mm)	85
Width (mm)	85

Table 11. Specifications of Astroscope 9350

Figure 39. Complete Assembly of Astroscope 9350 with Camera

C. SUBJECTIVE TEST AND EVALUATION

1. Method

a. Experiment Setup

For this test, the setup of the target area and the control of illumination level for the darkened room are similar to the setup for evaluation of the two existing NVDs discussed in Chapter III. The same USAF 1951 test pattern shown in Figure 18 is also used. The setup of the equipment for the test is shown in Figure 40.

In converting the photometric readings from Footlamberts (FL) to Lux, the same set of Equations from (12) to (14) are used. In this test setup, R is 15 cm and r_d is 1.65 cm. From Equation (14), the solid angle is found to be 0.0380 sr. Therefore, Equation (13) can be simplified to:

$$1\ \text{Lux} = 1\ \text{FL} \times 0.2930 \tag{18}$$

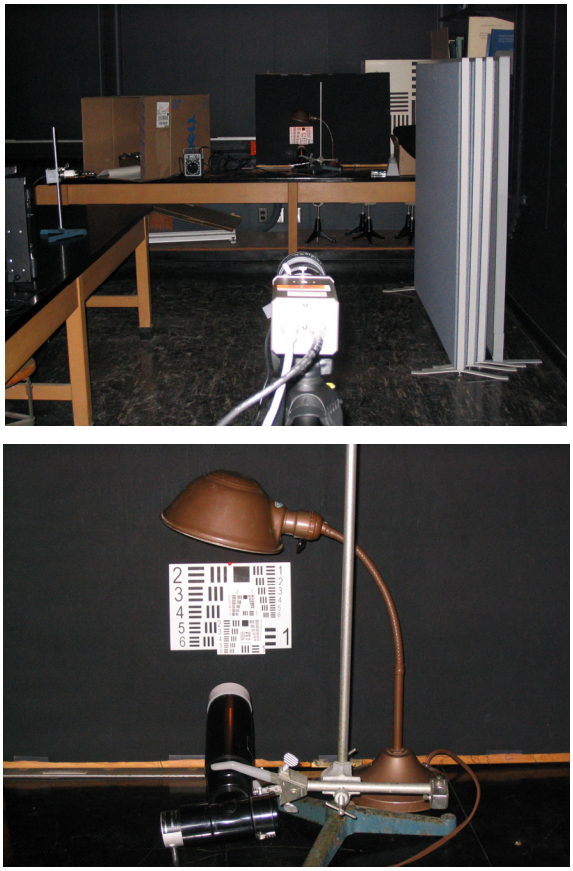

Figure 40. Experiment Setup for Subjective Testing of Astroscope 9350

b. Test Procedures

The test procedures are similar to those described in Chapter III for the two existing NVDs. The same calibration process is applied to calibrate the photometer [Gamma Scientific, 1969] and the minimum detectable scene illumination is 0.005 FL for the case of the Astroscope 9350.

The Astroscope 9350 is tested at two different stand-off starting distances of S = 3 and 5 m respectively. Observations are made at these two distances to determine the smallest bar target that can be resolved. The scope is then moved 0.1m further away from the target to obtain another set of resolvable bar targets. This process is repeated until S=3.5 and 5.5 m respectively. Using Equation (16), the spatial frequency can be converted from lp/mm to lp/mrad.

$$f = S \times v \tag{16}$$

After the conversion of spatial frequencies to lp/mrad, the bar target (taking into account stand-off distance) that produces the highest resolvable spatial frequency for a particular scene illumination will be selected as the highest resolvable bar target. The procedures described above are repeated for incremental scene illuminations adjusted by the variac driver up to the highest level achievable by the photometer, or until saturation of the Astroscope 9350 occurs.

2. Results

The results obtained are summarized in Table 12. In particular, the readings for Set 6 of the results are extended to the maximum illumination that can be measured by the photometer. From the results in Table 12, the graphs of spatial frequency versus scene illumination are plotted for all six sets of readings, as shown in Figure 41. In addition, Figure 42 shows the sensitivity of the Astroscope 9350 based on the results obtained from the extended scene illumination (i.e. Set 6).

Photometer Reading		Set 1			Set 2		
FL	Lux	*v* (lp/mm)	S (m)	*f* (lp/mrad)	*v* (lp/mm)	S (m)	*f* (lp/mrad)
0.005	6.51E-04	0.224	3.2	0.7168	0.224	3.2	0.7168
0.010	1.30E-03	0.224	3.4	0.7616	0.224	3.5	0.7840
0.015	1.95E-03	0.283	3.0	0.8490	0.252	3.4	0.8568
0.020	2.60E-03	0.283	3.2	0.9056	0.283	3.1	0.8773
0.030	3.906E-03	0.283	3.3	0.9339	0.283	3.3	0.9339
0.040	5.21E-03	0.283	3.4	0.9622	0.283	3.4	0.9622
0.060	7.81E-03	0.283	3.5	0.9905	0.283	3.5	0.9905
0.080	1.04E-02	0.318	3.2	1.0176	0.318	3.2	1.0176
0.100	1.302E-02	0.318	3.3	1.0494	0.318	3.3	1.0494
0.150	1.953E-02	0.318	3.2	1.0176	0.283	3.5	0.9905
0.200	2.604E-02	0.283	3.5	0.9905	0.318	3.3	1.0494
0.300	3.906E-02	0.283	3.5	0.9905	0.283	3.5	0.9905
Photometer Reading		Set 3			Set 4		
FL	Lux	*v* (lp/mm)	S (m)	*f* (lp/mrad)	*v* (lp/mm)	S (m)	*f* (lp/mrad)
0.005	6.510E-04	0.126	5.5	0.6930	0.126	5.5	0.6930
0.010	1.302E-03	0.142	5.5	0.7810	0.142	5.5	0.7810
0.015	1.953E-03	0.159	5.2	0.8268	0.159	5.0	0.7950
0.020	2.604E-03	0.159	5.5	0.8745	0.159	5.5	0.8745
0.030	3.906E-03	0.178	5.1	0.9078	0.178	5.0	0.8900
0.040	5.208E-03	0.178	5.2	0.9256	0.178	5.1	0.9078
0.060	7.812E-03	0.178	5.5	0.9790	0.178	5.2	0.9256
0.080	1.042E-02	0.200	5.0	1.0000	0.200	5.0	1.0000
Photometer Reading		Set 5			Set 6		
FL	Lux	*v* (lp/mm)	S (m)	*f* (lp/mrad)	*v* (lp/mm)	S (m)	*f* (lp/mrad)
0.005	6.510E-04	0.126	5.5	0.6930	0.126	5.5	0.6930
0.010	1.302E-03	0.142	5.5	0.7810	0.142	5.5	0.7810
0.015	1.953E-03	0.159	5.1	0.8109	0.159	5.2	0.8268
0.020	2.604E-03	0.159	5.2	0.8268	0.159	5.5	0.8745
0.030	3.906E-03	0.178	5.3	0.9434	0.178	5.3	0.9434
0.040	5.208E-03	0.200	5.2	1.0400	0.200	5.0	1.0000
0.060	7.812E-03	0.200	5.3	1.0600	0.200	5.3	1.0600
0.080	1.042E-02	0.200	5.4	1.0800	0.200	5.4	1.0800
0.100	1.302E-02	0.200	5.5	1.1000	0.200	5.5	1.1000
0.150	1.953E-02	0.224	5.1	1.1424	0.224	5.2	1.1648
0.200	2.604E-02	0.224	5.1	1.1424	0.200	5.5	1.1000
0.300	3.906E-02	0.200	5.5	1.1000	0.200	5.5	1.1000
0.500	6.510E-02	-	-	-	0.200	5.0	1.0000
1.000	1.302E-01	-	-	-	0.200	5.0	1.0000
1.500	1.953E-01	-	-	-	0.200	5.0	1.0000
2.000	2.604E-01	-	-	-	0.200	5.0	1.0000
5.000	6.510E-01	-	-	-	0.200	5.0	1.0000
10.00	1.302E+00	-	-	-	0.200	5.0	1.0000
15.00	1.953E+00	-	-	-	0.200	5.0	1.0000
20.00	2.604E+00	-	-	-	0.200	5.0	1.0000
50.00	6.510E+00	-	-	-	0.200	5.0	1.0000
100.00	1.302E+01	-	-	-	0.200	5.0	1.0000

Table 12. Tabulated Results for the Astroscope 9350

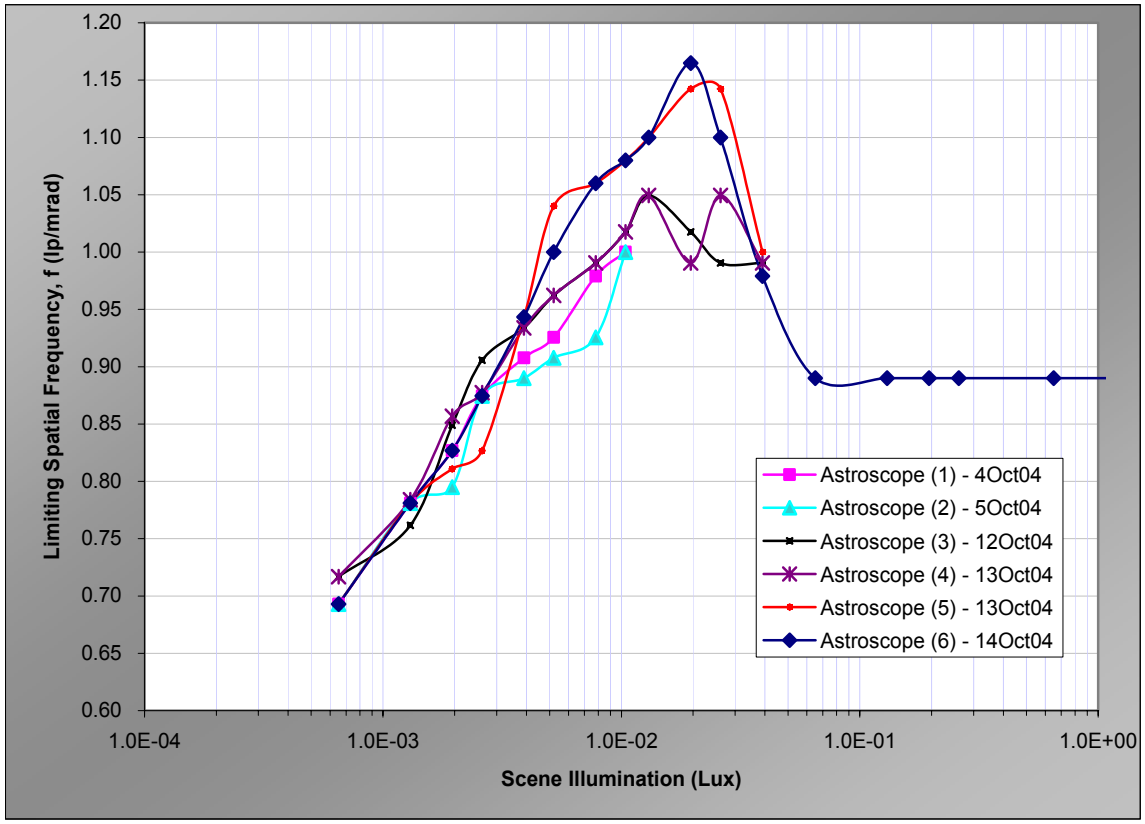

Figure 41. Sensitivity Plots of the Astroscope 9350

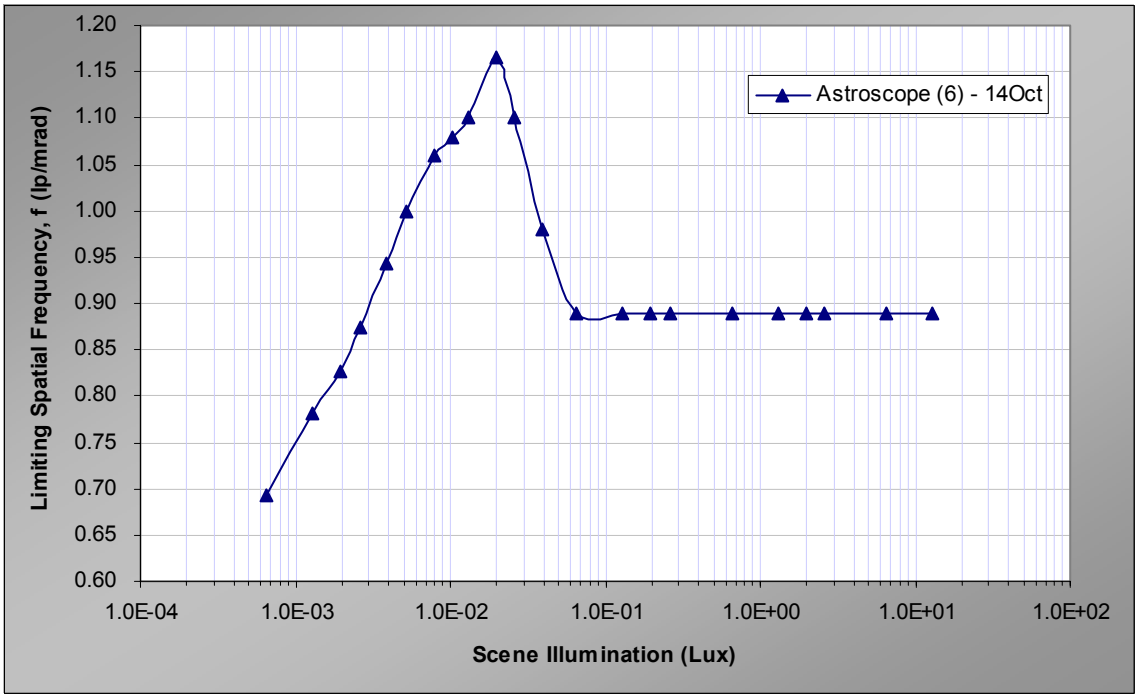

Figure 42. Sensitivity Plot for Set 6 of Test Results

3. Discussion

The plots in Figure 41 indicated consistency between the six sets of experimental results as the limiting spatial frequency points for the same scene illumination are relatively close with only minor deviations from each other. It is also observed that when the photometer reaches its limit in measurements, which is about 13 Lux (in the region of twilight), the Astroscope 9350 has yet to reach its saturation point. This shows that the Astroscope 9350 has a relatively wide dynamic range which is ideal for robust military applications. In view of the consistency in results obtained, the sensitivity plots can be used as the basis to characterize the Astroscope 9350 for further studies.

From the plot in Figure 42, it is observed that the sensitivity of the Astroscope 9350 peaks at a limiting spatial frequency of about 1.17 lp/mrad at 0.02 Lux and drops gradually to 0.89 lp/mrad from 0.062 Lux onwards. This drop in limiting spatial frequency may be caused by non-uniformity of the incandescent light source that is projected on the test pattern. The non-uniformity is suspected to result in a situation in which higher light intensities are being reflected from certain parts of the Test Pattern than others. These higher intensities may have eventually caused the saturation of certain portions of the Test Pattern (especially on the region directly below the incandescent source) when viewed by the Astroscope 9350.

Figure 43 shows the image of the scene at an illumination of 100 FL or 13 Lux. It is observed that though the majority of the scene is not saturated, there appears to be some blurring of the bar target -3,1 which showed discontinuity from bar target -4,6. An additional test was conducted, inverting the test pattern, as shown in Figure 44. In the latter figure, it is observed that bar target -4,6 appears saturated and can barely be resolved. Therefore, the comparison of the two images indicates an obvious lack of projection uniformity of the incandescent lamp on the test pattern. The comparison also showed that at a scene illumination of 100 FL, the smallest resolvable target is -4,6 as bar target -3,1

cannot be resolved for both Figures 43 and 44. This shows that the results obtained indeed reflect the characteristics of the Astroscope 9350.

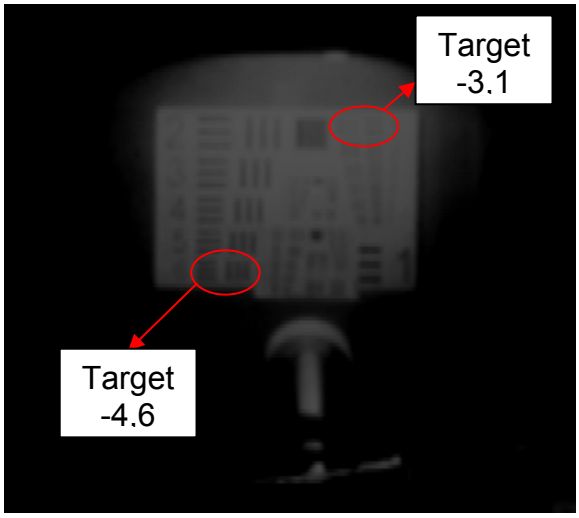

Figure 43. Image of Test Pattern at Illumination of 100 FL

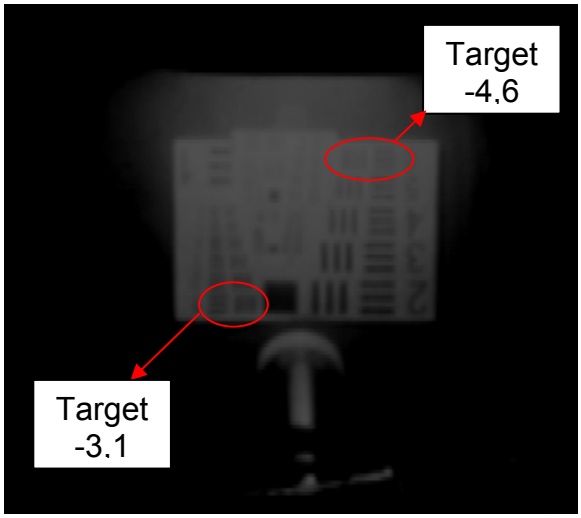

Figure 44. Image of Inverted Test Pattern at Illumination of 100 FL

One of the proposed solutions to the illumination non-uniformity problem is to replace the incandescent lamp with a collimated light source that is projected from a standoff distance. This arrangement can provide a uniform light irradiance projected on the Test Pattern, but may potentially obstruct the line-of-sight of the system on test. Another proposed solution is to project the Test Pattern digitally from a projector, which is able to produce a high quality and uniformly lit image. Illumination of the Test Pattern can also be electronically controlled via the projector to give different scene illuminations. A third solution is to redesign the target board to enable a collimated light source to be projected from the back of the Test Pattern. This solution would require a non-opaque target board to be constructed, and the development cost may become an issue.

A comparison of the sensitivities of the three tested NVDs (selected results) has been made. The sensitivity plots of these NVDs are plotted on the same graph in Figure 45. From the figure, it is observed that the Astroscope is the most sensitive amongst the three NVDs. The Astroscope can also start its operations from a significantly lower light level as compared to the other two

NVDs. When comparing the sensitivity figures of all NVDs, it is observed that the Astroscope is on average 30 % more sensitive than the ITT NQ-160 (for lower scene illuminations) and 400 % more sensitive than the Gen 2 equivalent NV-100. This further impresses the significance of the improvements made when the Gen 3 II systems are introduced. From the same sensitivity plots, it is also evident that the Astroscope 9350 has a significantly larger dynamic range as compared to the other two NVDs, thus making the Astroscope 9350 a better operational NVD than the others. However, the Astroscope 9350 is designed for aviation use, which is tailored towards higher end types of operational applications and is considerably more expensive.

Another observation made while performing the tests for the Astroscope 9350 is the significant reduction in the smearing of the scene when it is rapidly moved. This phenomenon becomes more evident when a comparison is made between the ITT NQ-160 and the Astroscope 9350. Therefore, it is noted that in a 'normal' Gen 3 II system, the smearing effect of the scene is more significant, especially if it is built for normal military operations. This comparison has shown the significant difference between two Gen 3 II systems of different grades and explains the premium required to acquire an aviation class of II system.

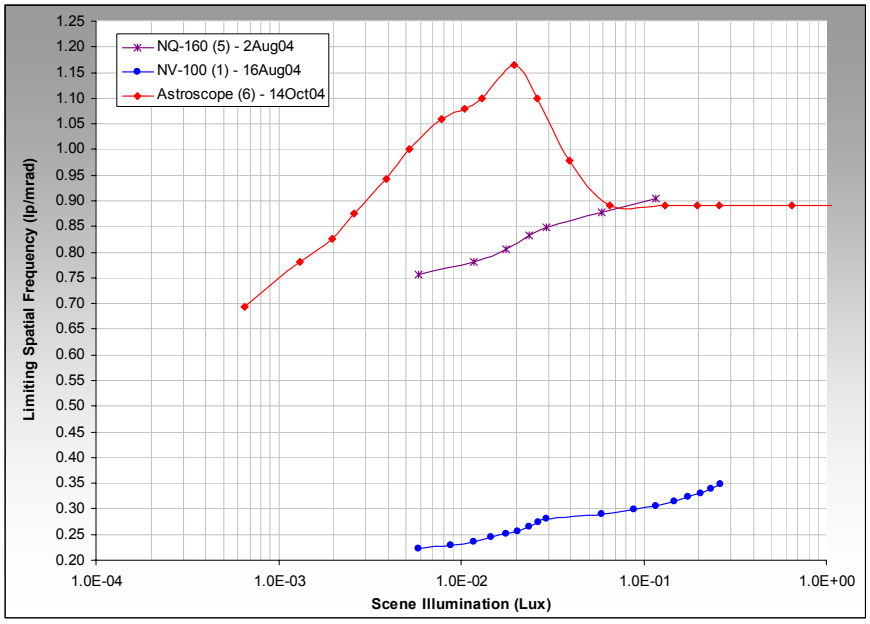

Figure 45. Sensitivity Plots of Astroscope 9350, ITT NQ-160 & NV-100

D. OBJECTIVE TEST AND EVALUATION

1. Method

a. Experiment Setup

For this test and evaluation, the setup of the equipment is similar to the subjective test with only a change in the Test Pattern. In this test, the modified USAF-1951 Test Pattern shown in Figure 46 is used. The setup of the target area for this test is shown in Figure 47. This Test Pattern is basically a modified version of the original USAF-1951 Test Pattern with the essential vertical bar targets extracted and lined up across a horizontal line. This modification is to facilitate the analysis task of scanning the image to measure the contrast intensities of the individual bar targets using the MATLAB program.

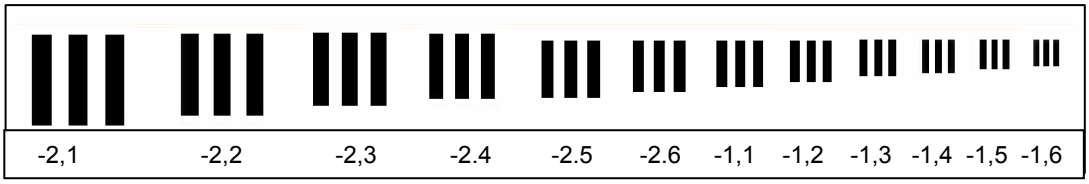

Figure 46. Modified USAF-1951 Test Pattern

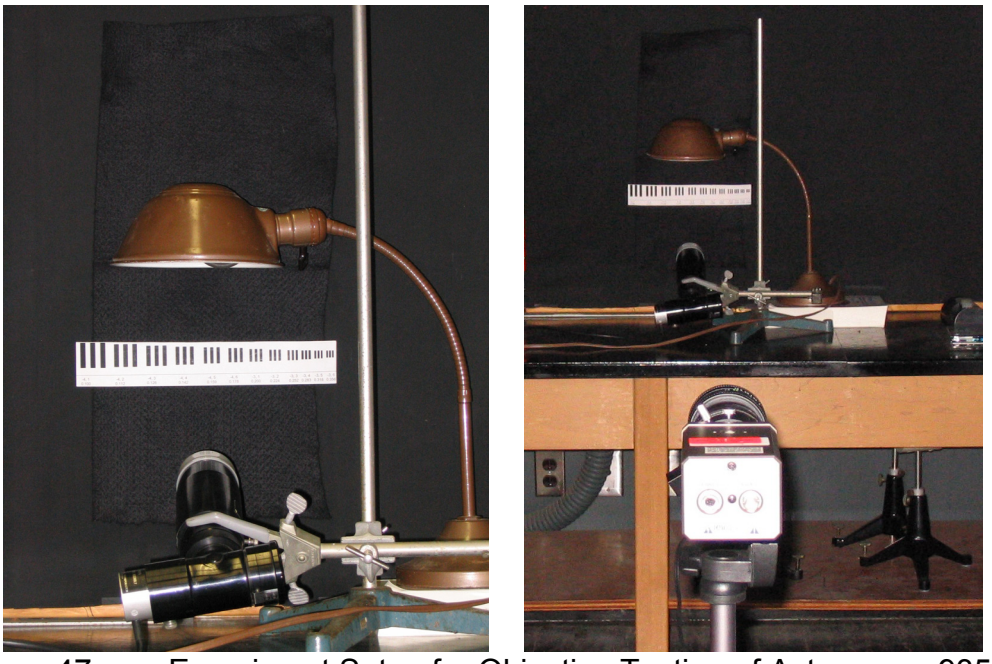

Figure 47. Experiment Setup for Objective Testing of Astroscope 9350

As this test requires the digital image of the scene to be captured for analysis, the same digital image capturing equipment and procedure used for

the Nitemax NM-1000 scene capturing (Chapter III) is used for this experiment. The images are captured and saved in 404x256 pixel format to match the resolution of the Panasonic TV Camera. A sample image of the captured scene is shown in Figure 48.

Figure 48. Sample of Captured Scene for the Astroscope 9350

b. Test Procedures

The scene illumination is first set to the lowest level at which the Astroscope 9350 can produce a resolvable image. The Astroscope 9350 is placed at a standoff distance of 3 m from the target and the first scene is captured. Subsequently, for the same scene illumination, the Astroscope 9350 is shifted and images are captured, at increments of 0.5 m away from the target area out to a distance of 5.5 m. A total of twelve scene images (two from each standoff distance) are captured for each scene illumination. From these captured scenes, one scene from each standoff distance is used for analysis. This procedure is repeated for several incremental scene illuminations until either the maximum illumination measurable by the photometer or saturation of the Astroscope 9350 is reached. Figures 49 to 54 show the scenes of target area at a sample scene illumination of 0.04 FL or 0.0052 Lux (Equivalent to a moonless clear night sky).

Figure 49. Scene at 3.0 m for 0.04 FL

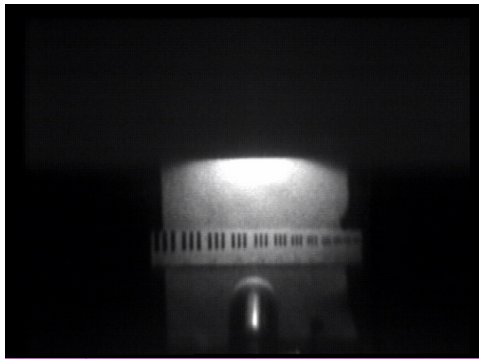

Figure 50. Scene at 3.5 m for 0.04 FL

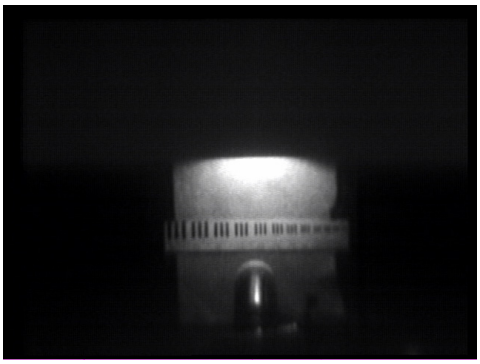

Figure 51. Scene at 4.0 m for 0.04 FL

Figure 52. Scene at 4.5 m for 0.04 FL

Figure 53. Scene at 5.0 m for 0.04 FL

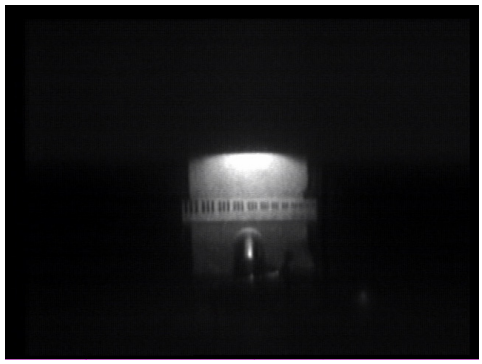

Figure 54. Scene at 5.5 m for 0.04 FL

2. Results

a. Experimental Results Tabulation

For the analysis of results, the same MATLAB program (used for analysis for the Nitemax NM-1000 in Chapter III) is used to measure the contrast intensity variations of the Test Pattern. The cropped images of the scene that show only the Test Patterns are analyzed and the contrast variations across one

horizontal line of pixels are presented in one contrast intensity plot for each image. Figures 55 through 60 show the results of the analysis using MATLAB.

From the contrast intensity plot of each bar target, the Contrast Transfer Function (CTF) of the individual bar targets can be calculated using Equation (8) that was discussed in Chapter II.

$$CTF = \frac{I_{max} - I_{min}}{I_{max} + I_{min}} \tag{8}$$

Table 13 summarizes the tabulation of the CTF with their respective spatial frequencies. In order to verify the results obtained from the MATLAB analysis, the 'traditional' tests using an oscilloscope for intensity measurement are also performed. From the data collection method described in Chapter II, the intensities are measured from the oscilloscope readout. The CTF can then be tabulated using Equation (8). Table 14 summarizes a sample set of results obtained from this 'traditional' test for a scene illumination of 0.04 FL.

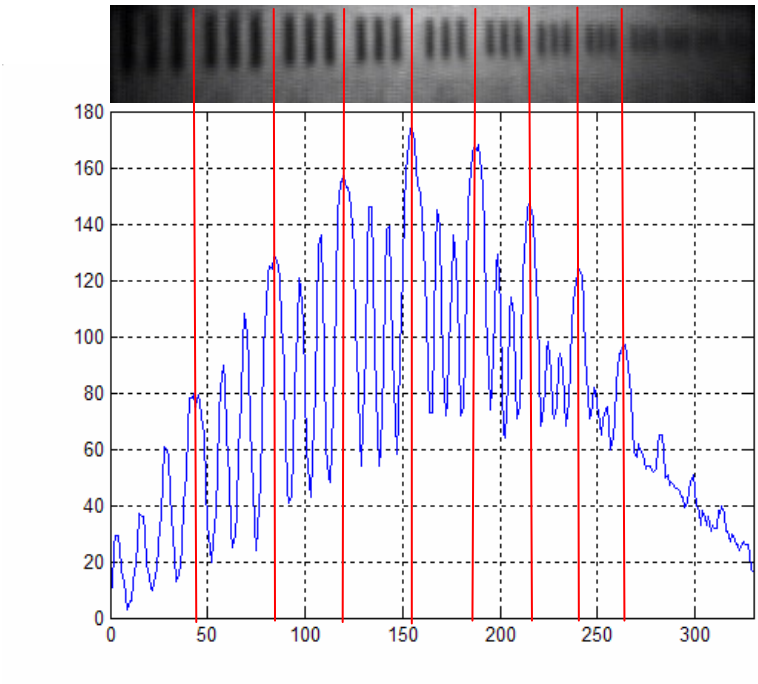

Figure 55. Contrast Intensity Plot for Scene Illumination of 0.04 FL at 3.0 m

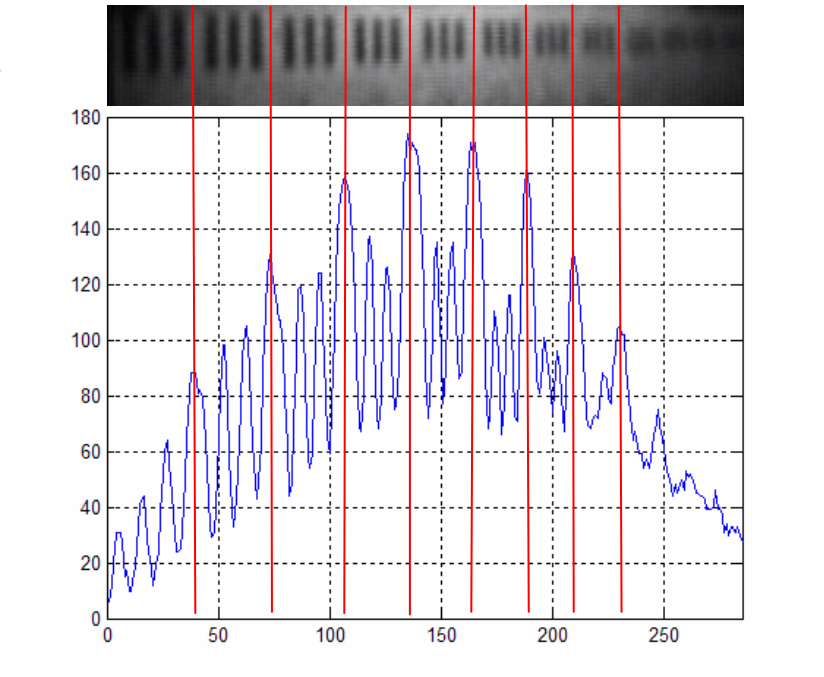

Figure 56. Contrast Intensity Plot for Scene Illumination of 0.04 FL at 3.5 m

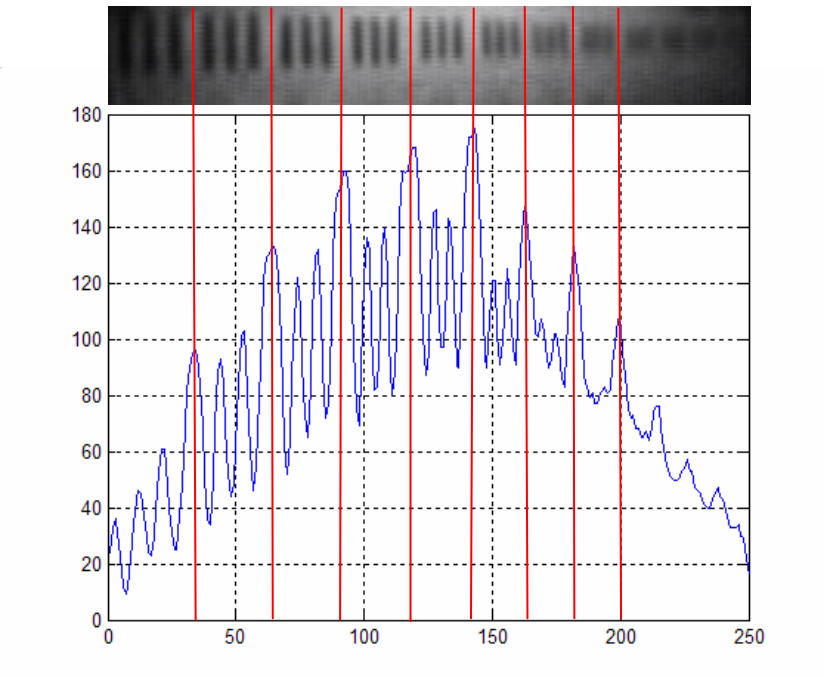

Figure 57. Contrast Intensity Plot for Scene Illumination of 0.04 FL at 4.0 m

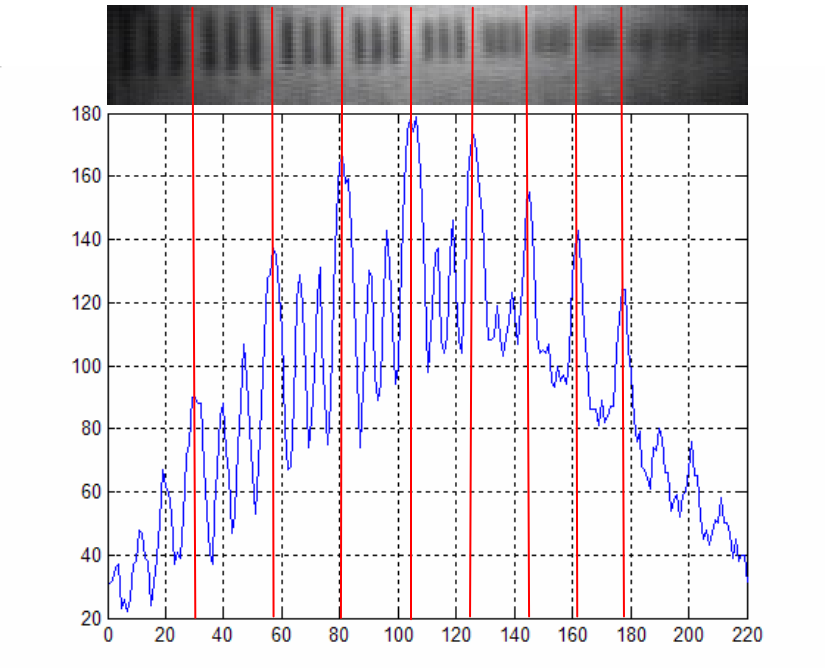

Figure 58. Contrast Intensity Plot for Scene Illumination of 0.04 FL at 4.5 m

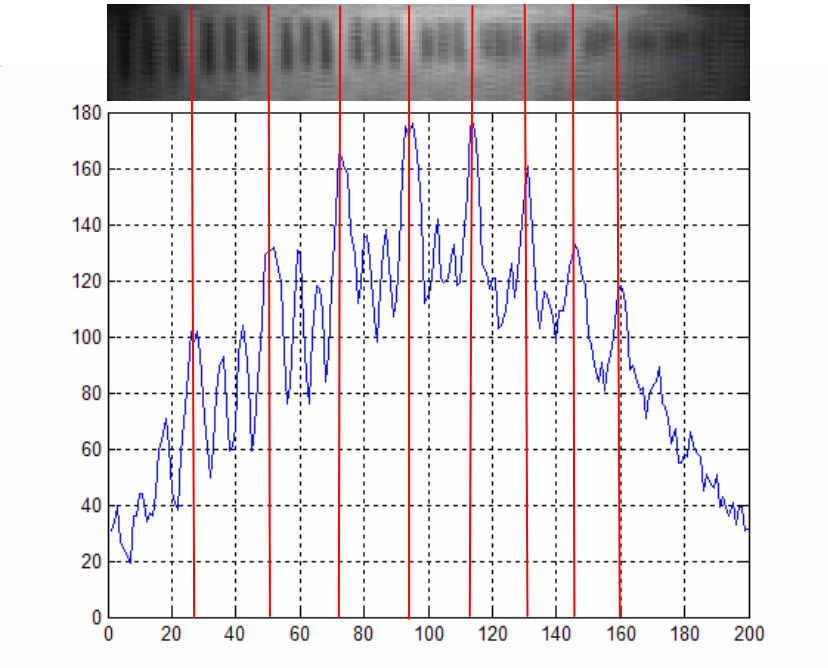

Figure 59. Contrast Intensity Plot for Scene Illumination of 0.04 FL at 5.0 m

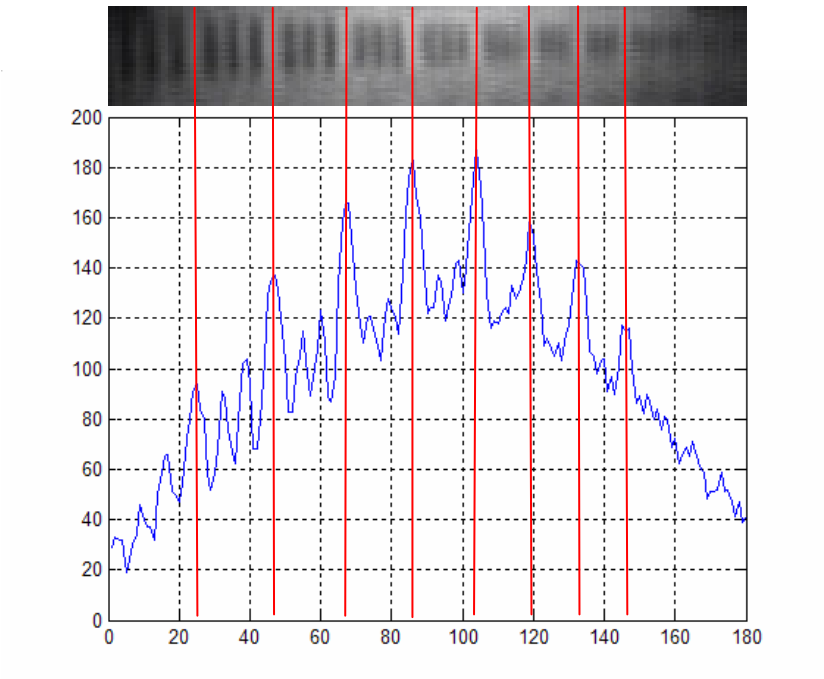

Figure 60. Contrast Intensity Plot for Scene Illumination of 0.04 FL at 5.5 m

I_{max}	I_{min}	CTF	Spatial Frequency, *v* (lp/mm)	Distance (m)	Spatial Frequency, *f* (lp/mrad)
60	14	0.622	0.100	3.0	0.300
100	25	0.600	0.112	3.0	0.336
130	40	0.529	0.126	3.0	0.378
145	55	0.450	0.142	3.0	0.426
144	70	0.346	0.159	3.0	0.477
130	70	0.300	0.178	3.0	0.534
95	72	0.138	0.200	3.0	0.600
82	60	0.155	0.224	3.0	0.672
105	34	0.511	0.112	3.5	0.392
120	50	0.412	0.126	3.5	0.441
138	70	0.327	0.142	3.5	0.497
135	80	0.256	0.159	3.5	0.557
110	70	0.222	0.178	3.5	0.623
100	75	0.143	0.200	3.5	0.700
102	42	0.417	0.112	4.0	0.448
134	60	0.381	0.126	4.0	0.504
138	80	0.266	0.142	4.0	0.568
145	95	0.208	0.159	4.0	0.636
122	90	0.151	0.178	4.0	0.712
108	85	0.119	0.200	4.0	0.800
60	24	0.429	0.100	4.5	0.450
100	45	0.379	0.112	4.5	0.504
128	72	0.280	0.126	4.5	0.567
138	84	0.243	0.142	4.5	0.639
143	105	0.153	0.159	4.5	0.716
120	105	0.067	0.178	4.5	0.801
60	20	0.500	0.100	5.0	0.500
104	60	0.268	0.112	5.0	0.560
130	80	0.238	0.126	5.0	0.630
138	102	0.150	0.142	5.0	0.710
140	120	0.077	0.159	5.0	0.795
60	20	0.500	0.100	5.5	0.550
103	52	0.329	0.112	5.5	0.616
120	83	0.182	0.126	5.5	0.693
126	106	0.086	0.142	5.5	0.781
142	120	0.084	0.159	5.5	0.875

Table 13. CTF vs Spatial Frequency for Scene Illumination of 0.04 FL or 0.0052 Lux

I_{max}	I_{min}	CTF	Spatial Frequency, *v* (lp/mm)	Distance (m)	Spatial Frequency, *f* (lp/mrad)
250	65	0.587	0.100	3.0	0.300
326	94	0.552	0.112	3.0	0.336
310	86	0.566	0.126	3.0	0.378
321	104	0.511	0.142	3.0	0.426
321	124	0.443	0.159	3.0	0.477
268	128	0.354	0.178	3.0	0.534
222	120	0.298	0.200	3.0	0.600
166	52	0.523	0.100	3.5	0.350
275	74	0.576	0.112	3.5	0.392
327	123	0.453	0.126	3.5	0.441
338	134	0.432	0.142	3.5	0.497
325	169	0.316	0.159	3.5	0.557
280	144	0.321	0.178	3.5	0.623
175	54	0.528	0.100	4.0	0.400
234	74	0.519	0.112	4.0	0.448
297	142	0.353	0.126	4.0	0.504
302	154	0.325	0.142	4.0	0.568
283	175	0.236	0.159	4.0	0.636

Table 14. CTF vs Spatial Frequency for 'Traditional' Test for Scene Illumination of 0.04 FL

The contrast intensity plots and CTF tabulations for ten different other scene illuminations are appended in Appendix A. Figure 61 presents a scatter plot of data points of the CTF versus Spatial Frequencies for all eleven scene illuminations.

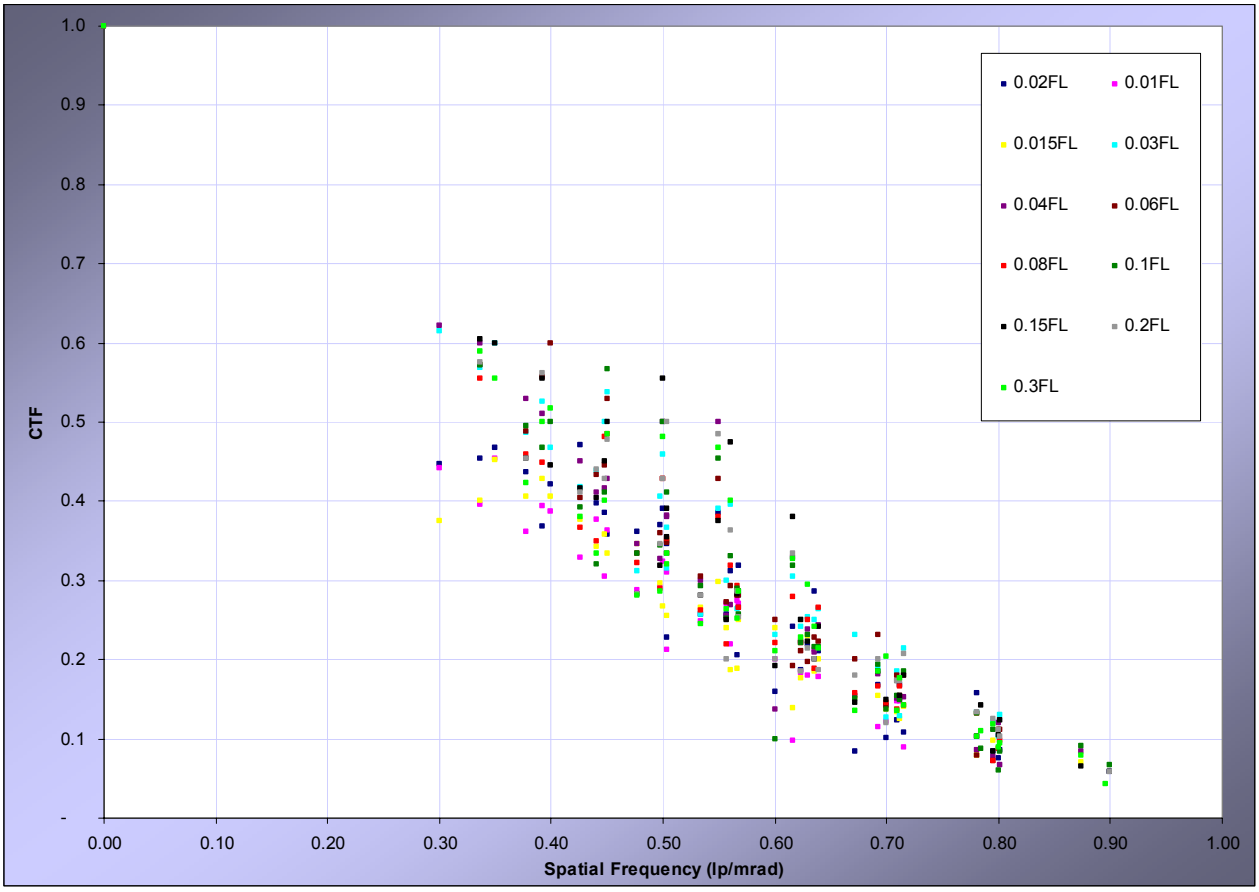

Figure 61. Plots of Experiment Data Points for CTF vs Spatial Frequency for Eleven Different Scene Illuminations

b. CTF and MTF Curve Fit

The CTF of the eleven scene illuminations are fitted using the Origin 6.1 curve fitting software with a Gaussian approximation. The parameters of the fitted CTF that correspond to Equation (17) of the Gaussian curve are summarized in Table 15 for all eleven sets of results.

$$CTF = CTF_0 + \frac{A}{w\sqrt{\pi/2}} e^{\frac{-2(f-f_c)^2}{w^2}} \qquad (17)$$

Scene Illumination (FL)	Parameters			
	CTF_0	f_c	w	A
0.010	-0.0655	-1.9787	1.9948	18.807
0.015	-0.0759	-2.1951	2.1362	23.335
0.020	-0.1612	-2.1142	2.3298	17.285
0.030	-0.0787	-0.3412	1.1747	1.8764
0.040	-0.0841	-0.2373	1.0560	1.5889
0.060	-0.0258	-0.1219	0.8874	1.1758
0.080	-0.1871	-0.8644	1.6717	4.2327
0.100	-0.2070	-0.8354	1.6877	4.2024
0.150	-0.1905	-0.6302	1.5314	3.2313
0.200	-0.1854	-0.7451	1.6053	3.7017
0.300	-0.1721	-0.8967	1.6965	4.3434

Table 15. Gaussian Approximation Parameters

The fitted CTFs for the eleven sets of results are shown in Figure 62. Figure 63 shows the tabulated MTF of these fitted CTF using Equation (9).

$$MTF = M(N) = \frac{\pi}{4}\left[C(N) + \frac{C(3N)}{3} - \frac{C(5N)}{5} + \frac{C(7N)}{7} - .....\right] \qquad (9)$$

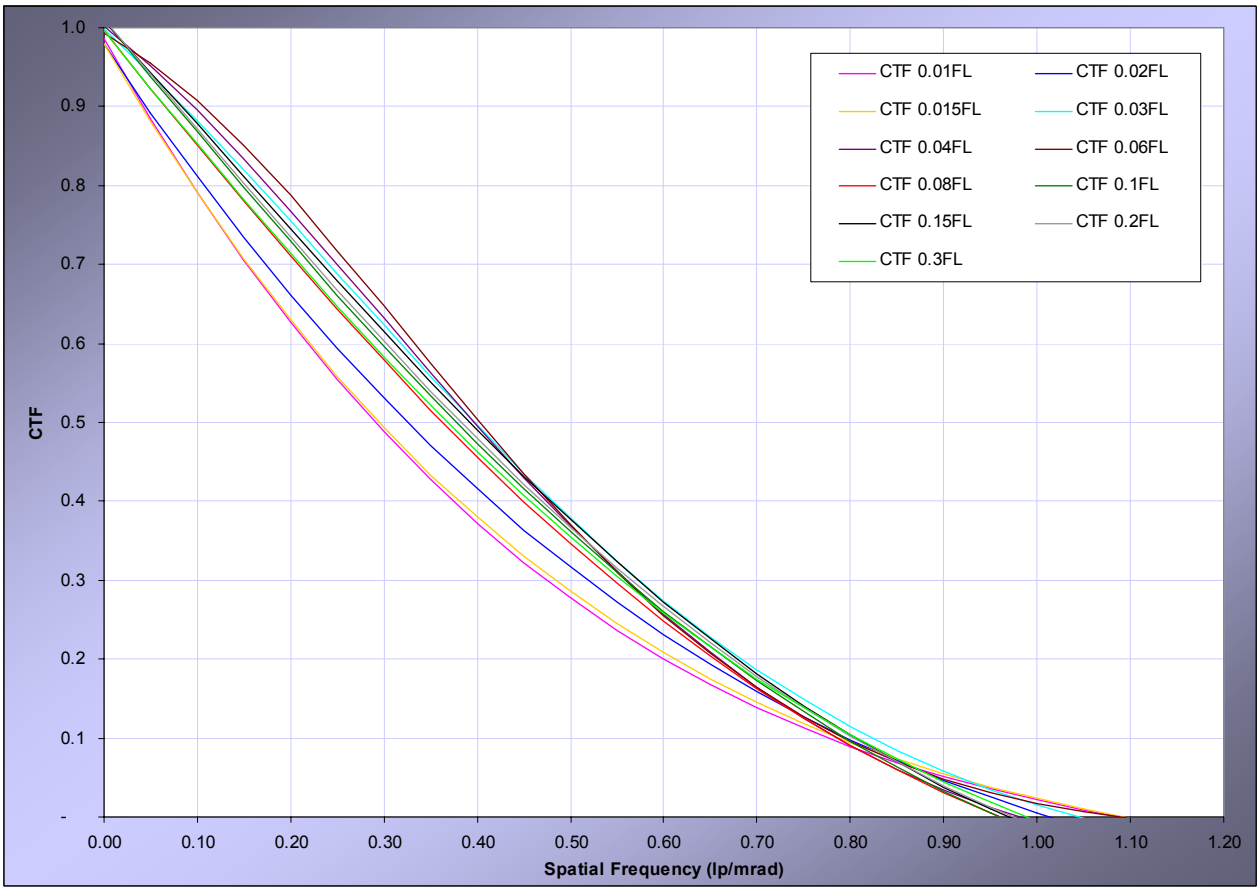

Figure 62. Fitted Plots of CTF vs Spatial Frequency for Eleven Different Scene Illuminations

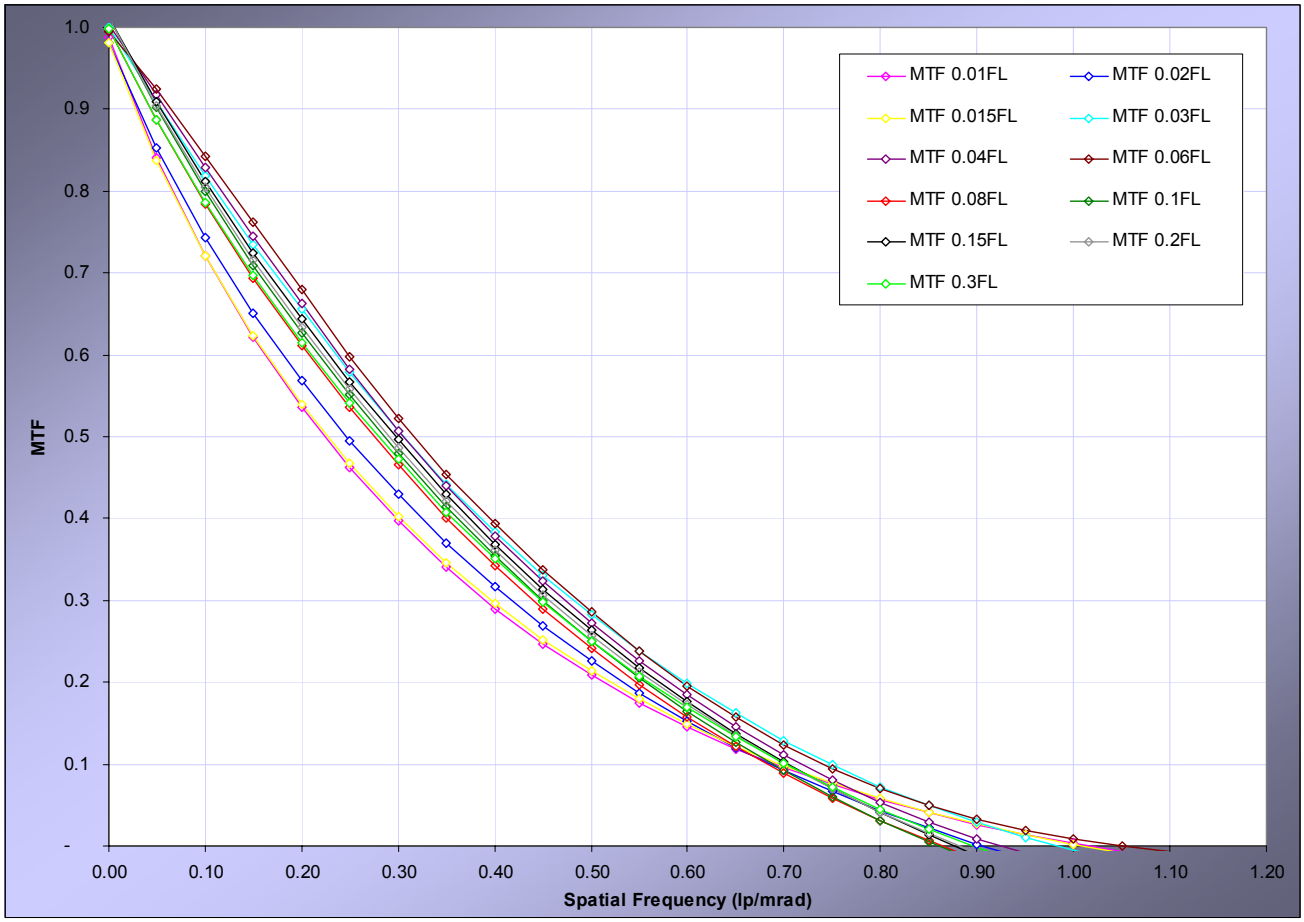

Figure 63. Plots of Tabulated MTF vs Spatial Frequency for Eleven Different Scene Illuminations

Figure 64 shows the combination of all eleven sets of CTF and MTF plotted on the same graph.

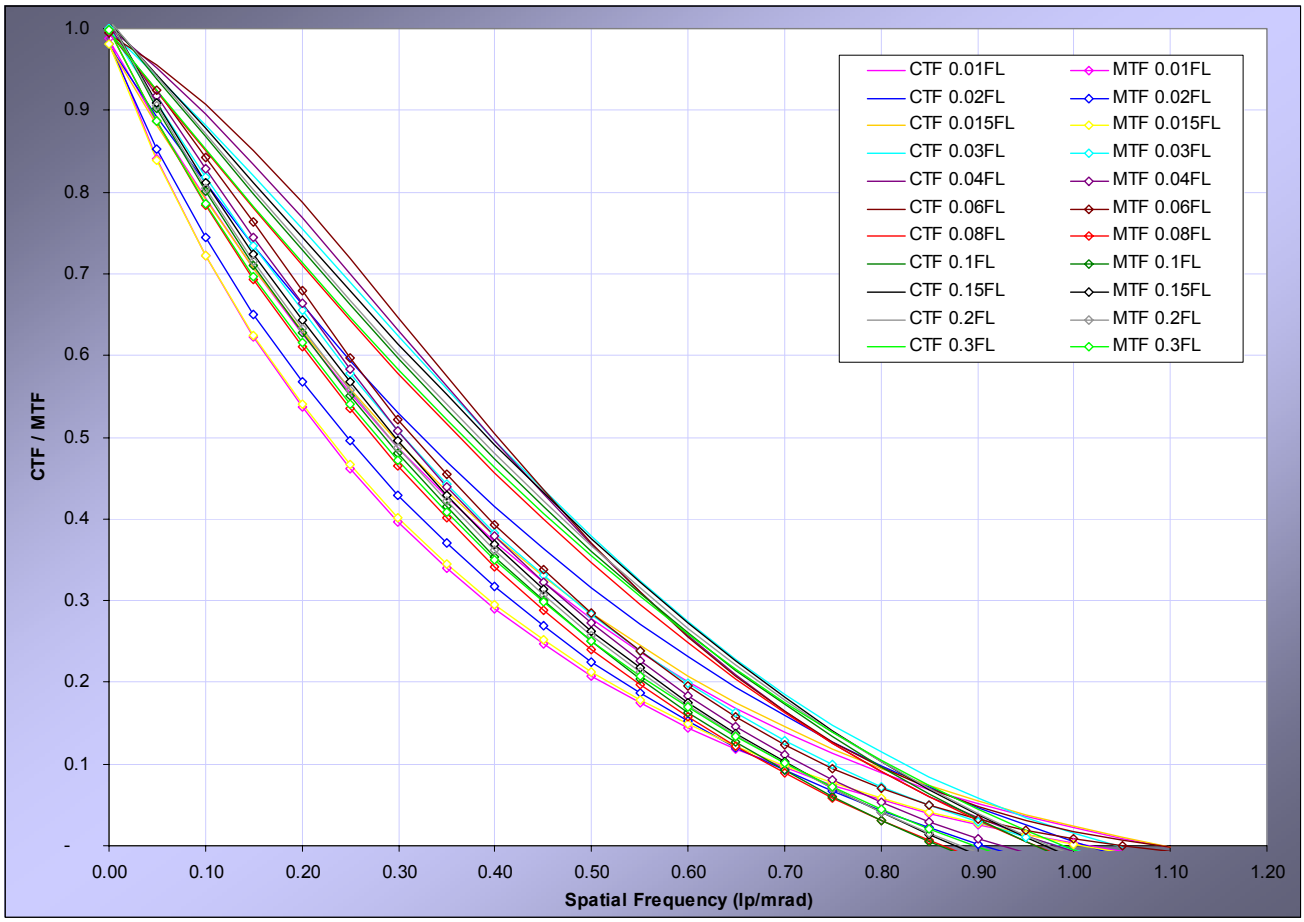

Figure 64. Combined Plots of Fitted CTF and Tabulated MTF vs Spatial Frequency for Eleven Different Scene Illuminations

3. Discussion

a. Intensity Plots

From Figures 55 to 60, it is observed that there is a consistent variation in the overall intensity across all the images of the Test Pattern. The bar targets nearer to the edges are observed to return lower overall intensity levels as compared to those in the middle of the Test Pattern. This is mainly due to the non-uniformity in the projection of the incandescent lamp on the target board. This issue had also been discussed in Chapter III and the possible solutions were proposed.

A unique solution in addressing this issue for the MATLAB test is by normalization. Figure 65 shows that raw intensity plot for the image at 3.0 m for a scene illumination 0.04 FL. The intensity plot is a result of the line scan for Row 16 as shown in Figure 67. Figure 66 shows the intensity plot of Row 38 to capture the contrast intensity variation of the scene without any bar targets (Figure 67). By dividing the two contrast plots, a normalized contrast intensity plot of the image is produced (Figure 68). Therefore, the variation of contrast in the scene is being cancelled. Of course, the most effective way of addressing this issue is still to work on the uniform projection of light on the Test Pattern itself.

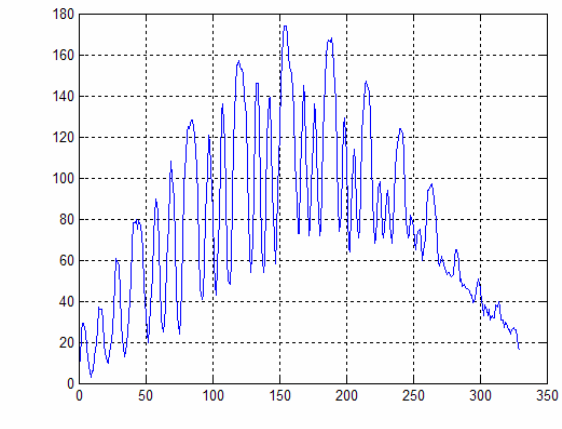

Figure 65. Contrast Intensity Plot of Test Pattern

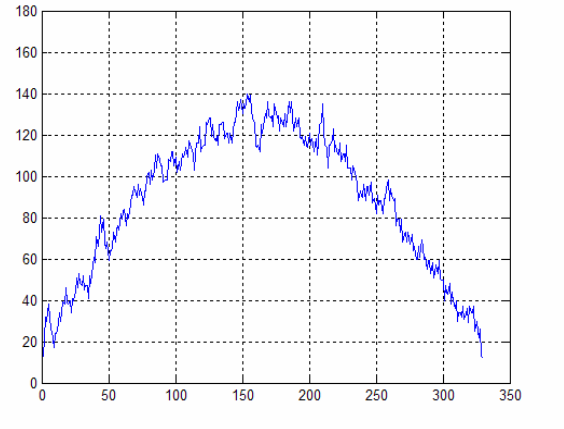

Figure 66. Contrast Intensity Plot of Scene without Bar Target

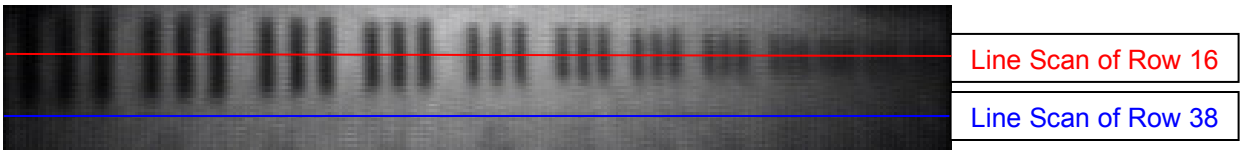

Figure 67. Illustration of Line Scans for Contrast Intensity Plots of Image

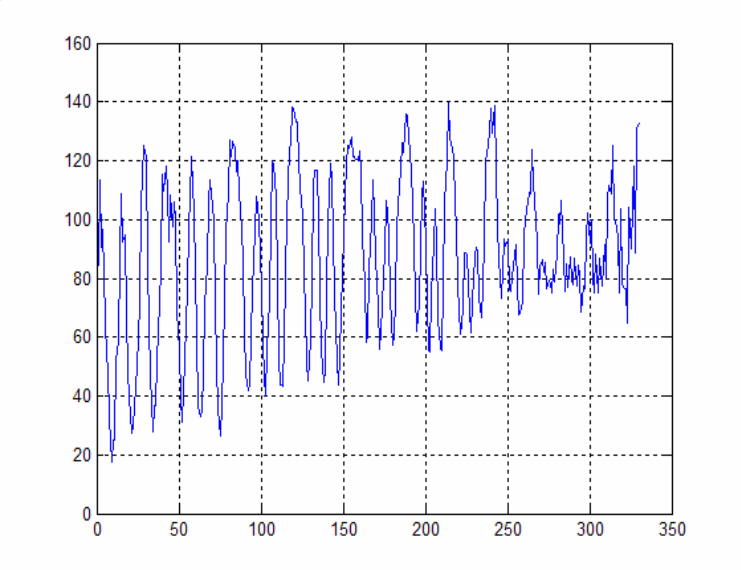

Figure 68. Normalized Contrast Intensity Plot for Test Pattern at Scene Illumination of 0.04 FL

b. CTF and MTF

From Figure 62, the CTF plots for all the different scene illuminations demonstrated only slight deviations from each other. The cut-off spatial frequencies that are read off from the plots range from 0.95 to 1.08 lp/mrad. This gives an average cut-off frequency of about 1.02 lp/mrad for the Astroscope 9350.

Figure 63 represents the tabulated MTF which also shows the slight deviations between all eleven scene illuminations. The cut-off frequencies measured range from 0.88 to 1.05 lp/mrad. The average cut-off spatial frequency is calculated to be about 0.97 lp/mrad. The average cut-off spatial frequencies obtained from the tests can be used to characterize the performance of the Astroscope 9350.

Figure 69 presents the plot for scene illumination 0.04 FL or 0.0052 Lux, showing experimental data (for both 'traditional' and MATLAB method of analysis), fitted CTF and tabulated MTF curves. It is observed that the experimental data obtained from the proposed MATLAB method are well distributed to the fitted CTF. Only about two points are slightly out of the curve fit

from observations. When the data for the 'traditional' and MATLAB methods are compared, it is observed that both cases produced relatively similar results. This demonstrated consistency in the results obtained from both experiments. It also validates the approach of using MATLAB to perform analysis in place of the 'traditional' oscilloscope approach. By adopting this approach, the analysis time to tabulate experiment data for CTF computations is also noted to be significantly shortened.

As the plots in Figure 69 are observed to reasonably represent the averages of the CTF and MTF for all eleven scene illuminations, it is chosen as the representation of the Astroscope 9350 for comparison with the Nitemax NM-1000.

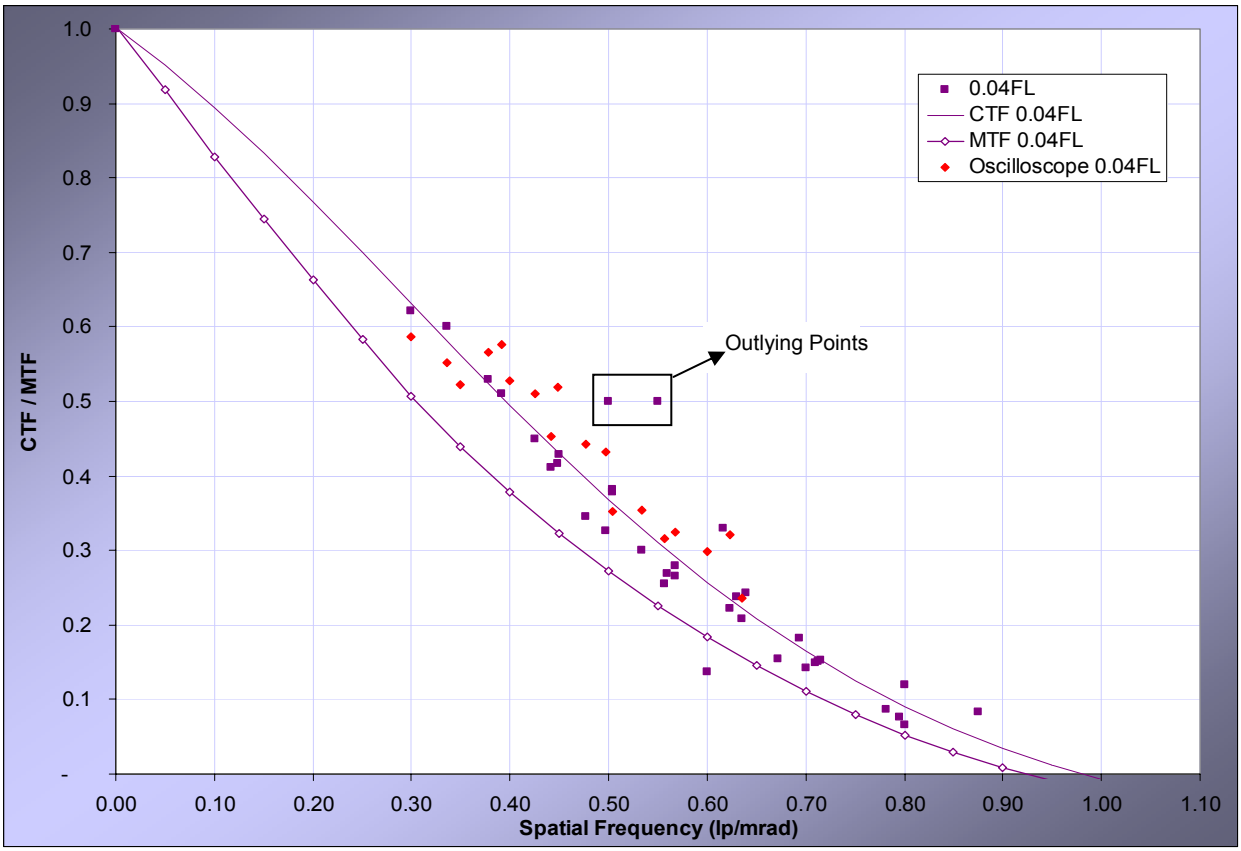

Figure 69. Plots of CTF/MTF vs Spatial Frequency for Scene Illumination of 0.04 FL

c. Comparison of MTF for Astroscope 9350 with Nitemax NM-1000

The CTF and MTF of the two systems are presented in Figure 70. From this figure, it is observed that the Astroscope 9350 performs at least a factor of two better than the Nitemax NM-1000 in terms of reproducing the contrast of the original scene. This is obvious in comparing first the cut-off spatial frequencies for both systems and the MTF for each individual spatial frequency. Using 0.2 lp/mrad as an example, the Astroscope 9350 could achieve a modulation level of 66 % while the NM-1000 could only achieve 35 %. This indicates a better performance of the Astroscope 9350 by about 88 %. This difference in performance between the two systems is expected as the Astroscope 9350 is a 'top of the line' II system while the NM-1000 is only an extended range night vision camera. Therefore, it is noted that II systems are still the main stream equipment used for robust night vision operations.

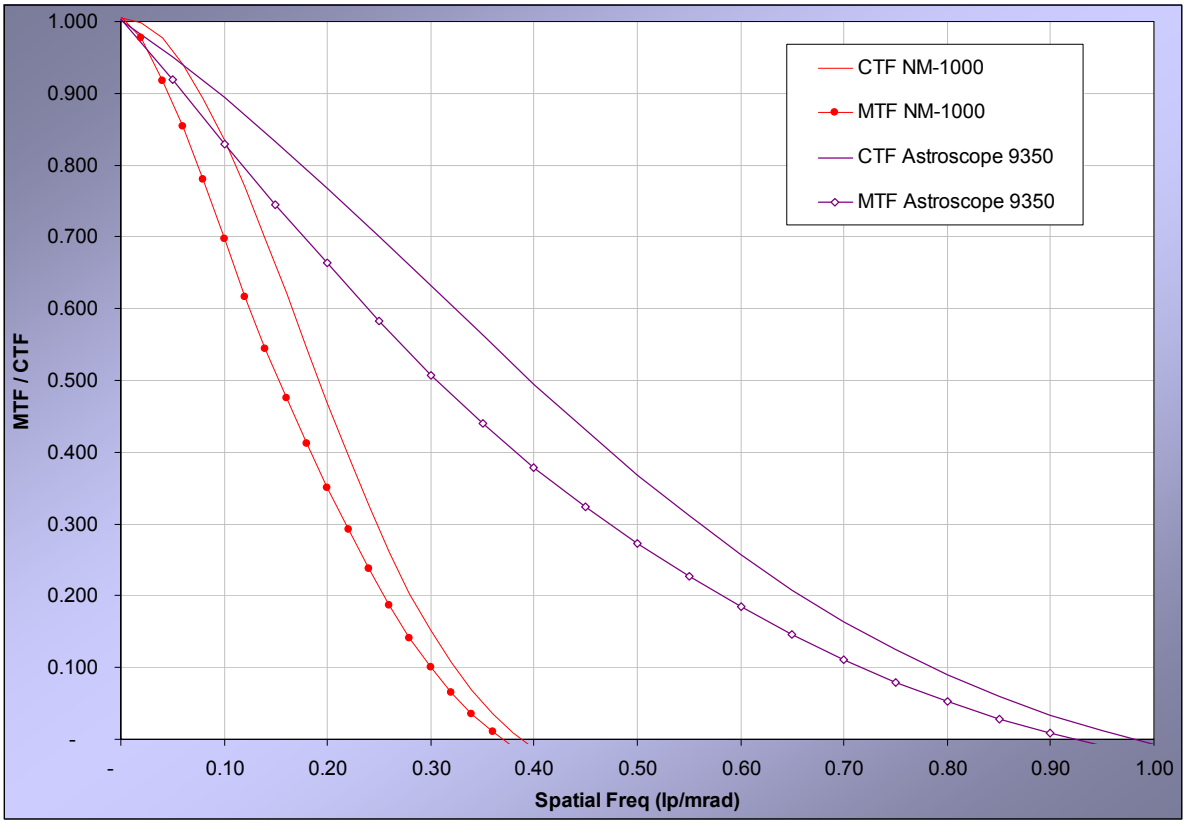

Figure 70. Plots of CTF/MTF vs Spatial Frequency for Nitemax NM-1000 and Astroscope 9350

d. Common Test Methods

It is successfully shown from the test and evaluation that this proposed method of characterization of a NVD can achieve a relatively good level of confidence. In view of this, the test method can also be applied to a Thermal Imaging system that has the capability of producing images of equal quality. This will enable the testing of both II and TI systems of similar resolution specifications under the same operational conditions looking at the 'same target'. The term 'same target' here does not explicitly mean using a common target board, but it essentially involves the integration of two different types of target boards (for II and TI systems) of the same scene into a single board for performing tests using both systems. The digitized images of the same scene can then be analyzed using the MATLAB program to obtain the respective systems CTF and MTF. As such, an accurate comparison of these two systems can be done concurrently to ensure consistency in operating conditions.

e. Image Fusion Potential

The capability of the Astroscope 9350 to produce good resolution images for digital readout makes it an outstanding system for objective performance analysis of these systems. From the good characterization results produced, it is concluded that the digitized output images produced by the Astroscope 9350 have met the image fusion criteria in terms of image quality. Thus, these images can be used for future image fusion studies. More scenes, such as outdoor scenarios consisting of different backgrounds, can be captured by the Astroscope 9350 to enable image fusion of II and TI images.

f. Operations

The high sensitivity and resolution of the Astroscope 9350 make it a powerful tool for effective night vision operations. It is shown in both subjective and objective tests that this system stands out above the rest of the 'lower grade' systems. Its robust design in the reduction of smearing effects on the scene also

makes it highly suitable for aviation use. However, the cost of acquiring this system is a premium to pay as it is easily 5-10 times more expensive than the other systems tested. It would be beneficial if a 'lower grade' Astroscope 9350 is obtained to perform like-to-like comparative tests to measure its sensitivity against the other systems.

V. CONCLUSIONS AND RECOMMENDATIONS FOR FUTURE WORK

A. SUMMARY

The testing and evaluation of NVD adopting Image Intensification (II) technology is performed both subjectively and objectively. The results from both tests indicate that the objective test is the preferred method as the 'human experience' factor is eliminated. However, NVD must have analogue or digital output which enables the performance of this test. For the objective test, a new method of using MATLAB to replace the 'traditional' method is proposed and verified. This method had demonstrated ease and efficiency of operations especially when a large number of tests and evaluations are required.

In testing and evaluation of optical systems, the MATLAB method can be extended to characterize Thermal Imaging (TI) systems for comparison with II systems. The testing of both II and TI systems with a common operational scenario can be carried out to evaluate and compare the performances of these two systems.

The newly acquired Astroscope 9350 is characterized for its performance and sensitivity. The sensitivity behavior and MTF are obtained for the system. The comparison, both subjectively and objectively, showed that the Astroscope 9350 is superior to the other systems tested. In addition, digitized images of good quality are produced from the Astroscope 9350 for future image fusion works.

B. PROPOSED FUTURE WORK

In continuation of this thesis, common tests for the Astroscope 9350 II and the Merlin InSb TI systems are proposed for both laboratory (indoor) and field (outdoor) conditions. The laboratory tests will focus on characterization of the II and TI systems under common controlled scenario to compare their performances objectively. Different operational scenarios such as sea surface, beach front, natural forest, desert and build-up area (BUA) terrains, should be

sought for these common tests. These field tests will enable the simulation of actual combat scenarios to verify the potential for the operations of these two systems. In addition, the field tests would serve as means to collect useful digitized images for fusion studies.

It is also proposed that image fusion analysis be carried out on the digitized images obtained from the Astroscope 9350 II and Merlin InSb TI systems. Different approaches of fusion should be evaluated to determine the optimal method to be used.

APPENDIX A: ASTROSCOPE 9350 ANALYSIS RESULTS

A. SCENE ILLUMINATION OF 0.01 FL OR 1.302E-3 LUX

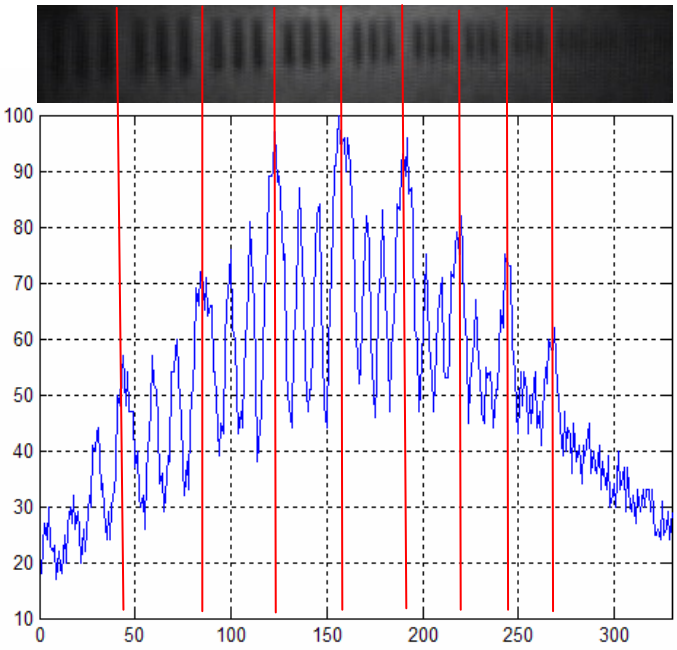

Figure A1. Contrast Intensity Plot of Scene Illumination of 0.01 FL at 3.0 m

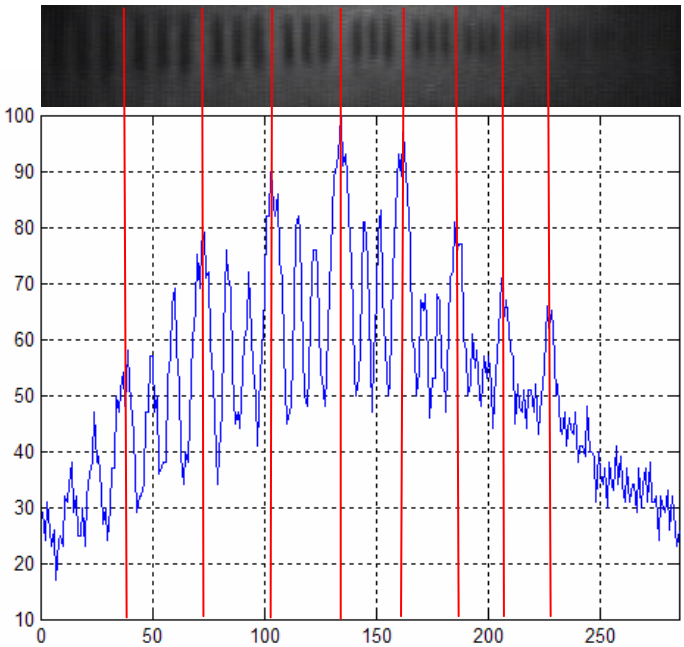

Figure A2. Contrast Intensity Plot of Scene Illumination of 0.01 FL at 3.5 m

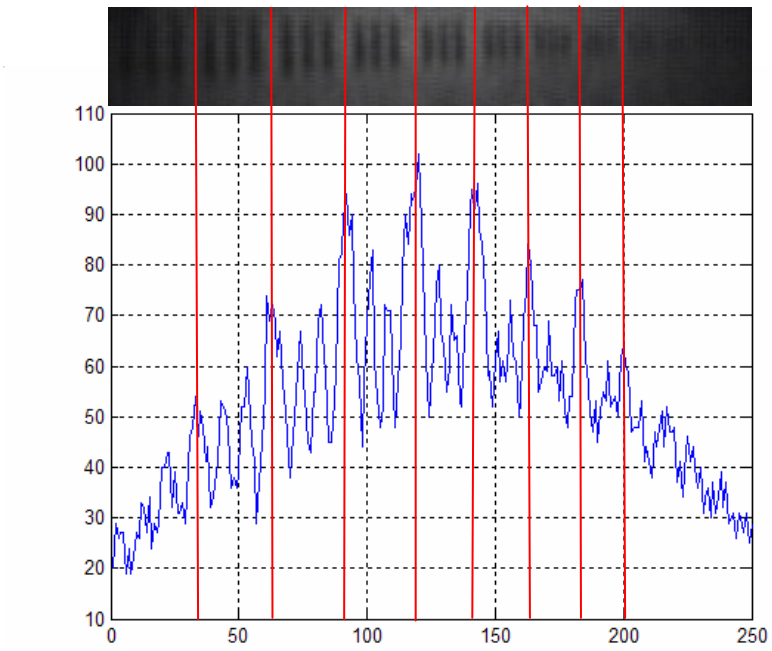

Figure A3. Contrast Intensity Plot of Scene Illumination of 0.01 FL at 4.0 m

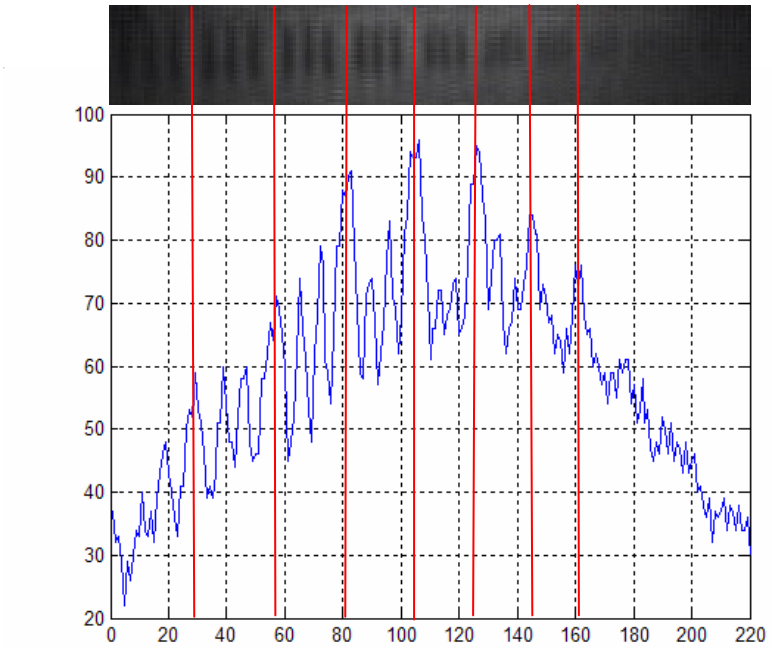

Figure A4. Contrast Intensity Plot of Scene Illumination of 0.01 FL at 4.5 m

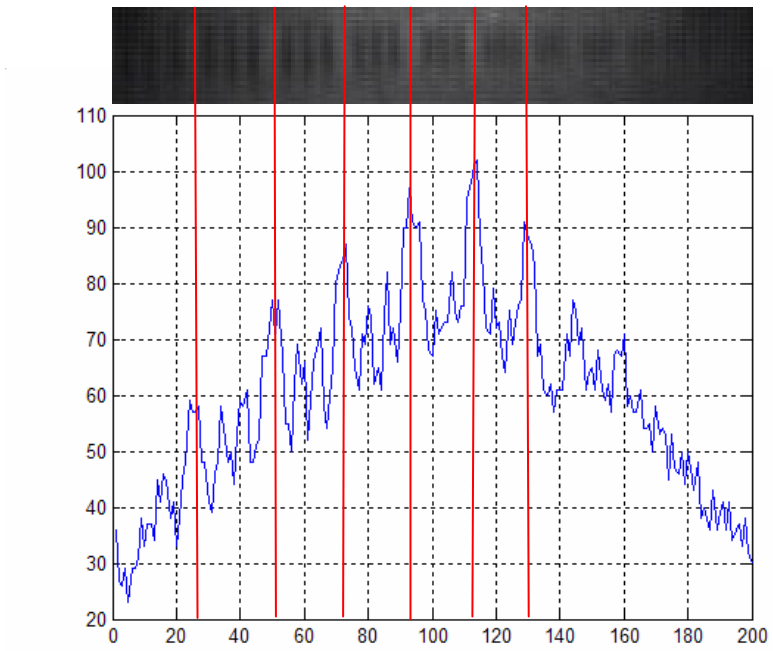

Figure A5. Contrast Intensity Plot of Scene Illumination of 0.01 FL at 5.0 m

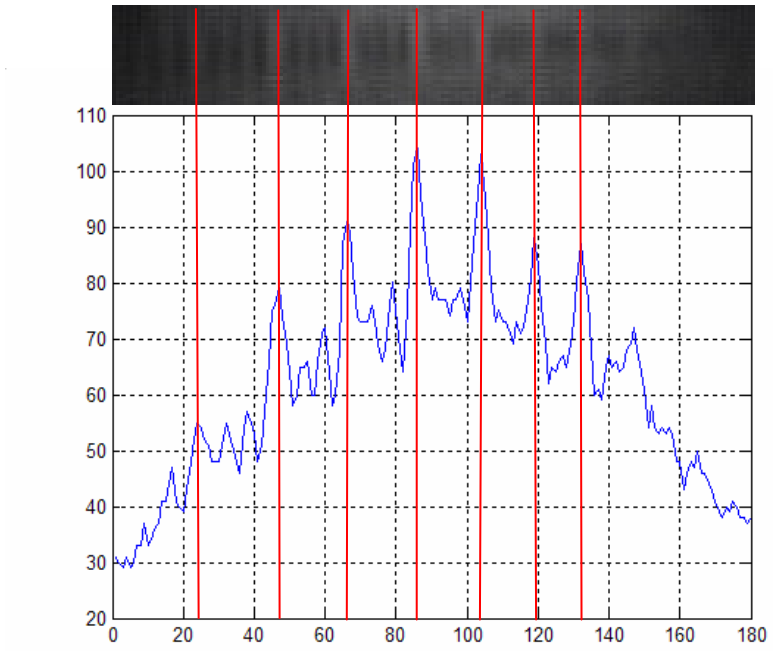

Figure A6. Contrast Intensity Plot of Scene Illumination of 0.01 FL at 5.5 m

I_{max}	I_{min}	CTF	Spatial Frequency, *v* (lp/mm)	Distance (m)	Spatial Frequency, *f* (lp/mrad)
44	17	0.443	0.100	3.0	0.300
60	26	0.395	0.112	3.0	0.336
81	38	0.361	0.126	3.0	0.378
87	44	0.328	0.142	3.0	0.426
83	46	0.287	0.159	3.0	0.477
78	47	0.248	0.178	3.0	0.534
66	44	0.200	0.200	3.0	0.600
48	18	0.455	0.100	3.5	0.350
69	30	0.394	0.112	3.5	0.392
75	34	0.376	0.126	3.5	0.441
82	45	0.291	0.142	3.5	0.497
82	47	0.271	0.159	3.5	0.557
68	47	0.183	0.178	3.5	0.623
60	47	0.121	0.200	3.5	0.700
43	19	0.387	0.100	4.0	0.400
60	32	0.304	0.112	4.0	0.448
72	38	0.309	0.126	4.0	0.504
82	47	0.271	0.142	4.0	0.568
80	52	0.212	0.159	4.0	0.636
70	52	0.148	0.178	4.0	0.712
47	22	0.362	0.100	4.5	0.450
60	39	0.212	0.112	4.5	0.504
79	45	0.274	0.126	4.5	0.567
83	58	0.177	0.142	4.5	0.639
73	61	0.090	0.159	4.5	0.716
45	23	0.324	0.100	5.0	0.500
61	39	0.220	0.112	5.0	0.560
72	50	0.180	0.126	5.0	0.630
82	61	0.147	0.142	5.0	0.710
56	46	0.098	0.112	5.5	0.616
73	58	0.115	0.126	5.5	0.693
80	65	0.103	0.142	5.5	0.781

Table A1. CTF vs Spatial Frequency for Scene Illumination of 0.01 FL

B. SCENE ILLUMINATION OF 0.015 FL OR 1.953E-3 LUX

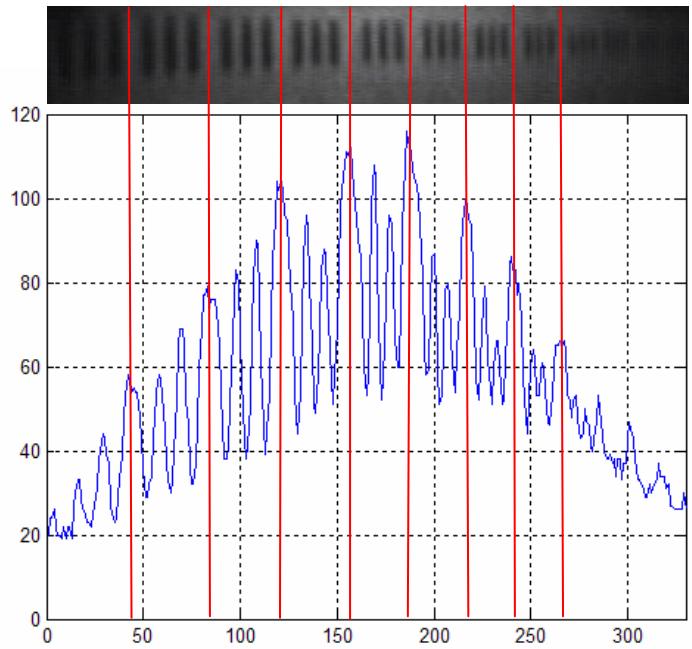

Figure A7. Contrast Intensity Plot of Scene Illumination of 0.015 FL at 3.0 m

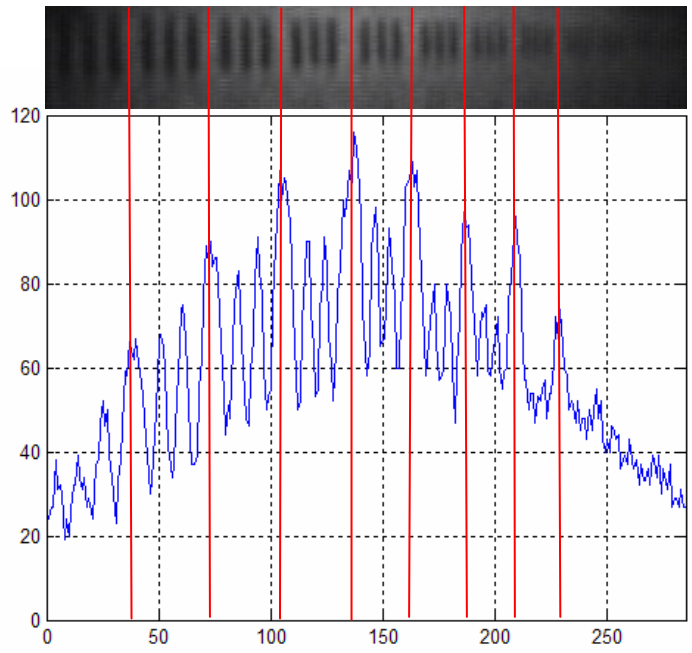

Figure A8. Contrast Intensity Plot of Scene Illumination of 0.015 FL at 3.5 m

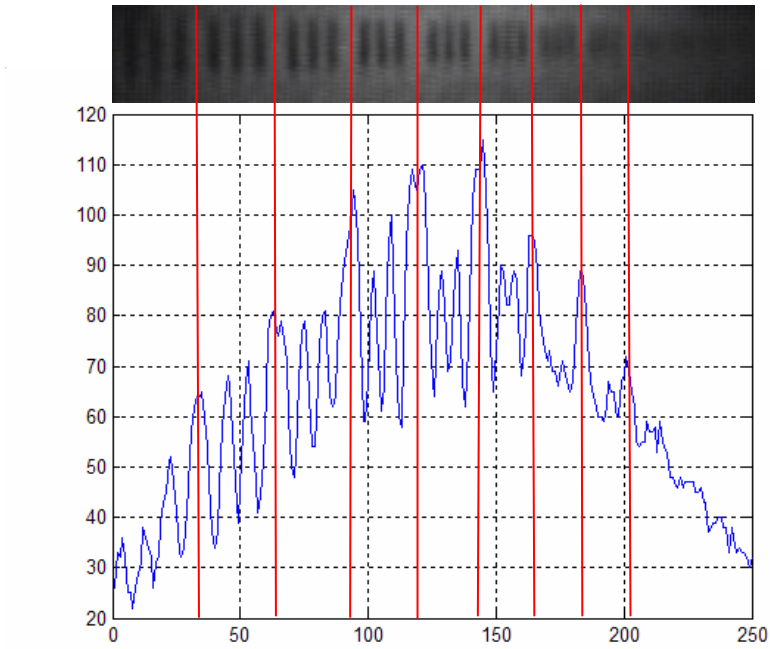

Figure A9. Contrast Intensity Plot of Scene Illumination of 0.015 FL at 4.0 m

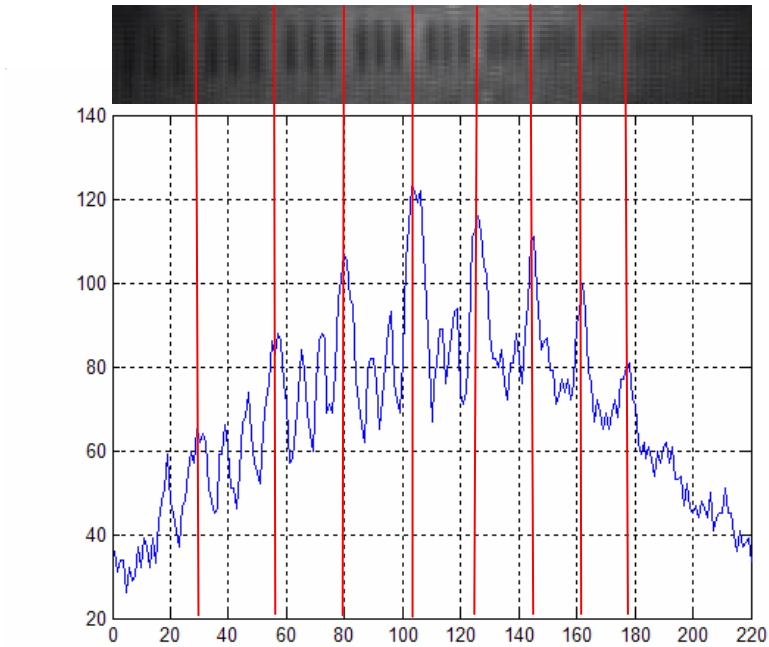

Figure A10. Contrast Intensity Plot of Scene Illumination of 0.015 FL at 4.5 m

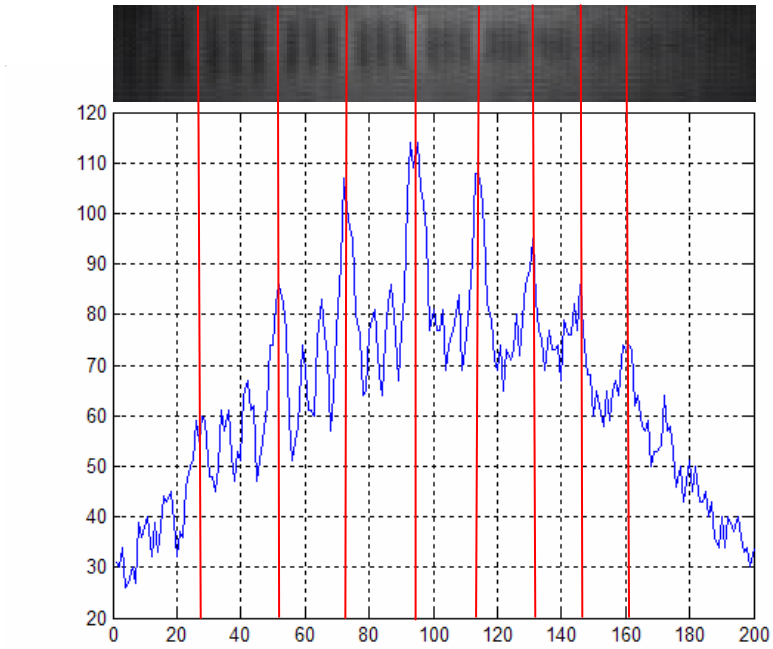

Figure A11. Contrast Intensity Plot of Scene Illumination of 0.015 FL at 5.0 m

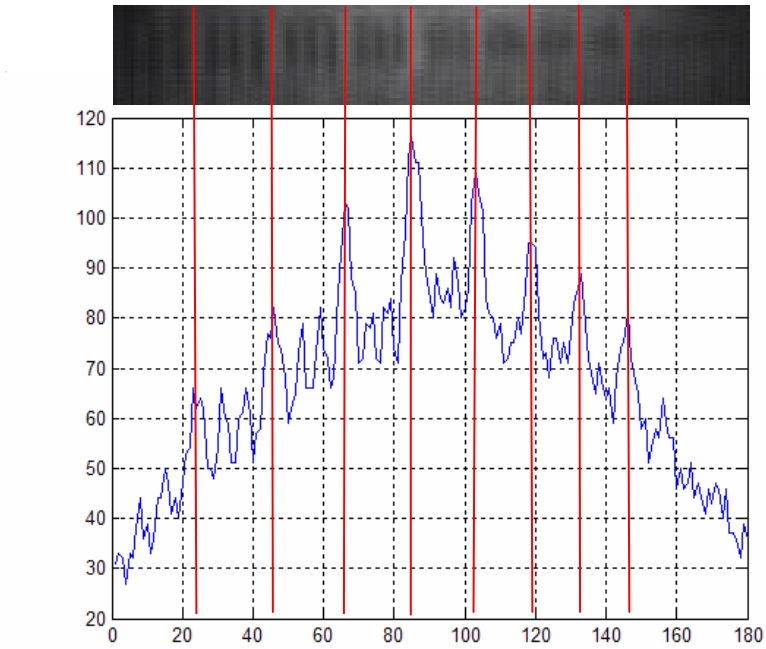

Figure A12. Contrast Intensity Plot of Scene Illumination of 0.015 FL at 5.5 m

I_{max}	I_{min}	CTF	Spatial Frequency, *v* (lp/mm)	Distance (m)	Spatial Frequency, *f* (lp/mrad)
44	20	0.375	0.100	3.0	0.300
70	30	0.400	0.112	3.0	0.336
90	38	0.406	0.126	3.0	0.378
95	43	0.377	0.142	3.0	0.426
109	53	0.346	0.159	3.0	0.477
86	50	0.265	0.178	3.0	0.534
80	49	0.240	0.200	3.0	0.600
64	47	0.153	0.224	3.0	0.672
53	20	0.452	0.100	3.5	0.350
75	30	0.429	0.112	3.5	0.392
92	45	0.343	0.126	3.5	0.441
92	50	0.296	0.142	3.5	0.497
98	60	0.241	0.159	3.5	0.557
80	56	0.176	0.178	3.5	0.623
75	57	0.136	0.200	3.5	0.700
52	22	0.405	0.100	4.0	0.400
72	34	0.358	0.112	4.0	0.448
81	48	0.256	0.126	4.0	0.504
100	60	0.250	0.142	4.0	0.568
93	64	0.185	0.159	4.0	0.636
90	70	0.125	0.178	4.0	0.712
60	30	0.333	0.100	4.5	0.450
75	36	0.351	0.112	4.5	0.504
88	60	0.189	0.126	4.5	0.567
93	62	0.200	0.142	4.5	0.639
93	70	0.141	0.159	4.5	0.716
45	26	0.268	0.100	5.0	0.500
67	46	0.186	0.112	5.0	0.560
83	52	0.230	0.126	5.0	0.630
85	65	0.133	0.142	5.0	0.710
84	69	0.098	0.159	5.0	0.795
50	27	0.299	0.100	5.5	0.550
66	50	0.138	0.112	5.5	0.616
82	60	0.155	0.126	5.5	0.693
83	71	0.078	0.142	5.5	0.781
92	80	0.070	0.159	5.5	0.875

Table A2. CTF vs Spatial Frequency for Scene Illumination of 0.015 FL

C. SCENE ILLUMINATION OF 0.02 FL OR 2.604E-3 LUX

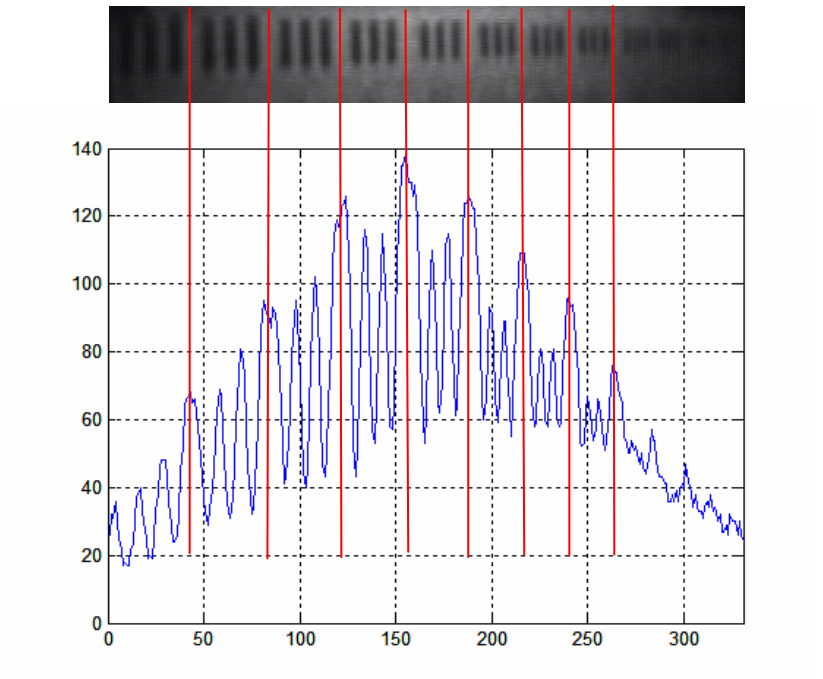

Figure A13. Contrast Intensity Plot of Scene Illumination of 0.02 FL at 3.0 m

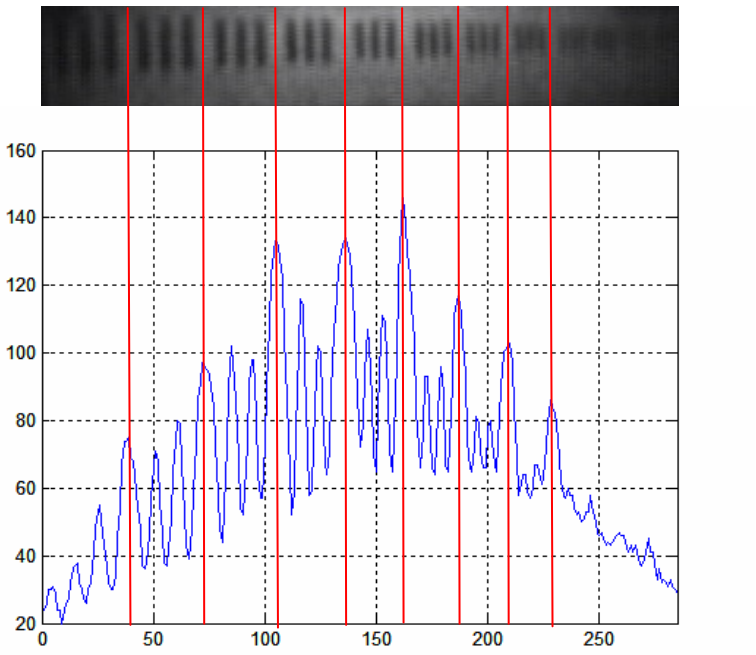

Figure A14. Contrast Intensity Plot of Scene Illumination of 0.02 FL at 3.5 m

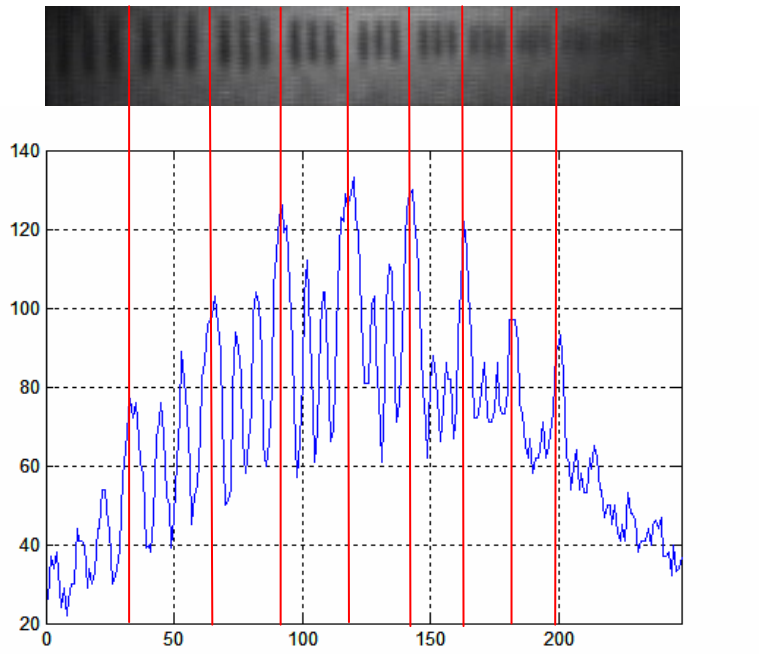

Figure A15. Contrast Intensity Plot of Scene Illumination of 0.02 FL at 4.0 m

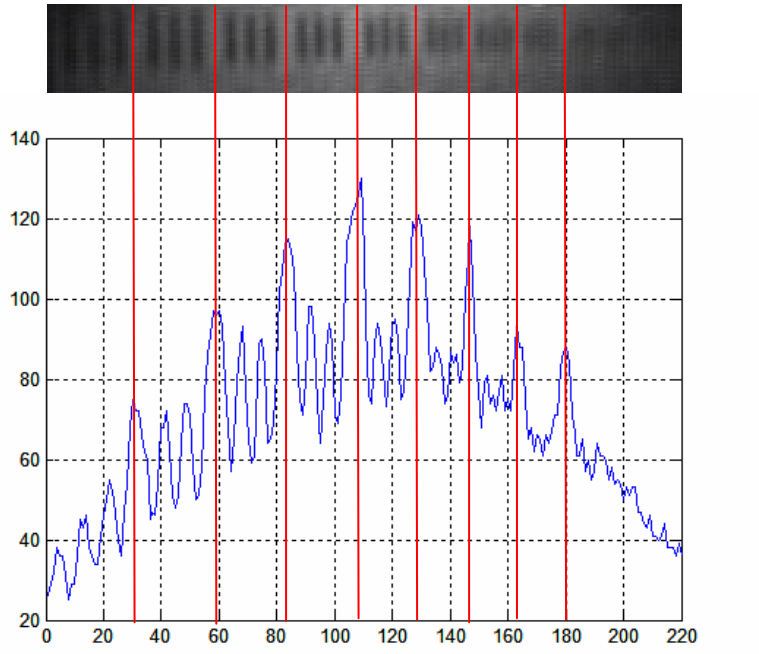

Figure A16. Contrast Intensity Plot of Scene Illumination of 0.02 FL at 4.5 m

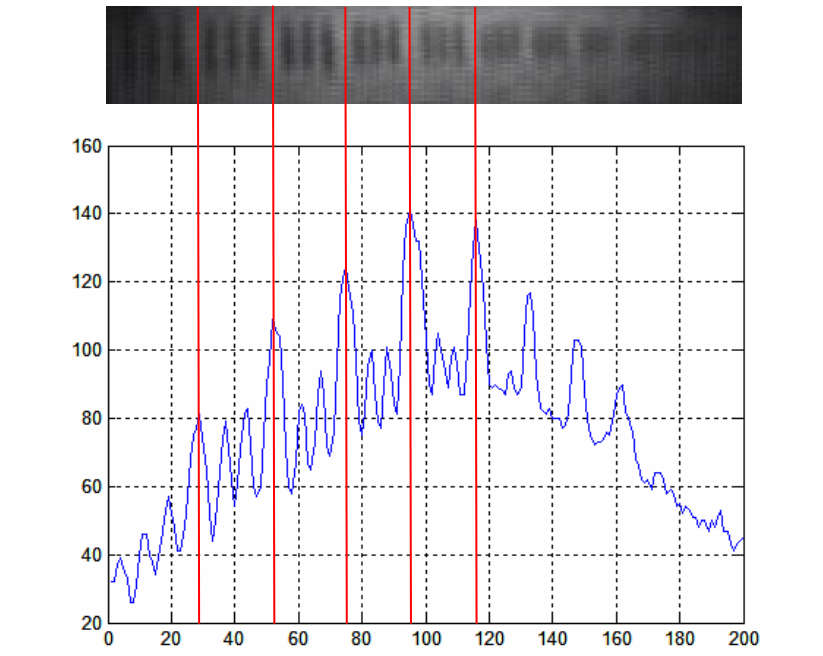

Figure A17 Contrast Intensity Plot of Scene Illumination of 0.02 FL at 5.0 m

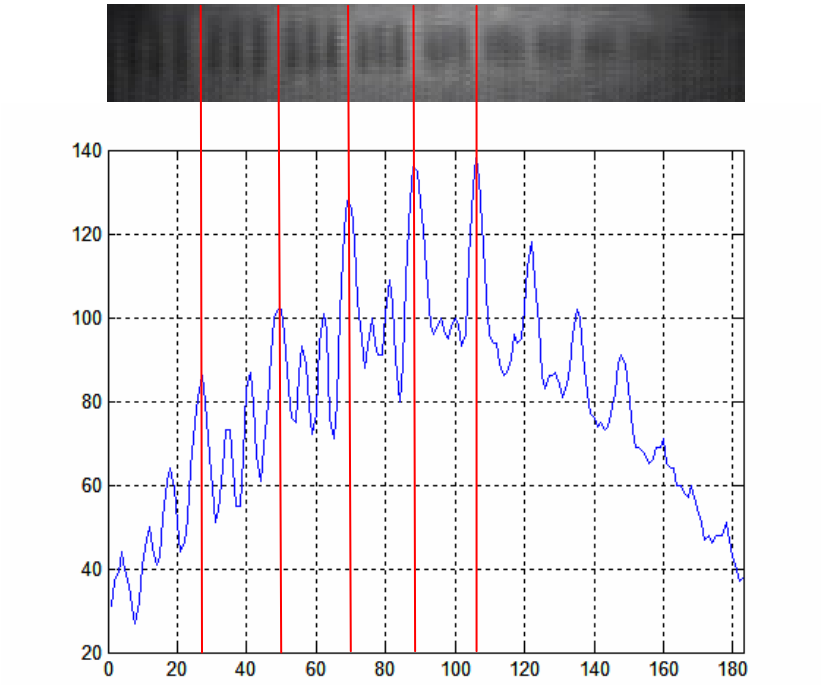

Figure A18. Contrast Intensity Plot of Scene Illumination of 0.02 FL at 5.5 m

I_{max}	I_{min}	CTF	Spatial Frequency, *v* (lp/mm)	Distance (m)	Spatial Frequency, *f* (lp/mrad)
47	18	0.446	0.100	3.0	0.300
80	30	0.455	0.112	3.0	0.336
102	40	0.437	0.126	3.0	0.378
117	42	0.472	0.142	3.0	0.426
115	54	0.361	0.159	3.0	0.477
93	55	0.257	0.178	3.0	0.534
80	58	0.159	0.200	3.0	0.600
65	55	0.083	0.224	3.0	0.672
55	20	0.467	0.100	3.5	0.350
80	37	0.368	0.112	3.5	0.392
102	44	0.397	0.126	3.5	0.441
115	53	0.369	0.142	3.5	0.497
110	65	0.257	0.159	3.5	0.557
95	65	0.188	0.178	3.5	0.623
82	67	0.101	0.200	3.5	0.700
54	22	0.421	0.100	4.0	0.400
88	39	0.386	0.112	4.0	0.448
103	50	0.346	0.126	4.0	0.504
112	58	0.318	0.142	4.0	0.568
110	61	0.287	0.159	4.0	0.636
87	62	0.168	0.178	4.0	0.712
85	73	0.076	0.200	4.0	0.800
55	26	0.358	0.100	4.5	0.450
73	46	0.227	0.112	4.5	0.504
91	60	0.205	0.126	4.5	0.567
98	64	0.210	0.142	4.5	0.639
93	75	0.107	0.159	4.5	0.716
88	74	0.086	0.178	4.5	0.801
81	72	0.059	0.200	4.5	0.900
57	25	0.390	0.112	5.0	0.560
82	43	0.312	0.126	5.0	0.630
92	59	0.219	0.142	5.0	0.710
100	78	0.124	0.159	5.0	0.795
104	88	0.083	0.178	5.0	0.890
63	28	0.385	0.100	5.5	0.550
85	52	0.241	0.112	5.5	0.616
101	72	0.168	0.126	5.5	0.693
110	80	0.158	0.142	5.5	0.781

Table A3. CTF vs Spatial Frequency for Scene Illumination of 0.02 FL

D. SCENE ILLUMINATION OF 0.03 FL OR 3.906E-3 LUX

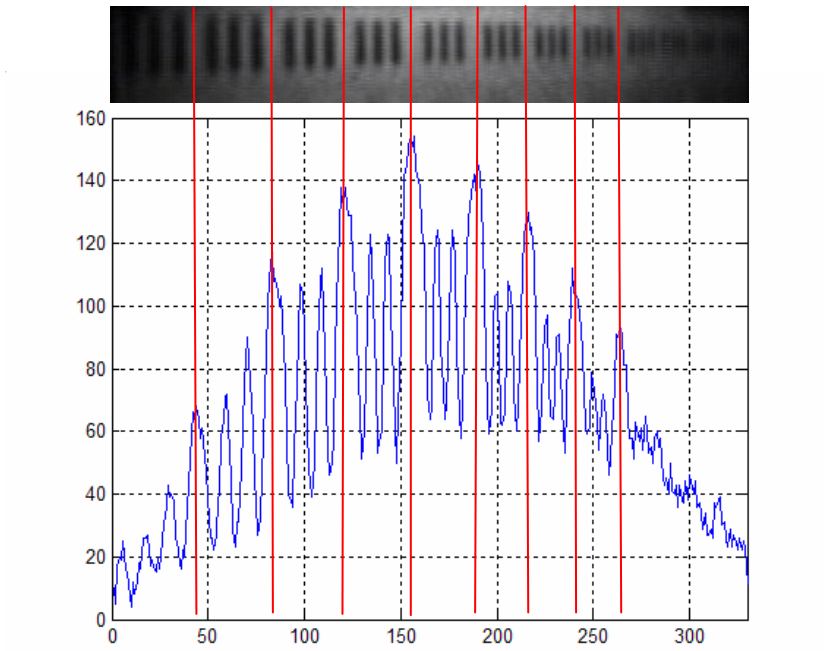

Figure A19. Contrast Intensity Plot of Scene Illumination of 0.03 FL at 3.0 m

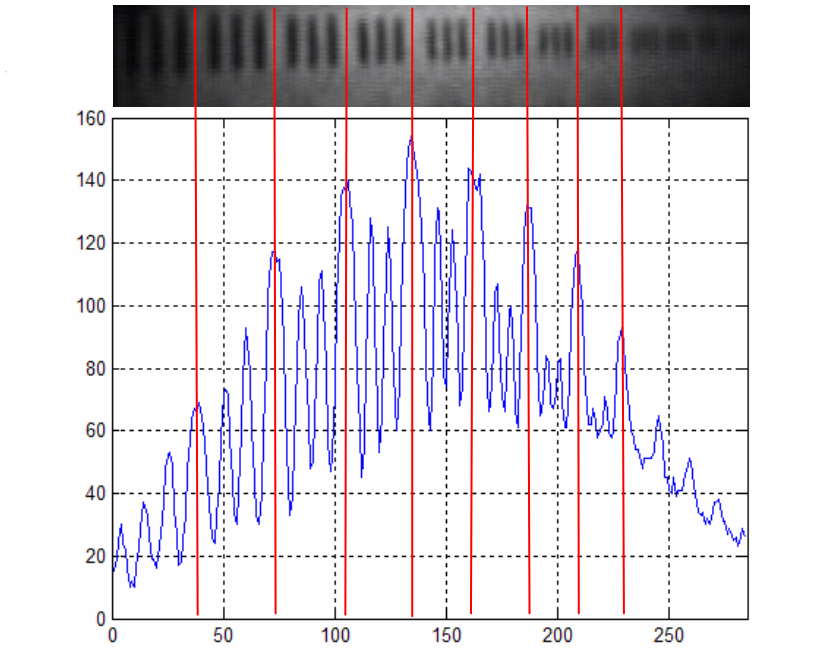

Figure A20. Contrast Intensity Plot of Scene Illumination of 0.03 FL at 3.5 m

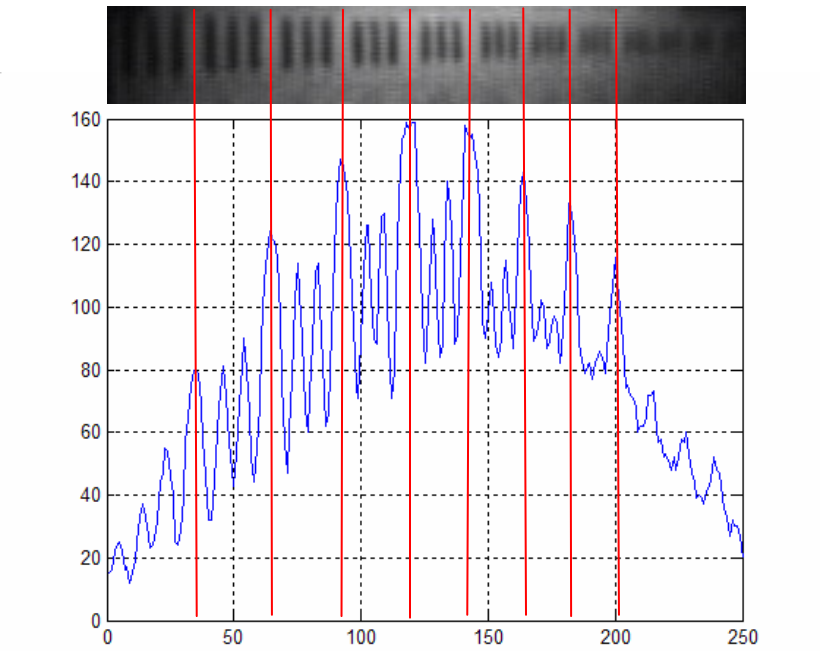

Figure A21. Contrast Intensity Plot of Scene Illumination of 0.03 FL at 4.0 m

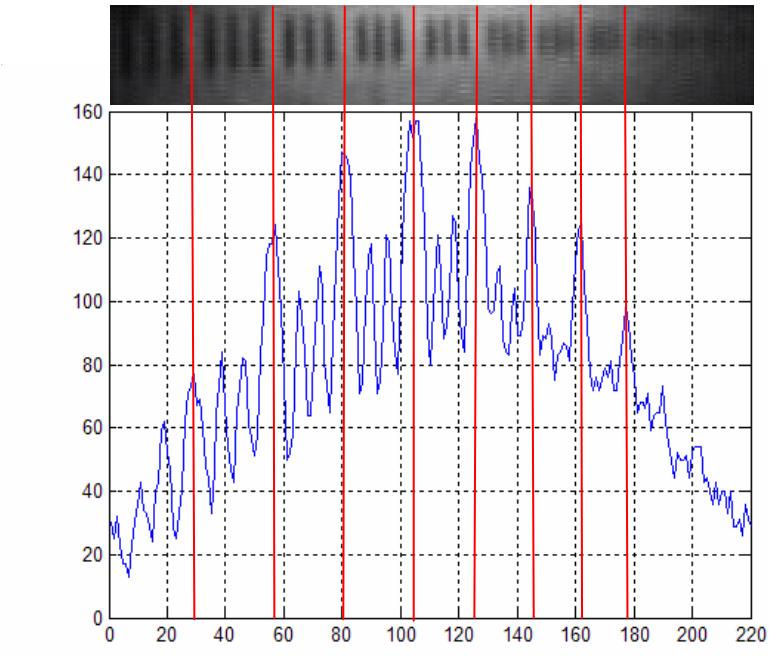

Figure A22. Contrast Intensity Plot of Scene Illumination of 0.03 FL at 4.5 m

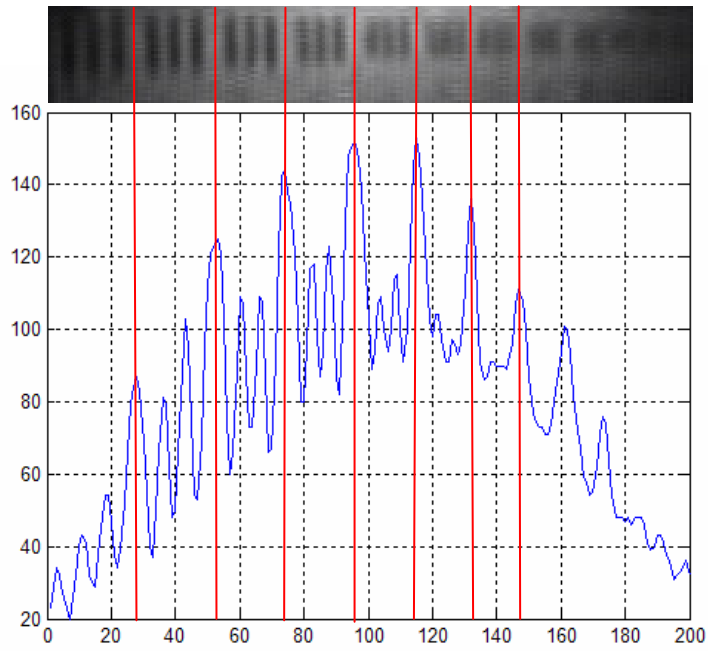

Figure A23. Contrast Intensity Plot of Scene Illumination of 0.03 FL at 5.0 m

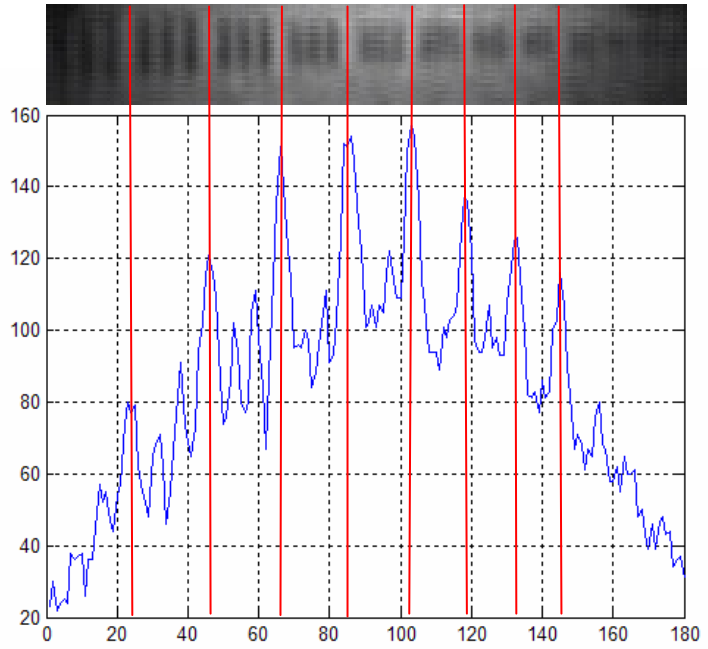

Figure A24. Contrast Intensity Plot of Scene Illumination of 0.03 FL at 5.5 m

I_{max}	I_{min}	CTF	Spatial Frequency, *v* (lp/mm)	Distance (m)	Spatial Frequency, *f* (lp/mrad)
42	10	0.615	0.100	3.0	0.300
80	22	0.569	0.112	3.0	0.336
110	38	0.486	0.126	3.0	0.378
122	50	0.419	0.142	3.0	0.426
122	64	0.312	0.159	3.0	0.477
105	62	0.257	0.178	3.0	0.534
96	60	0.231	0.200	3.0	0.600
80	50	0.231	0.224	3.0	0.672
40	10	0.600	0.100	3.5	0.350
90	28	0.525	0.112	3.5	0.392
110	43	0.438	0.126	3.5	0.441
130	55	0.405	0.142	3.5	0.497
130	70	0.300	0.159	3.5	0.557
108	66	0.241	0.178	3.5	0.623
84	65	0.128	0.200	3.5	0.700
55	20	0.467	0.100	4.0	0.400
90	30	0.500	0.112	4.0	0.448
115	60	0.314	0.126	4.0	0.504
128	72	0.280	0.142	4.0	0.568
140	84	0.250	0.159	4.0	0.636
110	85	0.128	0.178	4.0	0.712
102	83	0.103	0.200	4.0	0.800
50	15	0.538	0.100	4.5	0.450
82	38	0.367	0.112	4.5	0.504
108	63	0.263	0.126	4.5	0.567
120	70	0.263	0.142	4.5	0.639
128	83	0.213	0.159	4.5	0.716
108	83	0.131	0.178	4.5	0.801
54	20	0.459	0.100	5.0	0.500
104	45	0.396	0.112	5.0	0.560
109	65	0.253	0.126	5.0	0.630
122	84	0.184	0.142	5.0	0.710
115	90	0.122	0.159	5.0	0.795
57	25	0.390	0.100	5.5	0.550
90	48	0.304	0.112	5.5	0.616
110	75	0.189	0.126	5.5	0.693
110	84	0.134	0.142	5.5	0.781

Table A4. CTF vs Spatial Frequency for Scene Illumination of 0.03 FL

E. SCENE ILLUMINATION OF 0.06 FL OR 7.812E-3 LUX

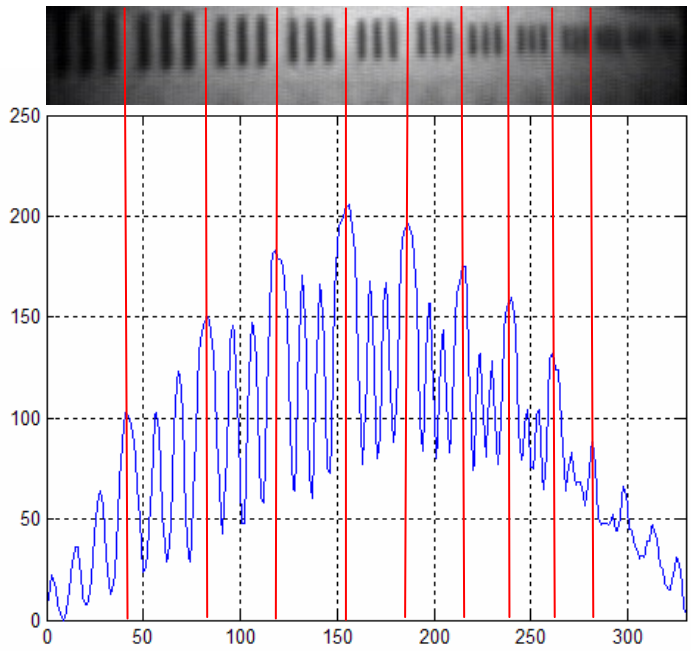

Figure A25. Contrast Intensity Plot of Scene Illumination of 0.06 FL at 3.0 m

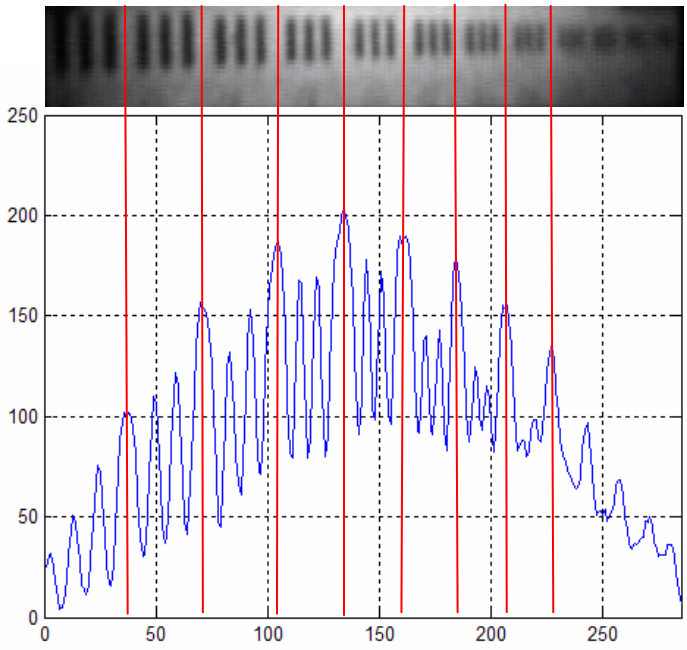

Figure A26. Contrast Intensity Plot of Scene Illumination of 0.04 FL at 3.5 m

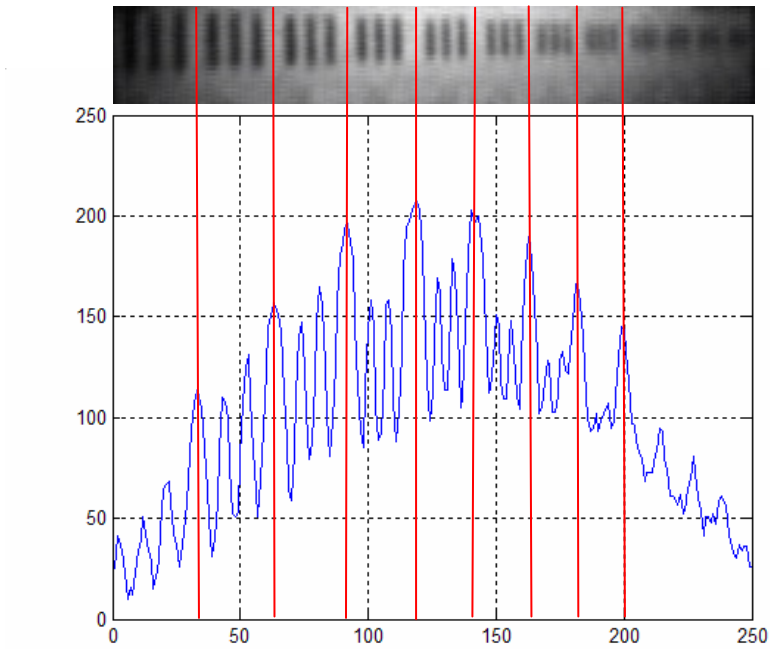

Figure A27. Contrast Intensity Plot of Scene Illumination of 0.06 FL at 4.0 m

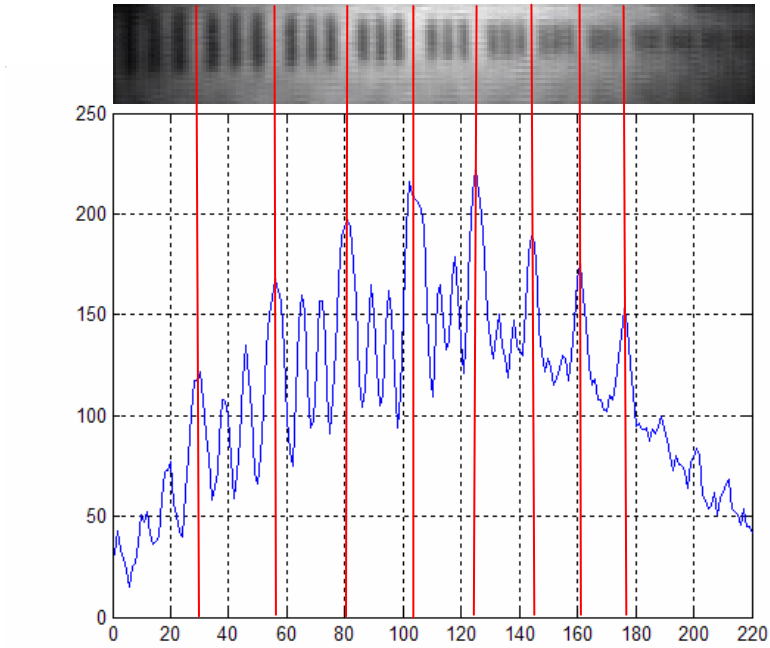

Figure A28. Contrast Intensity Plot of Scene Illumination of 0.06 FL at 4.5 m

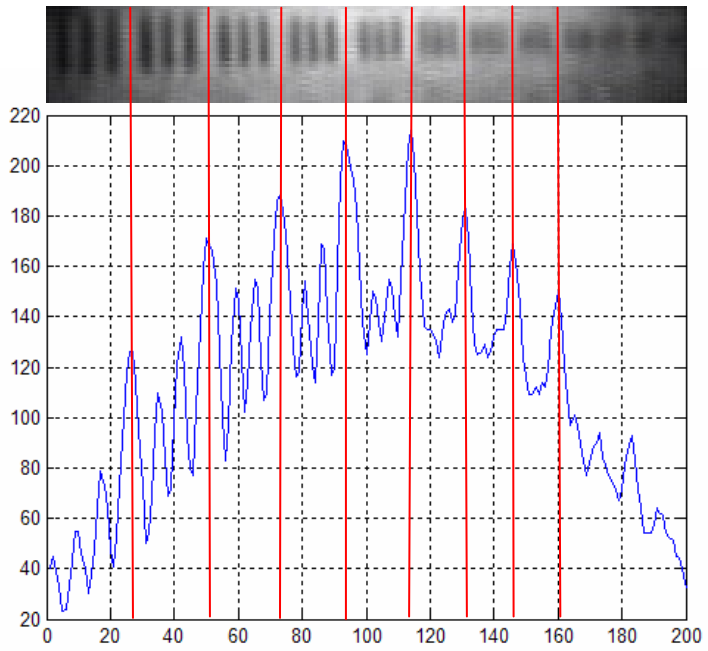

Figure A29. Contrast Intensity Plot of Scene Illumination of 0.06 FL at 5.0 m

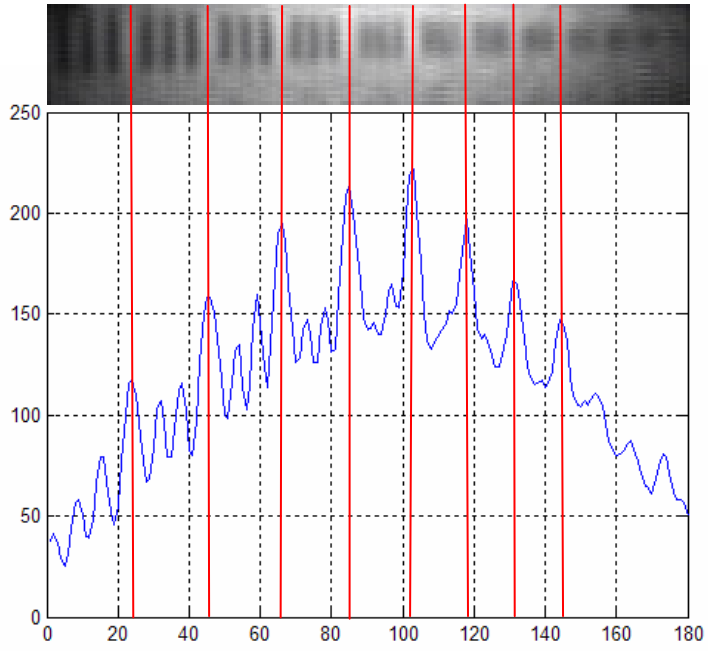

Figure A30. Contrast Intensity Plot of Scene Illumination of 0.06 FL at 5.5 m

I_{max}	I_{min}	CTF	Spatial Frequency, *v* (lp/mm)	Distance (m)	Spatial Frequency, *f* (lp/mrad)
110	30	0.571	0.112	3.0	0.336
145	50	0.487	0.126	3.0	0.378
165	70	0.404	0.142	3.0	0.426
160	80	0.333	0.159	3.0	0.477
150	80	0.304	0.178	3.0	0.534
125	75	0.250	0.200	3.0	0.600
105	70	0.200	0.224	3.0	0.672
123	35	0.557	0.112	3.5	0.392
152	60	0.434	0.126	3.5	0.441
170	80	0.360	0.142	3.5	0.497
175	100	0.273	0.159	3.5	0.557
138	90	0.211	0.178	3.5	0.623
120	90	0.143	0.200	3.5	0.700
60	15	0.600	0.100	4.0	0.400
130	50	0.444	0.112	4.0	0.448
165	80	0.347	0.126	4.0	0.504
160	90	0.280	0.142	4.0	0.568
175	110	0.228	0.159	4.0	0.636
150	110	0.154	0.178	4.0	0.712
130	104	0.111	0.200	4.0	0.800
65	20	0.529	0.100	4.5	0.450
135	65	0.350	0.112	4.5	0.504
160	90	0.280	0.126	4.5	0.567
165	105	0.222	0.142	4.5	0.639
180	125	0.180	0.159	4.5	0.716
150	120	0.111	0.178	4.5	0.801
75	30	0.429	0.100	5.0	0.500
128	70	0.293	0.112	5.0	0.560
152	102	0.197	0.126	5.0	0.630
170	118	0.181	0.142	5.0	0.710
150	130	0.071	0.159	5.0	0.795
70	28	0.429	0.100	5.5	0.550
118	80	0.192	0.112	5.5	0.616
160	100	0.231	0.126	5.5	0.693
152	130	0.078	0.142	5.5	0.781

Table A5. CTF vs Spatial Frequency for Scene Illumination of 0.06 FL

F. SCENE ILLUMINATION OF 0.08 FL OR 1.042E-2 LUX

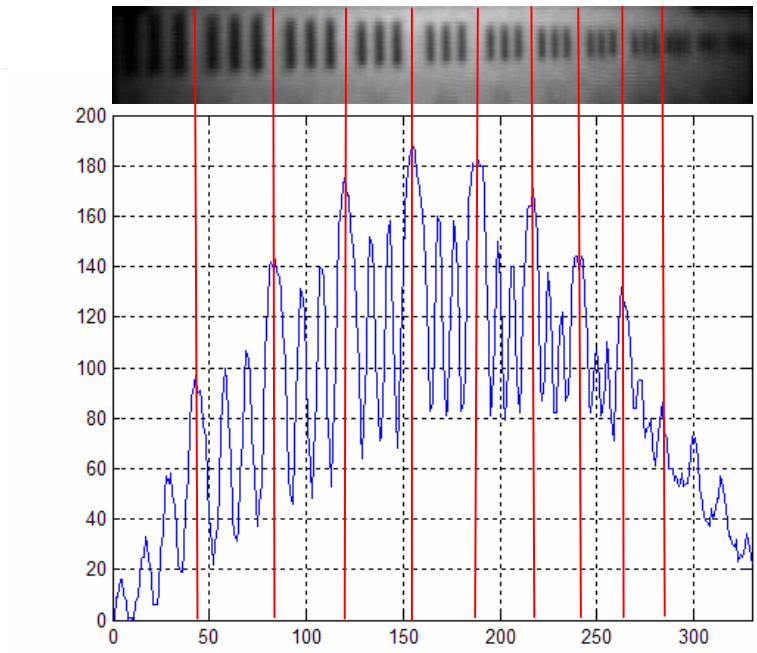

Figure A31. Contrast Intensity Plot of Scene Illumination of 0.08 FL at 3.0 m

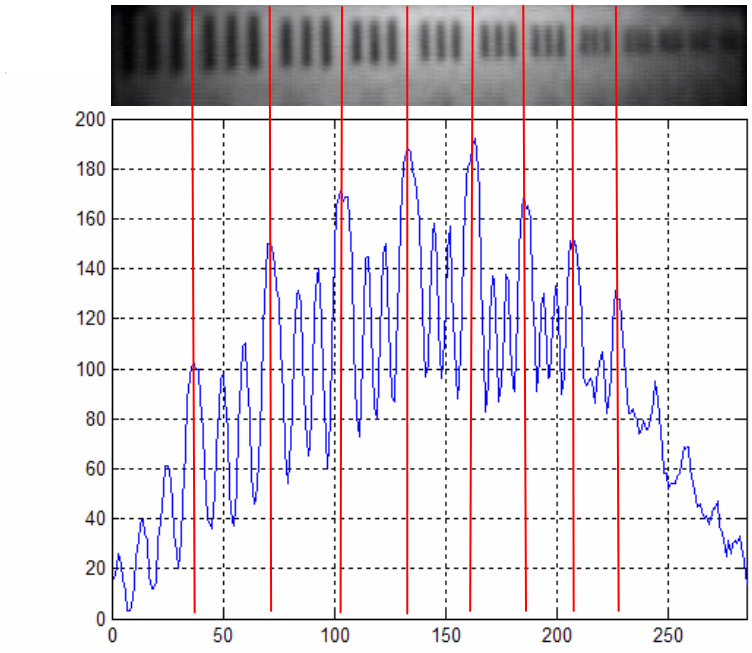

Figure A32. Contrast Intensity Plot of Scene Illumination of 0.08 FL at 3.5 m

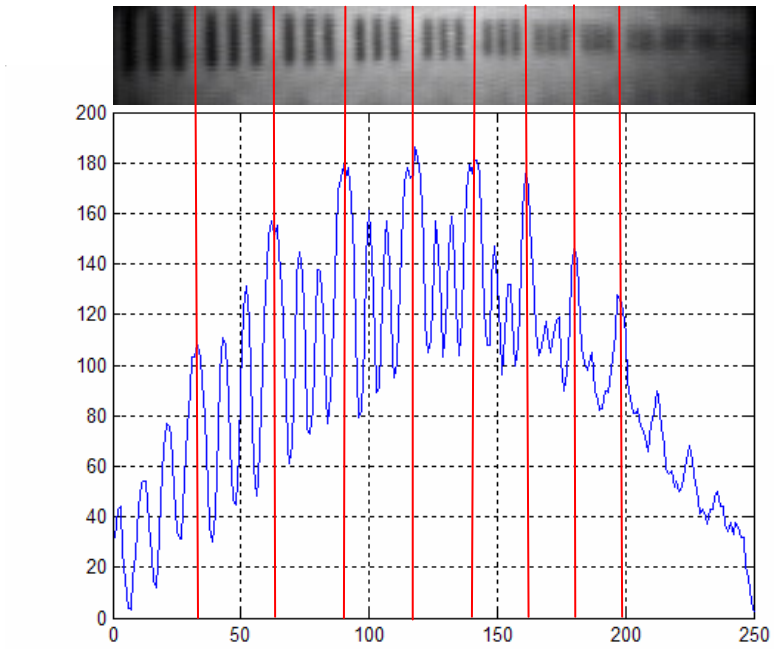

Figure A33. Contrast Intensity Plot of Scene Illumination of 0.08 FL at 4.0 m

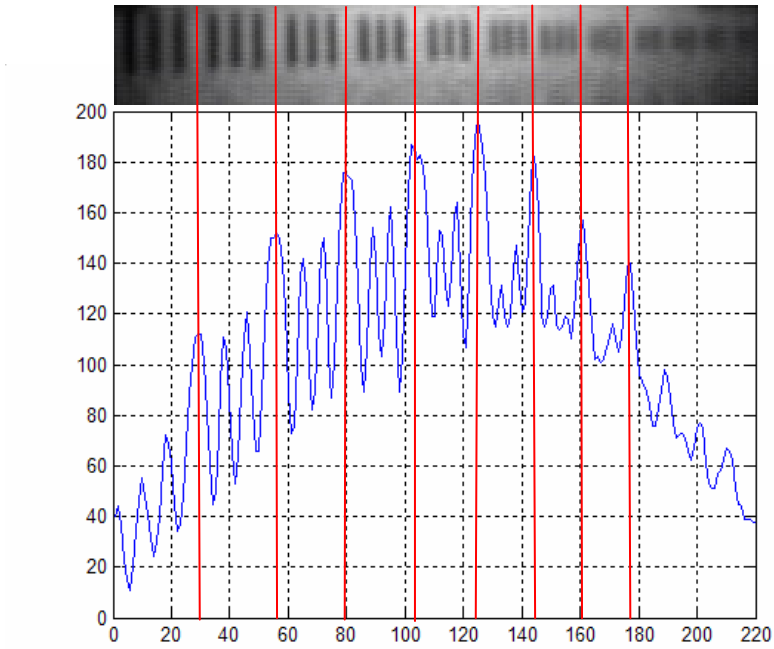

Figure A34. Contrast Intensity Plot of Scene Illumination of 0.08 FL at 4.5 m

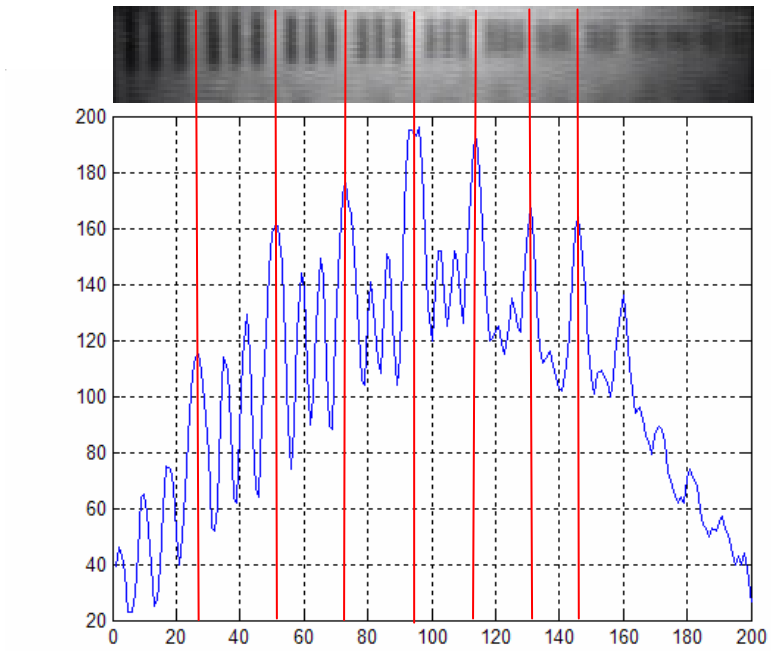

Figure A35. Contrast Intensity Plot of Scene Illumination of 0.08 FL at 5.0 m

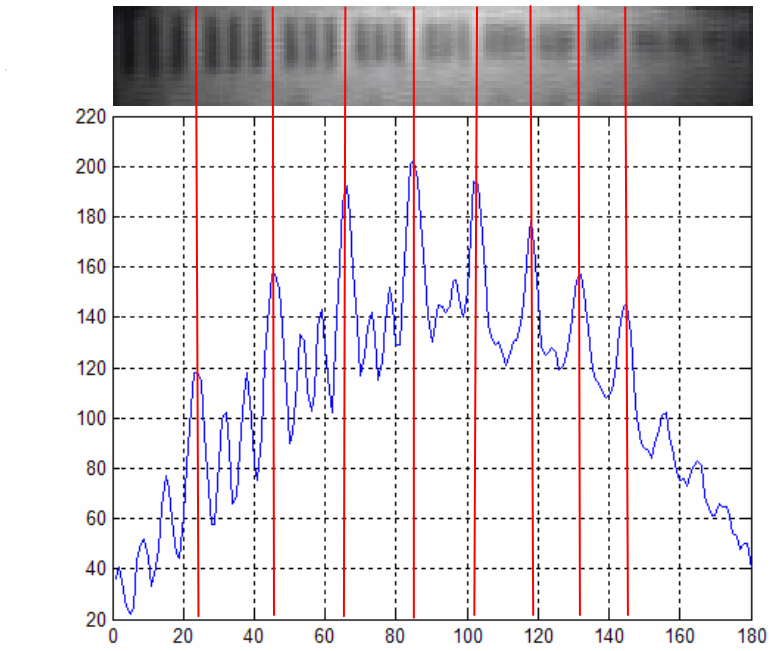

Figure A36. Contrast Intensity Plot of Scene Illumination of 0.08 FL at 5.5 m

I_{max}	I_{min}	CTF	Spatial Frequency, *v* (lp/mm)	Distance (m)	Spatial Frequency, *f* (lp/mrad)
105	30	0.556	0.112	3.0	0.336
135	50	0.459	0.126	3.0	0.378
155	72	0.366	0.142	3.0	0.426
160	82	0.322	0.159	3.0	0.477
140	82	0.261	0.178	3.0	0.534
130	83	0.221	0.200	3.0	0.600
110	80	0.158	0.224	3.0	0.672
105	40	0.448	0.112	3.5	0.392
135	65	0.350	0.126	3.5	0.441
145	80	0.289	0.142	3.5	0.497
156	100	0.219	0.159	3.5	0.557
138	88	0.221	0.178	3.5	0.623
130	97	0.145	0.200	3.5	0.700
120	42	0.481	0.112	4.0	0.448
140	70	0.333	0.126	4.0	0.504
155	90	0.265	0.142	4.0	0.568
158	108	0.188	0.159	4.0	0.636
140	100	0.167	0.178	4.0	0.712
119	100	0.087	0.200	4.0	0.800
72	25	0.485	0.100	4.5	0.450
115	55	0.353	0.112	4.5	0.504
150	82	0.293	0.126	4.5	0.567
155	90	0.265	0.142	4.5	0.639
160	120	0.143	0.159	4.5	0.716
140	115	0.098	0.178	4.5	0.801
75	30	0.429	0.100	5.0	0.500
120	62	0.319	0.112	5.0	0.560
150	90	0.250	0.126	5.0	0.630
145	110	0.137	0.142	5.0	0.710
150	130	0.071	0.159	5.0	0.795
78	35	0.381	0.100	5.5	0.550
110	62	0.279	0.112	5.5	0.616
140	100	0.167	0.126	5.5	0.693
150	115	0.132	0.142	5.5	0.781

Table A6. CTF vs Spatial Frequency for Scene Illumination of 0.08 FL

G. SCENE ILLUMINATION OF 0.1 FL OR 1.302E-2 LUX

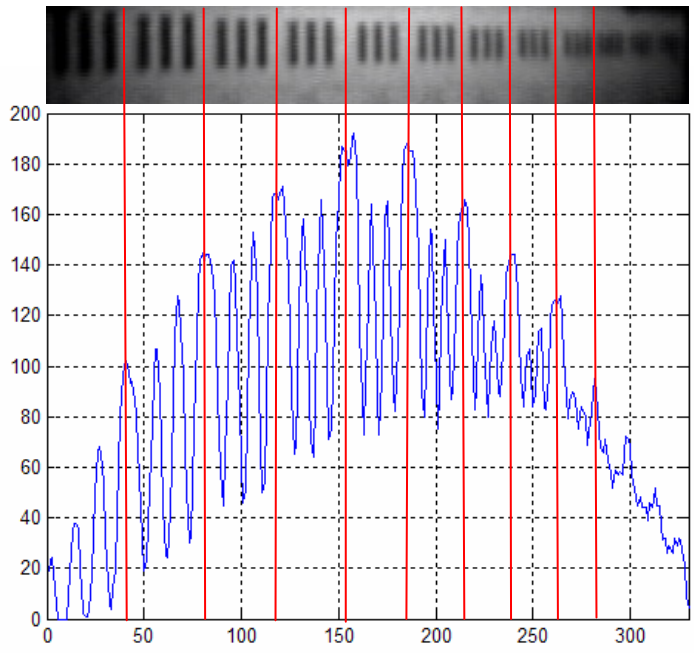

Figure A37. Contrast Intensity Plot of Scene Illumination of 0.1 FL at 3.0 m

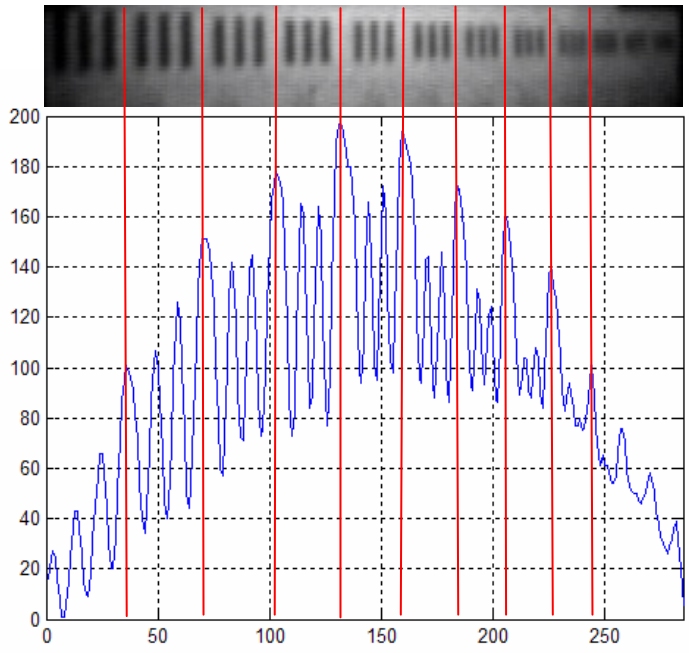

Figure A38. Contrast Intensity Plot of Scene Illumination of 0.1 FL at 3.5 m

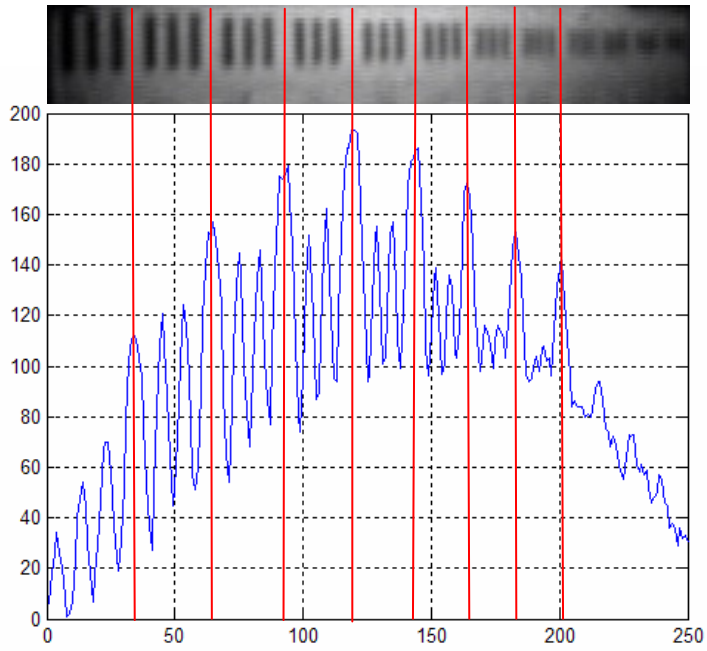

Figure A39. Contrast Intensity Plot of Scene Illumination of 0.1 FL at 4.0 m

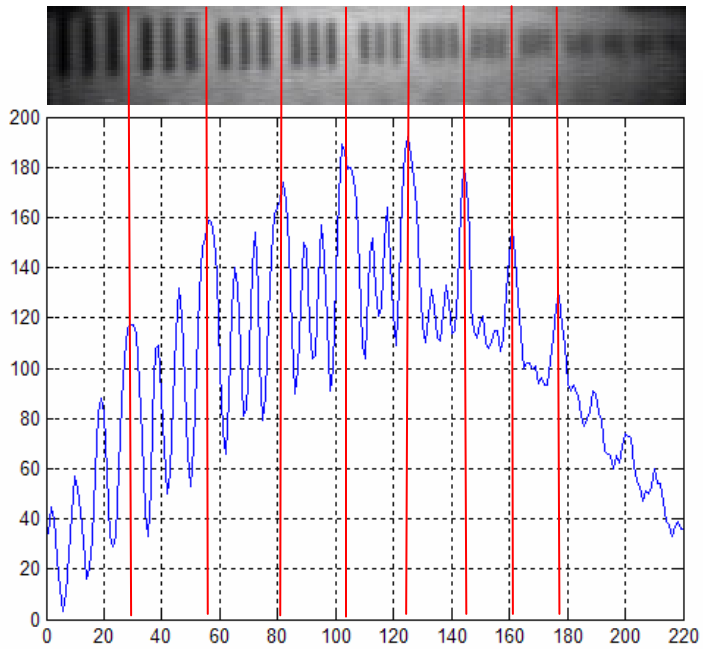

Figure A40. Contrast Intensity Plot of Scene Illumination of 0.1 FL at 4.5 m

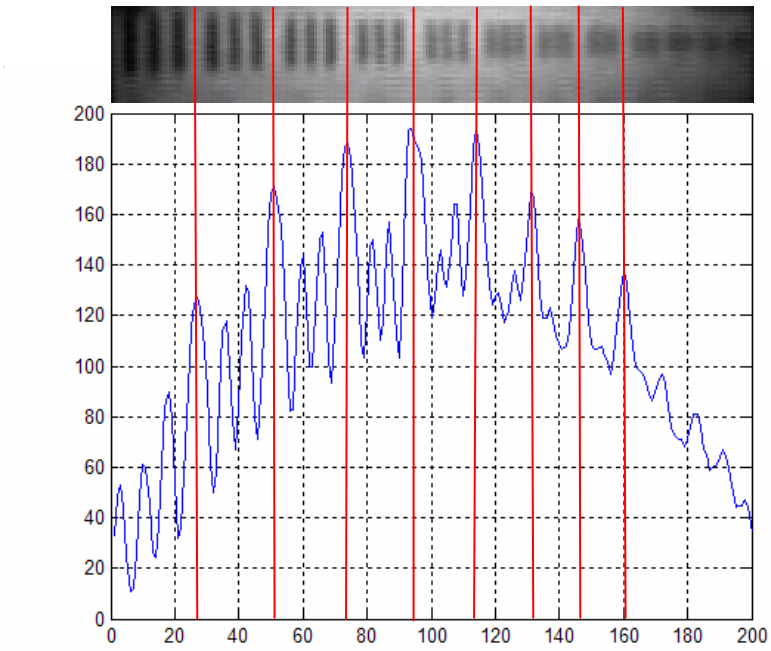

Figure A41. Contrast Intensity Plot of Scene Illumination of 0.1 FL at 5.0 m

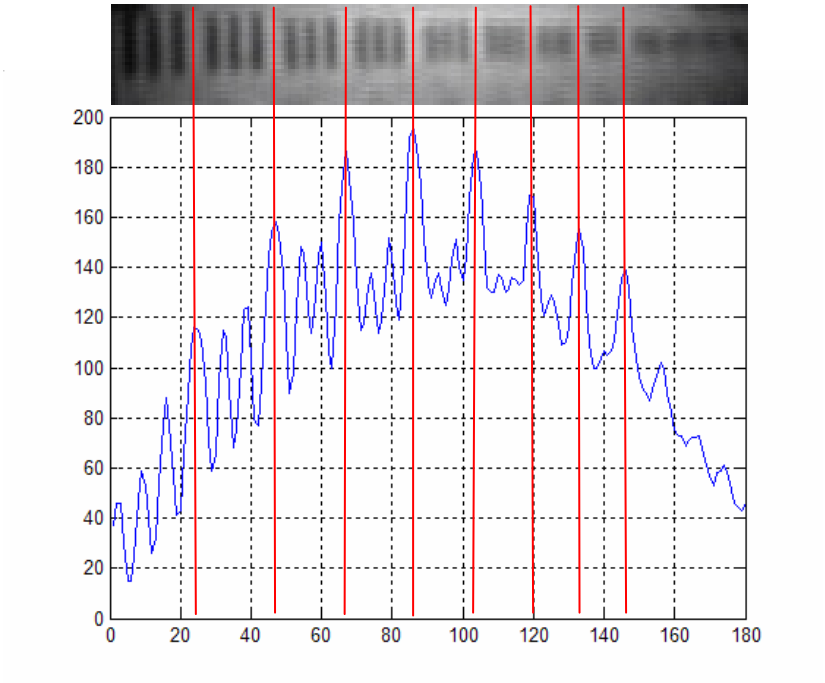

Figure A42. Contrast Intensity Plot of Scene Illumination of 0.1 FL at 5.5 m

I_{max}	I_{min}	CTF	Spatial Frequency, *v* (lp/mm)	Distance (m)	Spatial Frequency, *f* (lp/mrad)
110	30	0.571	0.112	3.0	0.336
148	50	0.495	0.126	3.0	0.378
160	70	0.391	0.142	3.0	0.426
160	80	0.333	0.159	3.0	0.477
150	82	0.293	0.178	3.0	0.534
110	90	0.100	0.200	3.0	0.600
115	85	0.150	0.224	3.0	0.672
110	40	0.467	0.112	3.5	0.392
140	72	0.321	0.126	3.5	0.441
164	80	0.344	0.142	3.5	0.497
164	98	0.252	0.159	3.5	0.557
144	92	0.220	0.178	3.5	0.623
125	95	0.136	0.200	3.5	0.700
105	88	0.088	0.224	3.5	0.784
60	20	0.500	0.100	4.0	0.400
120	50	0.412	0.112	4.0	0.448
140	70	0.333	0.126	4.0	0.504
152	90	0.256	0.142	4.0	0.568
155	100	0.216	0.159	4.0	0.636
135	100	0.149	0.178	4.0	0.712
115	102	0.060	0.200	4.0	0.800
65	18	0.566	0.100	4.5	0.450
120	50	0.412	0.112	4.5	0.504
145	80	0.289	0.126	4.5	0.567
155	100	0.216	0.142	4.5	0.639
160	110	0.185	0.159	4.5	0.716
130	110	0.083	0.178	4.5	0.801
120	105	0.067	0.200	4.5	0.900
75	25	0.500	0.100	5.0	0.500
135	68	0.330	0.112	5.0	0.560
152	95	0.231	0.126	5.0	0.630
150	110	0.154	0.142	5.0	0.710
160	128	0.111	0.159	5.0	0.795
80	30	0.455	0.100	5.5	0.550
120	62	0.319	0.112	5.5	0.616
148	100	0.194	0.126	5.5	0.693
150	115	0.132	0.142	5.5	0.781
150	125	0.091	0.159	5.5	0.875

Table A7. CTF vs Spatial Frequency for Scene Illumination of 0.1 FL

H. SCENE ILLUMINATION OF 0.15 FL OR 1.953E-2 LUX

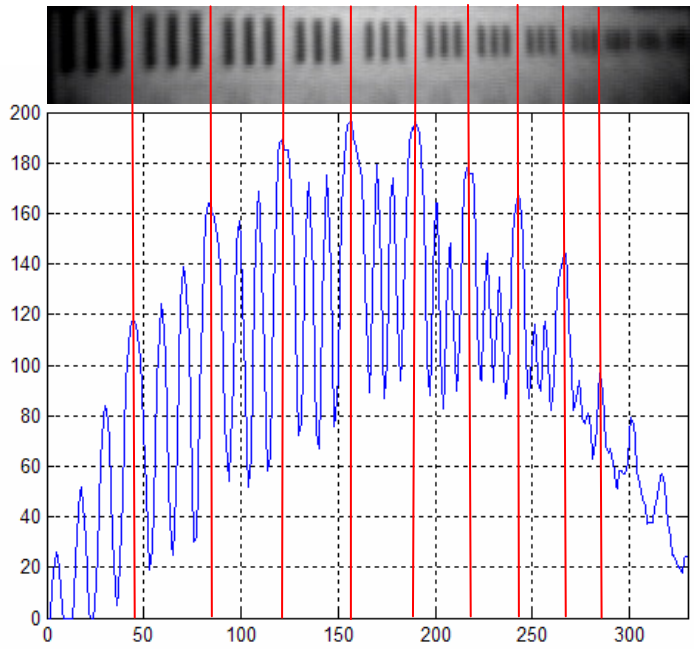

Figure A43. Contrast Intensity Plot of Scene Illumination of 0.15 FL at 3.0 m

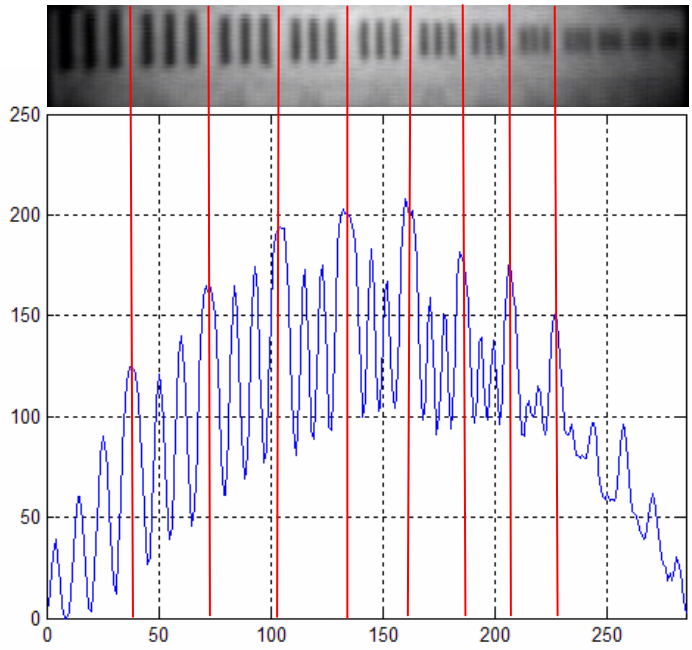

Figure A44. Contrast Intensity Plot of Scene Illumination of 0.15 FL at 3.5 m

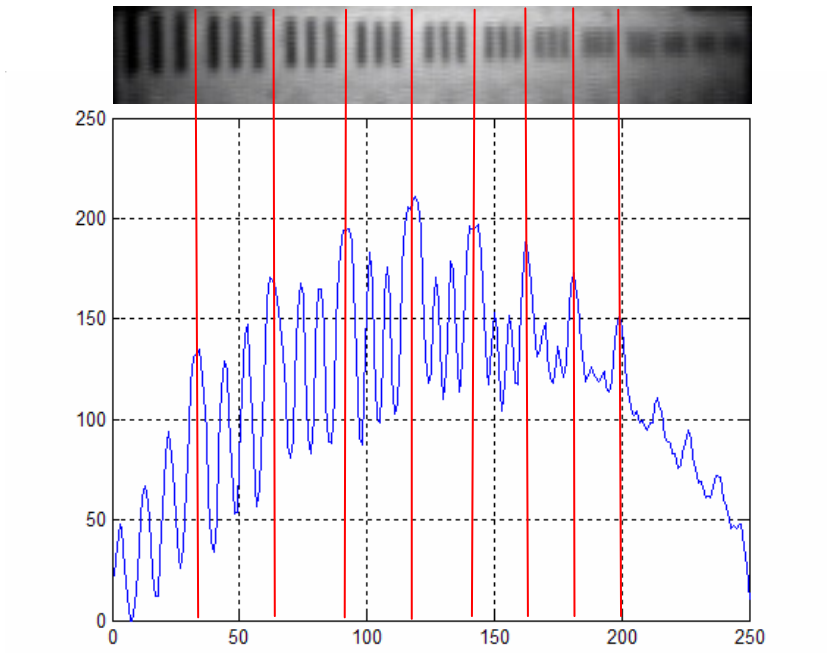

Figure A45. Contrast Intensity Plot of Scene Illumination of 0.15 FL at 4.0 m

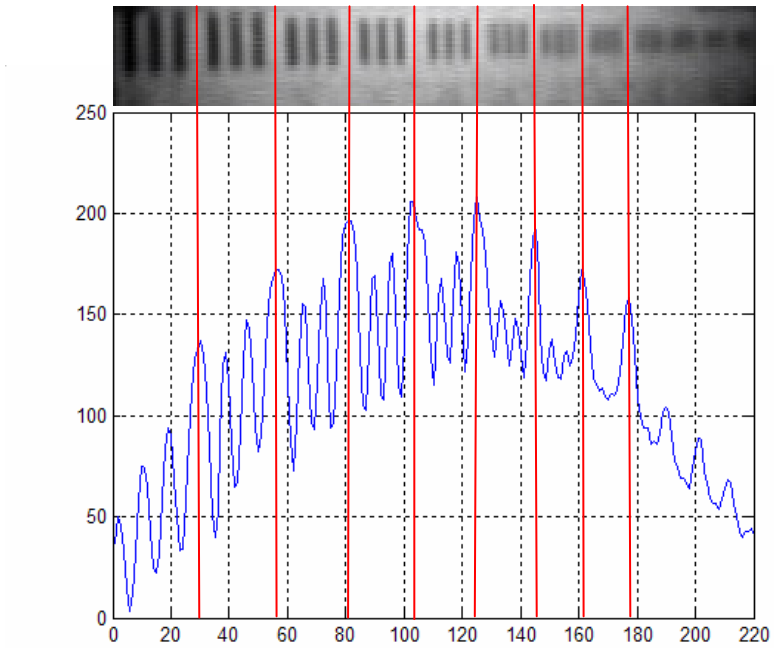

Figure A46. Contrast Intensity Plot of Scene Illumination of 0.15 FL at 4.5 m

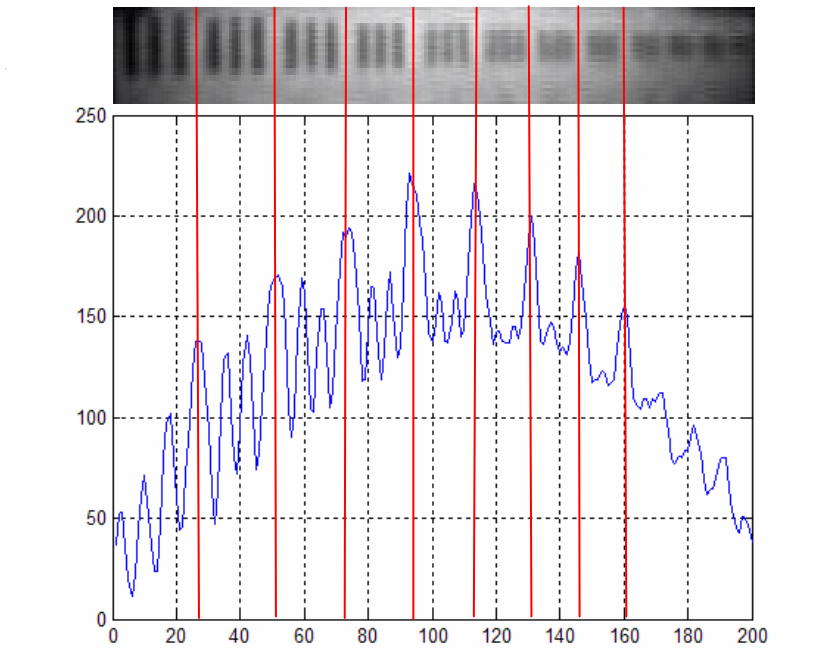

Figure A47. Contrast Intensity Plot of Scene Illumination of 0.15 FL at 5.0 m

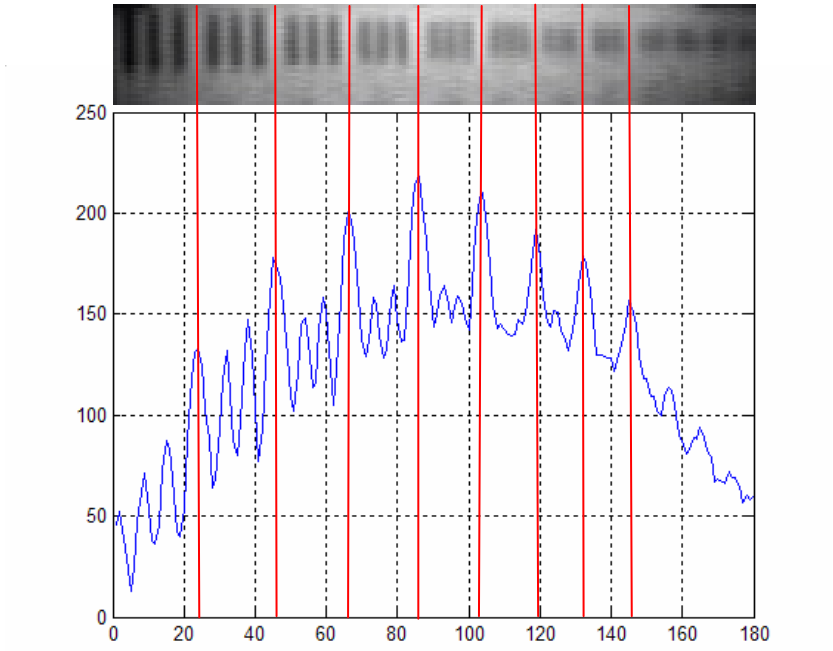

Figure A48. Contrast Intensity Plot of Scene Illumination of 0.15 FL at 5.5 m

I_{max}	I_{min}	CTF	Spatial Frequency, *v* (lp/mm)	Distance (m)	Spatial Frequency, *f* (lp/mrad)
122	30	0.605	0.112	3.0	0.336
160	60	0.455	0.126	3.0	0.378
170	70	0.417	0.142	3.0	0.426
170	95	0.283	0.159	3.0	0.477
160	90	0.280	0.178	3.0	0.534
140	95	0.191	0.200	3.0	0.600
118	88	0.146	0.224	3.0	0.672
60	15	0.600	0.100	3.5	0.350
140	40	0.556	0.112	3.5	0.392
170	72	0.405	0.126	3.5	0.441
170	88	0.318	0.142	3.5	0.497
175	105	0.250	0.159	3.5	0.557
150	90	0.250	0.178	3.5	0.623
135	100	0.149	0.200	3.5	0.700
120	90	0.143	0.224	3.5	0.784
65	25	0.444	0.100	4.0	0.400
145	55	0.450	0.112	4.0	0.448
168	80	0.355	0.126	4.0	0.504
180	100	0.286	0.142	4.0	0.568
180	120	0.200	0.159	4.0	0.636
150	110	0.154	0.178	4.0	0.712
148	120	0.104	0.200	4.0	0.800
75	25	0.500	0.100	4.5	0.450
148	65	0.390	0.112	4.5	0.504
170	95	0.283	0.126	4.5	0.567
180	110	0.241	0.142	4.5	0.639
180	125	0.180	0.159	4.5	0.716
160	125	0.123	0.178	4.5	0.801
135	120	0.059	0.200	4.5	0.900
70	20	0.556	0.100	5.0	0.500
140	50	0.474	0.112	5.0	0.560
165	105	0.222	0.126	5.0	0.630
170	120	0.172	0.142	5.0	0.710
160	135	0.085	0.159	5.0	0.795
88	40	0.375	0.100	5.5	0.550
145	65	0.381	0.112	5.5	0.616
160	110	0.185	0.126	5.5	0.693
160	130	0.103	0.142	5.5	0.781
162	142	0.066	0.159	5.5	0.875

Table A8. CTF vs Spatial Frequency for Scene Illumination of 0.15 FL

I. SCENE ILLUMINATION OF 0.2 FL OR 2.604E-2 LUX

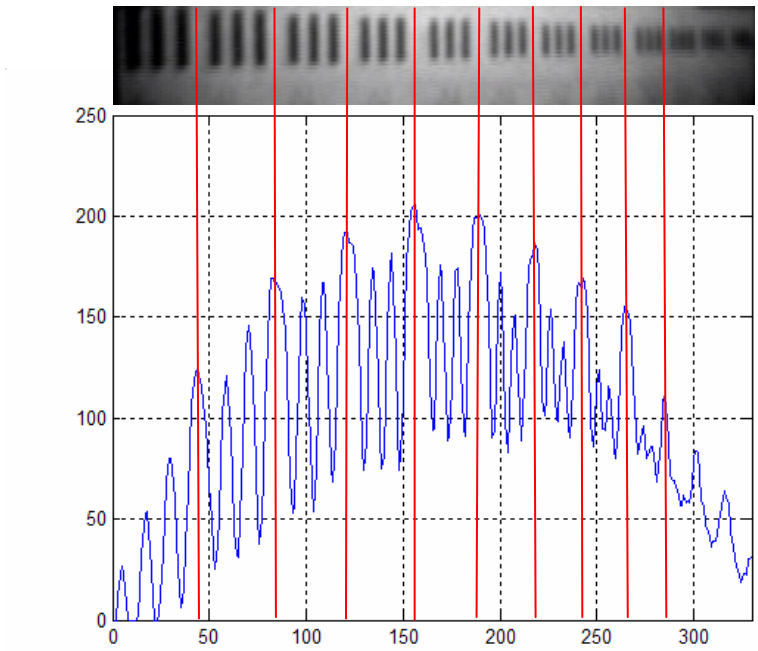

Figure A49. Contrast Intensity Plot of Scene Illumination of 0.2 FL at 3.0 m

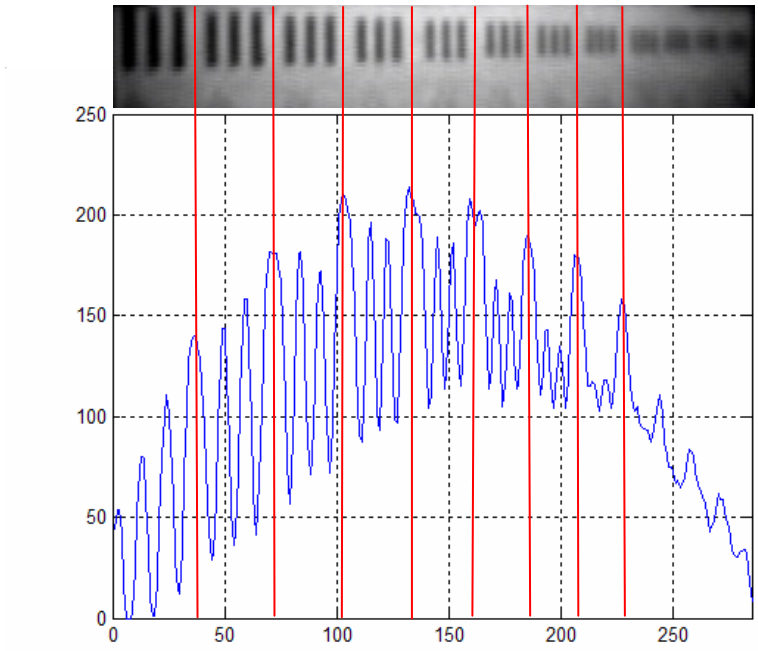

Figure A50. Contrast Intensity Plot of Scene Illumination of 0.2 FL at 3.5 m

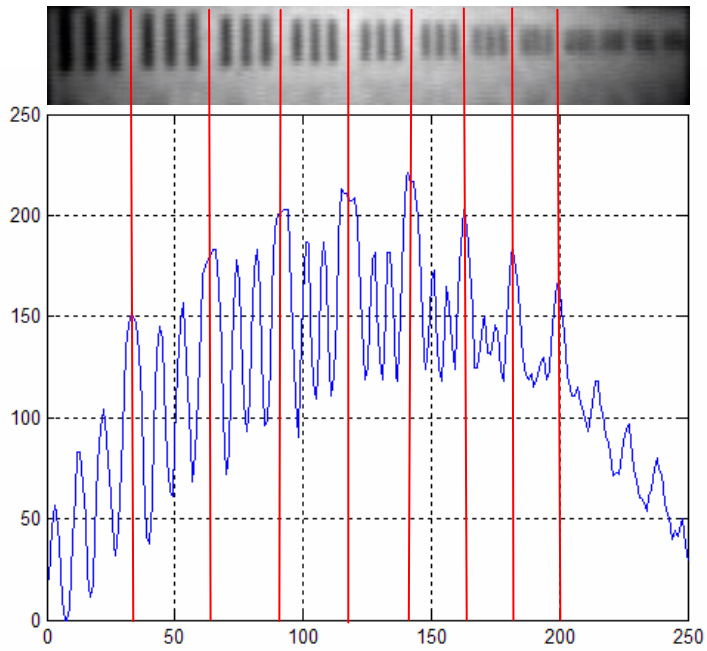

Figure A51. Contrast Intensity Plot of Scene Illumination of 0.2 FL at 4.0 m

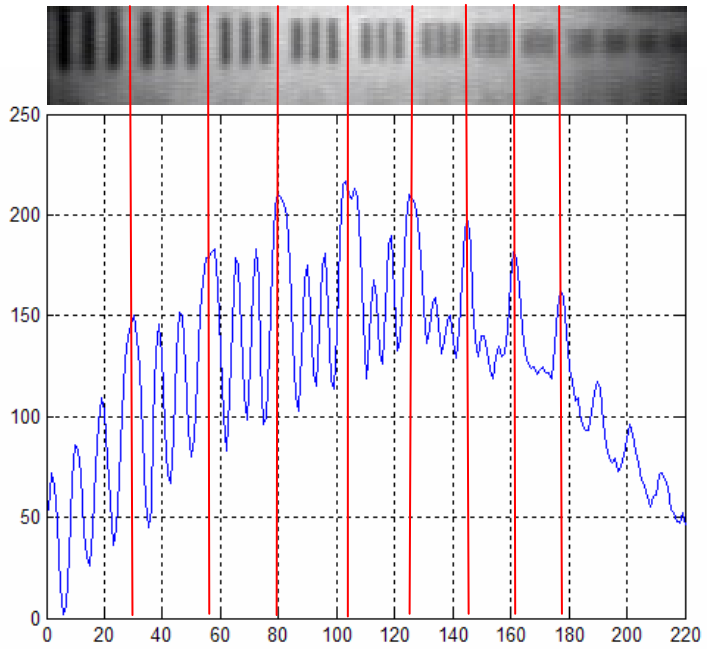

Figure A52. Contrast Intensity Plot of Scene Illumination of 0.2 FL at 4.5 m

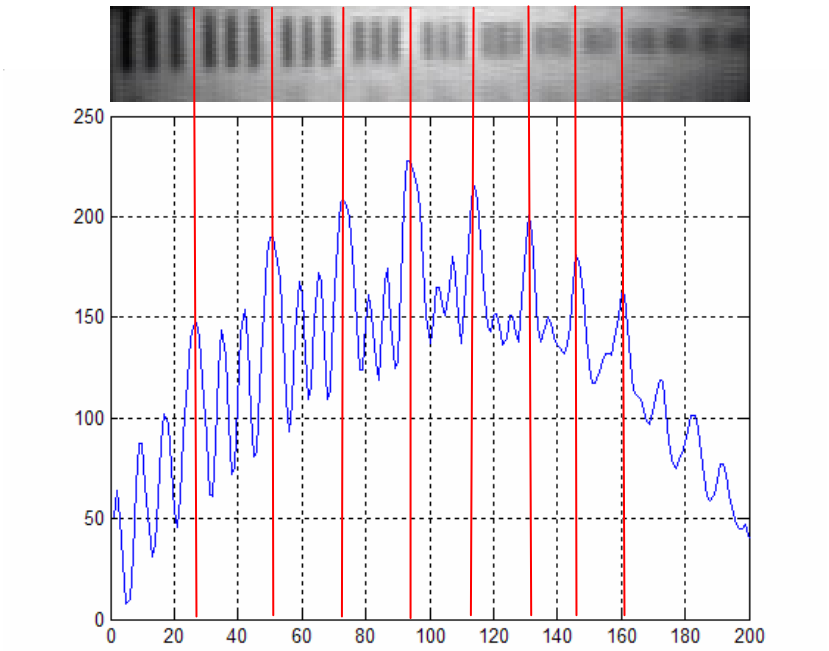

Figure A53. Contrast Intensity Plot of Scene Illumination of 0.2 FL at 5.0 m

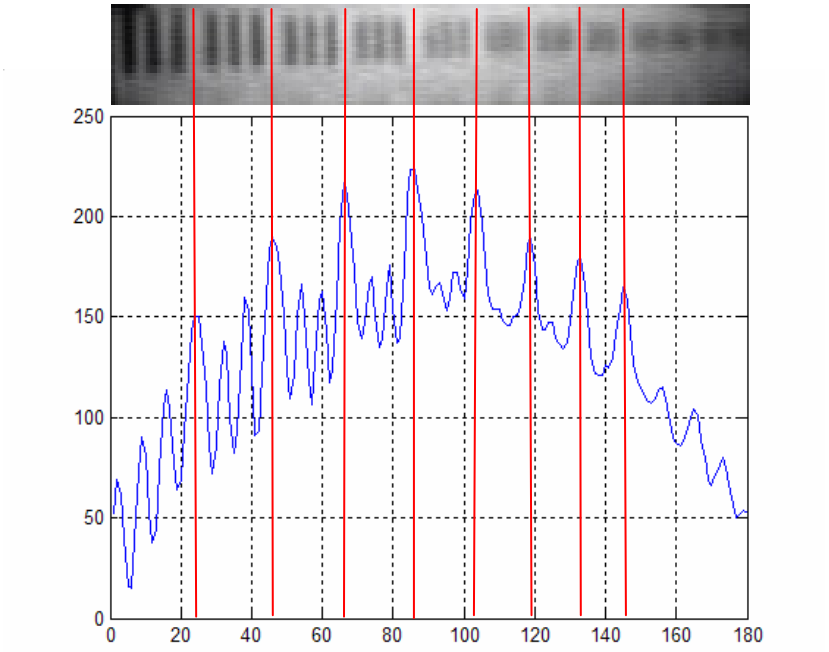

Figure A54. Contrast Intensity Plot of Scene Illumination of 0.2 FL at 5.5 m

I_{max}	I_{min}	CTF	Spatial Frequency, *v* (lp/mm)	Distance (m)	Spatial Frequency, *f* (lp/mrad)
130	35	0.576	0.112	3.0	0.336
160	60	0.455	0.126	3.0	0.378
180	75	0.412	0.142	3.0	0.426
170	95	0.283	0.159	3.0	0.477
160	90	0.280	0.178	3.0	0.534
150	100	0.200	0.200	3.0	0.600
115	80	0.179	0.224	3.0	0.672
150	42	0.563	0.112	3.5	0.392
180	70	0.440	0.126	3.5	0.441
185	90	0.345	0.142	3.5	0.497
180	120	0.200	0.159	3.5	0.557
160	110	0.185	0.178	3.5	0.623
140	110	0.120	0.200	3.5	0.700
150	60	0.429	0.112	4.0	0.448
180	90	0.333	0.126	4.0	0.504
185	110	0.254	0.142	4.0	0.568
180	120	0.200	0.159	4.0	0.636
170	120	0.172	0.178	4.0	0.712
150	120	0.111	0.200	4.0	0.800
85	30	0.478	0.100	4.5	0.450
150	50	0.500	0.112	4.5	0.504
180	100	0.286	0.126	4.5	0.567
175	120	0.186	0.142	4.5	0.639
190	125	0.206	0.159	4.5	0.716
160	130	0.103	0.178	4.5	0.801
135	120	0.059	0.200	4.5	0.900
100	40	0.429	0.100	5.0	0.500
150	70	0.364	0.112	5.0	0.560
170	110	0.214	0.126	5.0	0.630
170	120	0.172	0.142	5.0	0.710
180	140	0.125	0.159	5.0	0.795
115	40	0.484	0.100	5.5	0.550
160	80	0.333	0.112	5.5	0.616
165	110	0.200	0.126	5.5	0.693
170	130	0.133	0.142	5.5	0.781

Table A9. CTF vs Spatial Frequency for Scene Illumination of 0.2 FL

J. SCENE ILLUMINATION OF 0.3 FL OR 3.906E-2 LUX

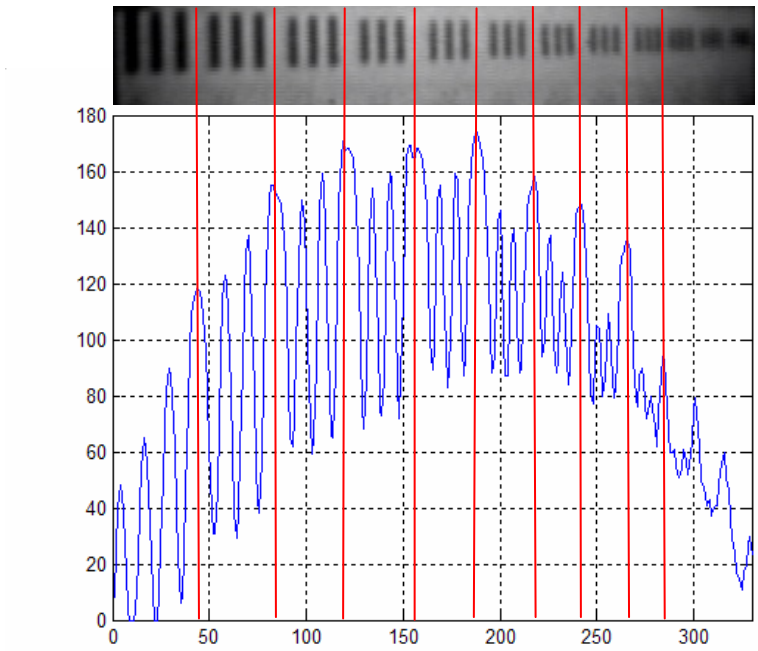

Figure A55. Contrast Intensity Plot of Scene Illumination of 0.3 FL at 3.0 m

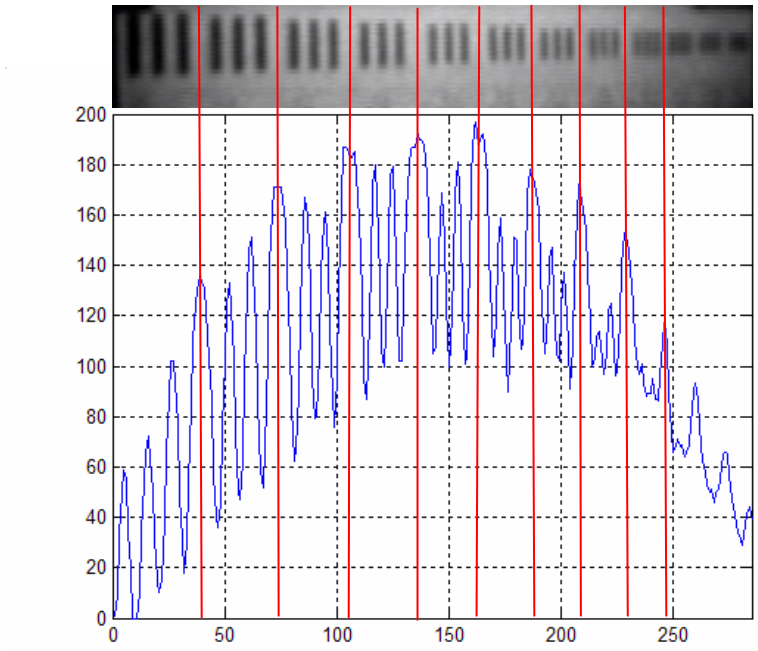

Figure A56. Contrast Intensity Plot of Scene Illumination of 0.3 FL at 3.5 m

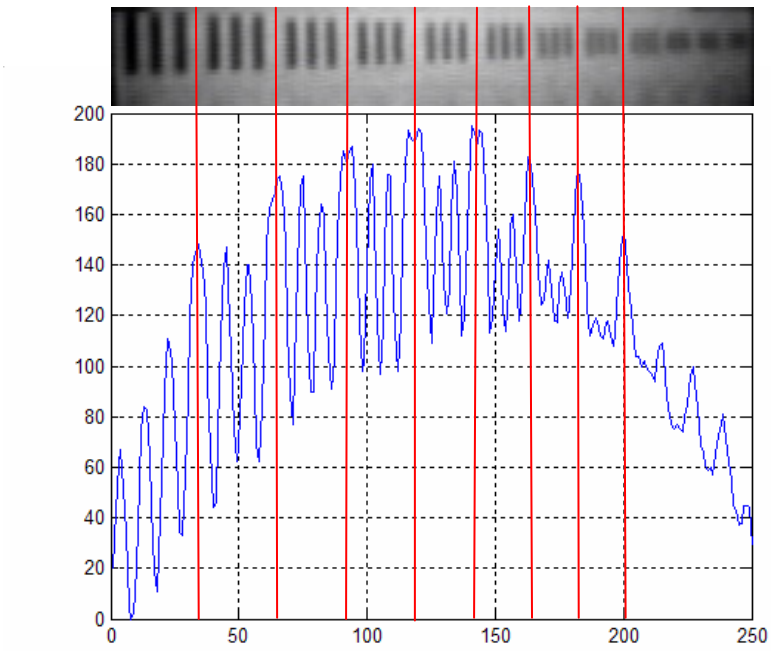

Figure A57. Contrast Intensity Plot of Scene Illumination of 0.3 FL at 4.0 m

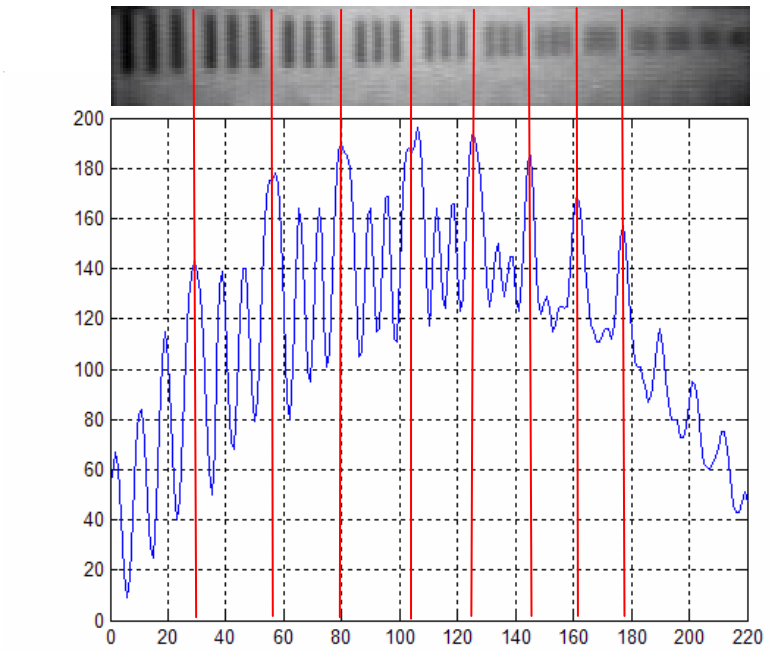

Figure A58. Contrast Intensity Plot of Scene Illumination of 0.3 FL at 4.5 m

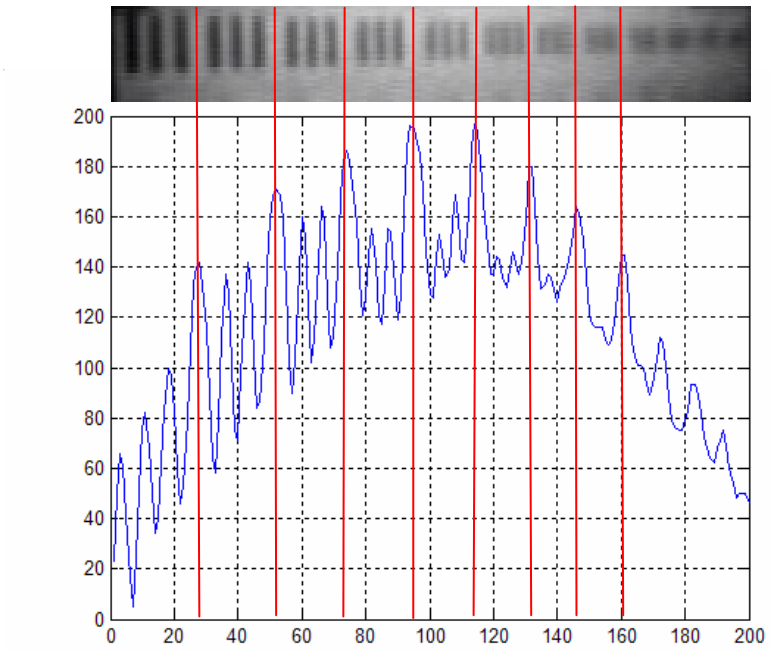

Figure A59. Contrast Intensity Plot of Scene Illumination of 0.3 FL at 5.0 m

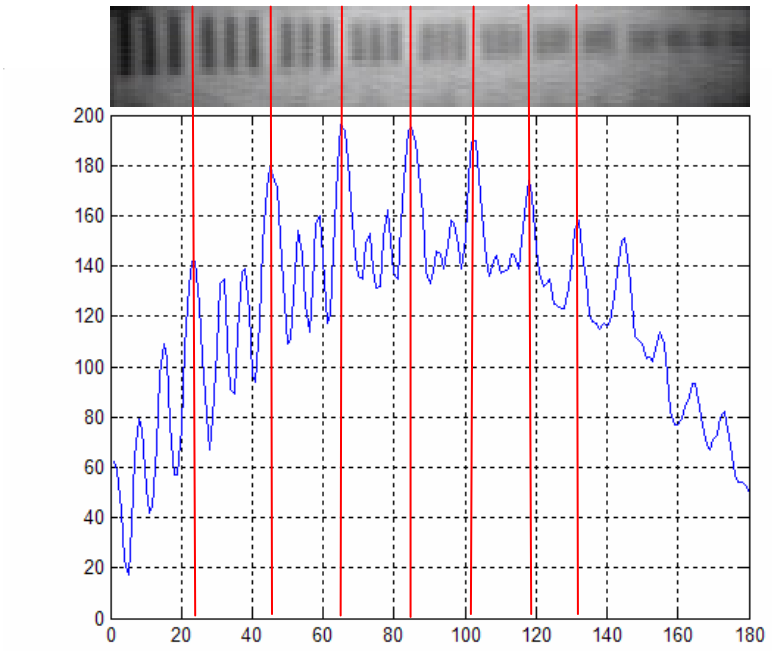

Figure A60. Contrast Intensity Plot of Scene Illumination of 0.3 FL at 5.5 m

I_{max}	I_{min}	CTF	Spatial Frequency, *v* (lp/mm)	Distance (m)	Spatial Frequency, *f* (lp/mrad)
135	35	0.588	0.112	3.0	0.336
160	65	0.422	0.126	3.0	0.378
160	72	0.379	0.142	3.0	0.426
160	90	0.280	0.159	3.0	0.477
145	88	0.245	0.178	3.0	0.534
138	90	0.211	0.200	3.0	0.600
105	80	0.135	0.224	3.0	0.672
70	20	0.556	0.100	3.5	0.350
150	50	0.500	0.112	3.5	0.392
160	80	0.333	0.126	3.5	0.441
180	100	0.286	0.142	3.5	0.497
180	105	0.263	0.159	3.5	0.557
159	100	0.228	0.178	3.5	0.623
148	98	0.203	0.200	3.5	0.700
122	98	0.109	0.224	3.5	0.784
110	35	0.517	0.100	4.0	0.400
145	62	0.401	0.112	4.0	0.448
175	90	0.321	0.126	4.0	0.504
180	100	0.286	0.142	4.0	0.568
180	110	0.241	0.159	4.0	0.636
160	112	0.176	0.178	4.0	0.712
141	118	0.089	0.200	4.0	0.800
120	110	0.043	0.224	4.0	0.896
115	40	0.484	0.100	4.5	0.450
140	70	0.333	0.112	4.5	0.504
164	98	0.252	0.126	4.5	0.567
170	110	0.214	0.142	4.5	0.639
165	124	0.142	0.159	4.5	0.716
150	124	0.095	0.178	4.5	0.801
100	35	0.481	0.100	5.0	0.500
140	60	0.400	0.112	5.0	0.560
165	90	0.294	0.126	5.0	0.630
155	118	0.136	0.142	5.0	0.710
165	130	0.119	0.159	5.0	0.795
110	40	0.467	0.100	5.5	0.550
138	70	0.327	0.112	5.5	0.616
160	110	0.185	0.126	5.5	0.693
160	130	0.103	0.142	5.5	0.781
158	135	0.078	0.159	5.5	0.875

Table A10. CTF vs Spatial Frequency for Scene Illumination of 0.3 FL

APPENDIX B: MATLAB CODES

```
% Point the directory to where you store the image file

X = input('Enter first image file name: ');

N_start = X;
N_end = X+10;

for n = N_start:2:N_end
   % Convert to grayscale intensity image from RGB image
   RGB1=imread([num2str(n), '.bmp']);
   A = rgb2gray(RGB1);
   % Extract line 16 for analysis
   D=im2double(A(16,:));
   D1=A(16,:);
   % Extract line 38 for analysis
   E=im2double(A(38,:));
   E1=A(38,:);
   % Normalization
   F=(D./E);
   F1=F.*100; % For ease of reading on graph
   figure, plot(D1)
   grid
   figure, plot(E1)
   grid
   figure, plot(F1)
   grid
end
```

THIS PAGE INTENTIONALLY LEFT BLANK

LIST OF REFERENCES

ATN Corp, “How Night Vision Works”, American Technologies Network Corporation, South San Francisco, CA, 30 July 2004. http://www.atncorp.com/HowNightVisionWorks

Bond, D. S. and Henderson, F. P., “Conquest of Darkness”, U.S. Army Night Vision Laboratory, July 1963.

Boreman, Glenn D., Basic Electro-Optics for Electrical Engineers, SPIE Optical Engineering Press, Bellingham, Washington, 1998.

Burt, Peter J. & Kolczynski, Raymond J., David Sarnoff Research Center, Enhanced Image Capture through Fusion, Princeton, NJ, 08543-5300, 1993.

Coltman, J. W., The Specification of Imaging Properties by Response to a Sine Wave Target, Journal of the Optical Society of America, Vol. 44, No. 6, pp. 468-471. June 1954

Csorba, Illes P., Image Tubes, Howard W. Sams, Indianapolis IN, 1985.

Edmund Optics, USAF 1951 Test Pattern, Edmund Industrial - Optics. 30 July 2004 http://www.edmundoptics.com/onlinecatalog/DisplayProduct.cfm?productid=1790

Electrophysics, Specifications for the Astroscope 9350CIU3-A Generation 3 Image Intensifier, Electrophysics Corp. Inc., Fairfield, NJ, 30 October 2004. http://www.electrophysics.com/Browse/Brw_ProductLineCategory.asp?CategoryId=27&Area=NV

Gamma Scientific, Operating Instructions for Model 2020 Photometer, Gamma Scientific, Inc, San Diego, CA, 1969.

Harney, Robert C., Combat Systems, Volume 2 - Sensor Elements - Part II, Sensor Technologies, Naval Postgraduate School, Monterey, CA, January 2004. Chapter 9.

Holst, Gerald C., Infrared Imaging System Testing, The Infrared & Electro-Optical Systems Handbook, Vol 4, Chapter 4. Infrared Information Analysis Center, Michigan and SPIE Optical Engineering Press, Washington, 1993.

Ji Wei, Electro-Optics Systems and Technology Review, TDSI, Singapore, 2003

Kjellberg, Lars, Resolution, Contrast and MTF, Photodo AB, 30 November 2004. http://www.photodo.com/art/Reso8.shtml

Lloyd, J.M., Thermal Imaging Systems, Honeywell Inc, Plenum Press, New York, 1975.

McDaniel, R., Scribner, D., Krebs, W., Warren, P., Ockman, N., McCarley, J. Image fusion for tactical applications. Proceedings of the SPIE - Infrared Technology and Applications XXIV, 3436, Pages 685-695, 1998.

OriginLab, Getting Started Booklet, Version 6.1, OriginLab Corporation, Northampton, MA, 2000.

Palmer, James M., Radiometry and Photometry, Optical Sciences Center University of Arizona, Tucson, AZ, 30 November 2004. http://www.optics.arizona.edu/Palmer/rpfaq/rpfaq.htm#radiometry

RCA, Electro-Optics Handbook, RCA Corporation, Lancaster, PA, 1974.

RCA, Photomultiplier Tubes, Photodiodes, Electron Multipliers, PIT-700B, December 1971.

Sitko, Michael L., Light Measurement, Department of Physics, University of Cincinnati, 15 November 2004. http://www.physics.uc.edu/~sitko/LightColor/8-Measuring/Measurement.htm

Stack, John, Machine Vision – Optics, Edmund Industrial, 30 July 2004. http://www.sensorsmag.com/articles/0400/34/main.shtml

Task, Harry L., Hartman, Richard T., Marasco, Peter L., Methods for Measuring Characteristics of Night Vision Goggles, Armstron Laboratory, Crew Systems Directorate, Human Engineering Division, Wright-Patterson AFB OH 45433-7022, Pages 481-483, October 1993.

Wolfram Research Inc., Discrete Wavelet Transform, Digital Image Processing Documentation, Wolfram Research Inc., 15 November 2004 http://documents.wolfram.com/applications/digitalimage/UsersGuide/8.6.htm

INITIAL DISTRIBUTION LIST

1. Defense Technical Information Center
   Ft. Belvoir, Virginia

2. Dudley Knox Library
   Naval Postgraduate School
   Monterey, California

3. Professor Alfred W. Cooper
   Physics Department
   Naval Postgraduate School
   Monterey, California

4. Professor Gamani Karunasiri
   Physics Department
   Naval Postgraduate School
   Monterey, California

5. Professor Yeo Tat Soon
   Temasek Defence Systems Institute
   Singapore

6. Mr. Cheng Wee Kiang
   Defence Science and Technology Agency
   Singapore